CHALMERS

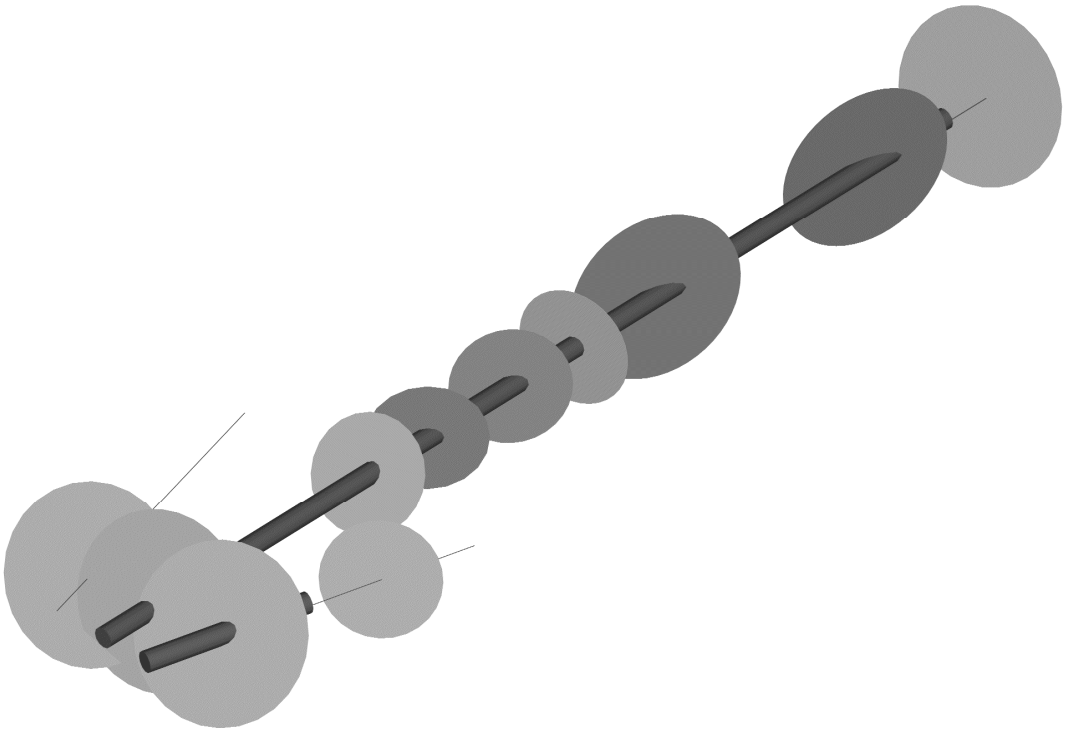

Hydrogeological characterisation of a fracture network

Case study of horizontal drifts at Äspö Hard Rock Laboratory

Master of Science Thesis in the Master's Programme Geo and Water Engineering

SARA KVARTSBERG

Department of Civil and Environmental Engineering
Division of GeoEngineering
Engineering Geology Research Group
CHALMERS UNIVERSITY OF TECHNOLOGY
Gothenburg, Sweden 2010
Master's Thesis 2010:88

MASTER'S THESIS 2010:88

Hydrogeological characterisation of a fracture network

Case study of horizontal drifts at Äspö Hard Rock Laboratory

Master of Science Thesis in the Master's Programme Geo and Water Engineering

SARA KVARTSBERG

Department of Civil and Environmental Engineering
Division of GeoEngineering
Engineering Geology Research Group
CHALMERS UNIVERSITY OF TECHNOLOGY

Gothenburg, Sweden 2010

Hydrogeological characterisation of a fracture network
Case study of horizontal drifts at Äspö Hard Rock Laboratory
Master of Science Thesis in the Master's Programme Geo and Water Engineering
SARA KVARTSBERG

Examensarbete / Institutionen för bygg- och miljöteknik,
Chalmers tekniska högskola 2010:88

Department of Civil and Environmental Engineering
Division of GeoEngineering
Engineering Geology Research Group
Chalmers University of Technology
SE-412 96 Göteborg
Sweden
Telephone: + 46 (0)31-772 1000

Cover:
3D-model of water-conducting fractures along drifts and core boreholes. Read more in Chapter 4.1.2.

Chalmers Reproservice
Gothenburg, Sweden 2010

Hydrogeological characterisation of a fracture network
Case study of horizontal drifts at Äspö Hard Rock Laboratory
Master of Science Thesis in the Master's Programme Geo and Water Engineering
SARA KVARTSBERG
Department of Civil and Environmental Engineering
Division of GeoEngineering
Engineering Geology Research Group
Chalmers University of Technology

ABSTRACT

Characterisation of a fracture system can provide a better understanding of its hydrogeological behaviour, hence facilitate underground construction. This project has been focusing on describing the hydrogeological conditions of the fracture system surrounding two horizontal drifts at 220 meters depth in Äspö Hard Rock Laboratory (HRL). These drifts are part of a project studying the KBS-3H repository design for storage of spent nuclear fuel. The inflow of groundwater is of particular importance for the KBS-3H design since sections with high inflow must be identified.

The characterisation has been performed by evaluating parameters found important for describing a water-conducting fracture system, e.g. fracture intensity, fracture orientations and distribution of hydraulic apertures. Other analyses concern grouting performance and flow dimensions in fractures, all used to give a representative description of the fracture network and its flow characteristics. The inputs for the evaluations are hydraulic tests, fracture mapping and grouting performed in core boreholes and drifts at Äspö HRL.

It was found that the fracture system surrounding the horizontal drifts can be described as poorly connected network, where the rock consists of a sparsely fractured crystalline rock mass intersected by water-conducting zones with higher fracture intensities. Indicators confirming this are few inflow positions, which are located in areas with higher fracture intensity than the rock in general. The sealing of these specific positions resulted in a significantly reduced inflow and a limited development of inflow relocation. The results from the evaluations showed that the generally described characteristics of the Äspö rock mass also were identified in this fracture system. The anisotropic hydraulic conductivity of the Äspö rock mass was found, as well as agreements in transmissivity distribution, fracture intensity and fracture set orientations.

Inflow predictions are often an important issue when constructing tunnels, but it was found that there are difficulties when making these prognoses. The largest and most important inflows were though possible to find and to simulate. Making consistent and precise measurements was identified as a central part of a hydraulic characterisation programme, since data with low accuracy or incomparable data make evaluations more difficult.

Key words: flow dimension, fracture system, fracture intensity, grouting, inflow prediction, KBS-3H, penetration length, transmissivity

Hydrogeologisk karakterisering av ett spricknätverk
Fallstudie av horisontella deponeringshål i Äspölaboratoriet
Examensarbete inom Mastersprogrammet Geo and Water Engineering
SARA KVARTSBERG
Institutionen för bygg- och miljöteknik
Avdelningen för Geologi och geoteknik
Chalmers tekniska högskola

SAMMANFATTNING

En karakterisering av ett bergs spricksystem kan ge en ökad förståelse för de hydrogeologiska förhållandena i berget och möjliggöra förbättringar i genomförandet av ett tunnelprojekt. Detta examensarbete fokuserar på att beskriva det spricknätverk som omger de horisontella deponeringshålen på 220 m-nivån i Äspölaboratoriet. Deponeringshålen är en del av KBS-3H projektet som undersöker ett designalternativ för slutförvar av kärnbränsleavfall. Grundvatteninflöden till deponeringshålen är en viktig fråga i ett KBS-3H förvar eftersom sektioner med höga flöden måste identifieras.

Karakteriseringen har genomförts genom att utvärdera parametrar som beskriver det vattenförande spricksystemet, bland annat sprickintensitet, sprickriktningar och fördelningar av transmissiviteter. Analyserna utfördes med data från hydrauliska tester och karteringar genomförda i kärnborrhål och i deponeringshål. Även injekteringsresultat och analyser av flödesdimensioner i sprickor har använts för att kunna ge en representativ beskrivning av spricknätverket med dess hydrauliska egenskaper.

En genomgång av utförda mätningar och analys av resultaten visar att spricksystemet runt deponeringshålen kan beskrivas som ett dåligt konnekterat spricknätverk, bestående av sprickfattiga plintar av kristallint berg som genomkorsas av mer sprickrika zoner. Indikationer på detta är få inflödespositioner vilka hänger samman med sektioner med ökade sprickintensiteter, samt att flödet i liten utsträckning länkades till omgivande sprickor då de stora inflödespositionerna tätades. Resultaten från de utvärderade parametrarna visade sig överrensstämma väl med andra utvärderingar utförda i Äspös bergmassa, exempelvis transmissivitetsfördelning, sprickintesitet, sprickset och anisotropin i bergets hydrauliska egenskaper.

Skattningarna av inflöden till deponeringshålen, baserat på hydrauliska tester i kärnborrhål, var förknippat med vissa osäkerheter. Dock kunde de största och mest betydelsefulla inflödena förutses, vilket visar att förundersökningar kan ge viktig information om hydrogeologiska förhållandena. Att utföra konsekventa och genomtänkta hydrauliska tester visade sig vara av stor betydelse för karakteriseringen, eftersom låg mätnoggrannhet och ej jämförbar data reducerar tillförlitligheten i analyserna.

Nyckelord: flödesdimension, inflödesskattning, injektering, inträngningslängd, KBS-3H, sprickintensitet, spricksystem, transmissivitet

Contents

Handledarnas förord

Följande examensarbete utgör en komplett analys av de hydrogeologiska förhållandena och resultatet av injektering i ett demonstrationsprojekt med horisontell deponering (KBS-3H) i SKBs Äspölaboratorium. Analysen har genomförts med utgångspunkt från den databas som framtagits under projektets gång. Analysen har utförts på grundval av nya erfarenheter och insikt om de hydrogeologiska egenskaperna hos ett sprickigt urberg. Likaledes har nyutvecklade verktyg för analys av hydrogeologiska egenskaper och injekteringsförlopp använts. Arbetet är föredömligt genomfört och kan rekommenderas till läsning för den som planerar eller genomför ett liknande projekt.

Sammanfattningsvis ett mycket bra examensarbete.

Göteborg i juni 2010

Gunnar Gustafson Åsa Fransson

Preface

This master thesis has been carried out at the Department of Civil and Environmental Engineering, Division of GeoEngineering at Chalmers University of Technology, Sweden. It has been supervised by Magnus Zetterlund (Vattenfall Power Consultant AB) and Gunnar Gustafson (Chalmers University of Technology). Examiner is Gunnar Gustafson.

I wish to express my gratitude to all whom have contributed to the progress of this master thesis project. Special thanks are directed to Magnus Zetterlund for his support and guidance during the progress of this thesis. Many thanks also to Åsa Fransson and Gunnar Gustafson for their support of information and ideas of how to develop the project. Further I would like to thank Johan Berglund at Vattenfall Power Consultant for his support of software, Magnus Eriksson and Linda Lindström for useful inputs in the understanding of the KBS-3H project and Swedish Nuclear Fuel and Waste Management Co. (SKB), especially Magnus Kronberg, for providing the data needed for this project.

Thanks also to my opponents, Edward Runslätt and Johan Thörn, for useful comments throughout the project, and the staff at Vattenfall Power Consultant and the staff at the GeoDivision at Chalmers for their encouragement and pleasant lunch and coffee breaks.

Göteborg, June 2010

Sara Kvartsberg

Notations

Roman letters

B	[m]	channel width
b	[m]	aperture, hydraulic aperture
b_{max}	[m]	the hydraulic aperture of the largest fracture
b_r	[m]	the hydraulic aperture of the fracture with rank r
g	[m/s^2]	the gravitational acceleration
h	[m]	hydraulic head
i	[-]	interval number
I	[m]	penetration length
I_D	[-]	dimensionless penetration length
I_{max}	[m]	maximum penetration
k	[-]	Pareto distribution parameter
N	[-]	total number of fractures
n	[-]	order number of a size-sorted sample
p	[Pa]	pressure
Q	[m^3/s]	flow
R_0	[m]	radius of influence
r	[-]	the rank of a value in an ordered sample
r_w	[m]	radius of a borehole
S	[-]	storativity
s	[m]	drawdown, pressure
T	[m^2/s]	transmissivity
T_{max}	[m^2/s]	transmissivity of the largest fracture
t	[s]	time
t'	[s]	recovery time
t_D	[-]	dimensionless time
t_e	[s]	adjusted time
t_G	[s]	gel induction time
t_p	[s]	flow time
V	[m^3]	volume

Greek letters

θ	[-]	parameter for penetration analysis
μ	[Pa·s]	fluid viscosity
μ_0	[Pa·s]	fluid initial viscosity
ξ	[-]	skin factor
ρ	[kg/m^3]	fluid density
σ	[MPa]	stress tensor
τ_0	[Pa]	fluid initial yield stress

Mathematical expressions

$-dh/dl$	[-]	hydraulic gradient
Q/dh	[m^2/s]	specific capacity
μ	[-]	mean value
σ	[-]	standard deviation
x	[-]	variable

Abbreviations

CBH	Core borehole
CDF	Cumulative density function
DFN	Discrete fracture network
HRL	Hard Rock Laboratory
NB	Negative binomial
PBT	Pressure build-up test
PDF	Probability density function
PVT	Pressure, volume and time
RQD	Rock Quality Designation
WPT	Water pressure test

1 Introduction

1.1 Background

The Swedish Nuclear Fuel and Waste Management Co, SKB, is planning to build a nuclear waste repository in the Forsmark area in Östhammar, Sweden. Different techniques for storage of spent nuclear fuel in the repository are evaluated; vertical deposition of spent fuel (KBS-3V) is the reference layout, but horizontal deposition in drifts (KBS-3H) is also considered (Eriksson & Lindström 2008). Both KBS-3V and KBS-3H are design variants of a multi barrier method called KBS-3, which is a disposal concept where spent nuclear fuel is stored in copper canisters with cast iron, surrounded by bentonite clay, placed at about 500 meters depth in granitic rock (Bäckblom & Lindgren 2005), see Figure 1.1.

The KBS-3H design is planned to consist of horizontal drifts, which have a diameter of 1.85 m and maximum length of about 300 m. In the drifts, canisters with spent nuclear fuel will be placed, separated with blocks of bentonite clay. The deposition method has several advantages compared to KBS-3V; there will be smaller quantities of bentonite and several other materials, probably less grouting required due to smaller cross-sectional area and there will be no tunnel backfill material (Antilla et al. 2008). This contributes to cost savings and reductions in environmental impact. But a potential problem may be groundwater flowing into the drift since the water may cause erosion and transport of buffer. There are also uncertainties related to the emplacement of the containers and the drift utilisation degree with risk for abandoned drifts if the requirements are not met.

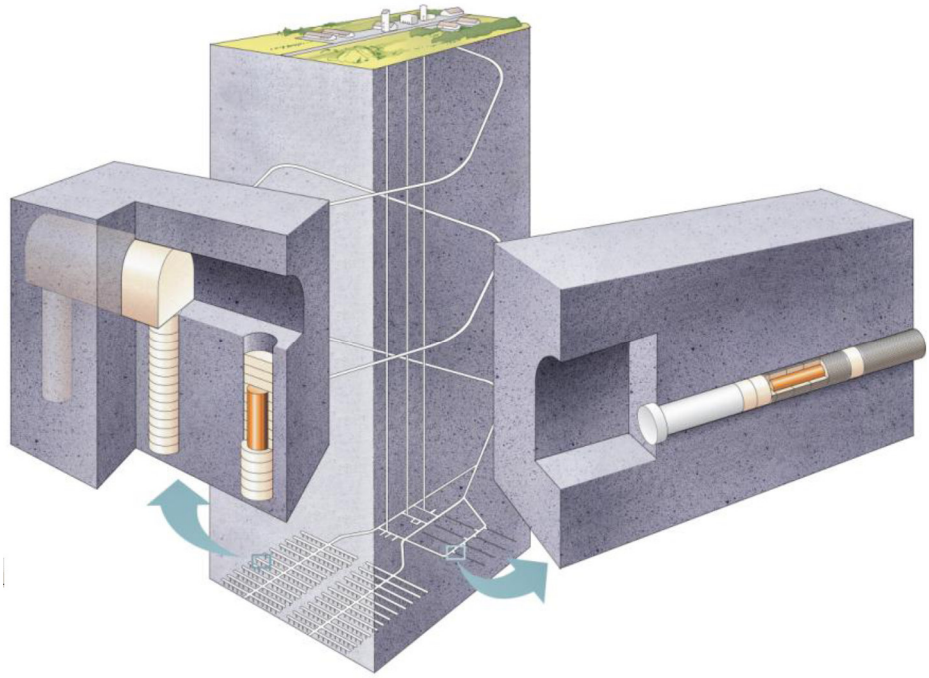

Figure 1.1 Principles of the KBS-3 repository designs, with KBS-3V to the left and KBS-3H to the right. From Antilla et al. (2008).

The host rock need to protect the buffer against piping and erosion, and it must provide an effective barrier against transport of radionuclides released in the event of canister failure. Smith et al. (2007) concluded that a value of inflow that can be accepted for deposition of canisters is 0.1 litres/minute per 10 meter long canister position. If this value is exceeded, either filling blocks or isolation by using compartment plugs are required (Antilla et al. 2008). One drawback is though that compartments significantly reduce the degree of utilization, which leads to higher costs. The groundwater control is thus an important issue in the KBS-3H design.

Demonstration and testing of different drift components and equipment have been carried out at the Äspö Hard Rock Laboratory (HRL). The project started with pre-investigations in 2003 at the -220 level. Three core drilled boreholes were placed in the positions of the projected drifts. The two final demonstration drifts were drilled in 2004 and 2005. Both are about 1.85 m in diameter, the long drift is 94.45 metres long and the short is 15.85 metres. During autumn 2007 and spring 2008, a post-grouting method for sealing horizontal deposition drifts was tested at the site. The long drift was used in the post-grouting test. In the shorter drift groundwater inflow measurements were performed in order to study how grouting in the longer drift affected the inflow to the shorter drift. The post grouting was performed in the five positions where inflow was noticed. The equipment used was a Mega-Packer (see Figure 1.2); a 2 m long tube, 1.82 m in diameter, which sealed sections using grout consisting of silica sol (Eriksson & Lindström 2008).

The five selected positions were hydraulically characterised (pre- and post-characterisation) in conjunction with the grouting. The pre-characterisation was used to create a base for the grouting design and consisted of three tests; groundwater pressure build up test, measurement of water leaking into the drift, and water pressure tests. The post characterisation consisted of measurement of water leaking into the drift in all positions after grouting and these values were used to evaluate the obtained sealing effect. The KBS-3H project was carried out over a period of five years, and there is a lack of consistency in the hydraulic tests performed. This since the focus has been more on practical aspects such as constructability of drifts or the Mega-Packer as a sealing method, rather than the hydrogeological behaviour of the host rock.

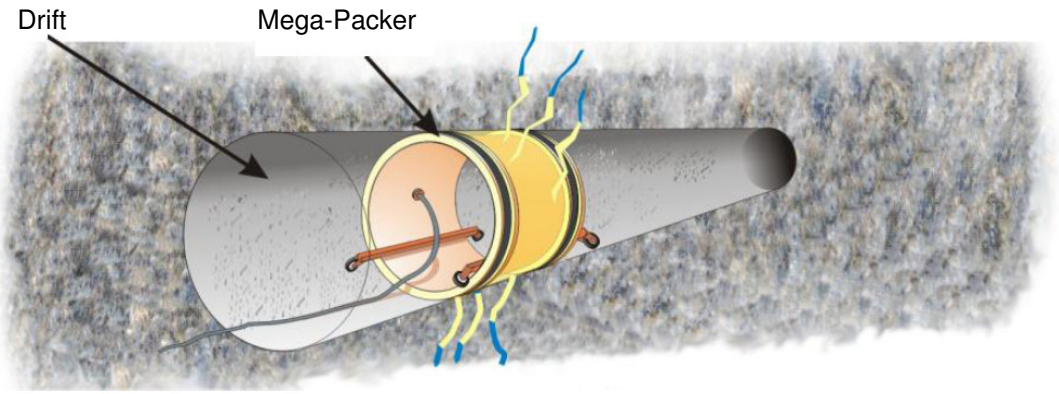

Figure 1.2 Illustration of post-grouting with the Mega-Packer. From Antilla et al. (2008).

1.2 Objective

The impact of groundwater may ultimately determine the feasibility of the KBS-3H design, and knowledge of the properties of the water-conducting fracture system in the rock is important in order to foresee and avoid sections with too high inflow before excavation of the drifts. This thesis has been focusing on the fracture system surrounding the horizontal demonstration drifts at Äspö HRL, which are a part of the KBS-3H design project. The objective is to make a description of the properties of the fracture system, in order to increase the understanding of the transport of groundwater in the rock. This is achieved by combining and interpreting the results from a number of characterisation methods, which are based on geological and hydrogeological data.

An essential part of the characterisation of the fracture system has been to understand the fracture network (how fractures are linked to each other) and how water is flowing within the fractures. This information has then been used to analyse observed results regarding water inflows and grouting performances.

1.3 Method

The central part of the thesis is the processing and evaluation of existing geological and hydrogeological data, which have been generated in the different phases of the KBS-3H project. First the components of a fracture system are studied, followed by a survey of characterisation methods appropriate for this thesis. Then the KBS-3H project at Äspö HRL are described, in order to understand all the phases of the project and how these could have affected the rock. The different characterisation methods are then applied on the data collected from these phases. The results are used to achieve a better understanding of the hydraulic behaviour of the rock, but also to interpret how the rock has been affected by the reaming and grouting of the drifts.

The two drifts are 15 m and 95 m long with corresponding pre-boreholes of 30 m and 100 m at their positions. The analysis is focusing on the data from the long drift simply because more data are collected from that part of the rock. There has been some inconsistency in the hydraulic tests performed, and the data generated are not always complete or comparable. In some of these situations assumptions are made. A 3D modelling of the fractures has been made in order to obtain a clearer view of how the fractures form a network. This modelling is performed with a deterministic approach describing fracture properties individually and no attempt of modelling the flow of water within the fractures has been made.

1.4 Delimitations

This project is focusing on characteristics of the fracture system surrounding the demonstration drifts at Äspö HRL, and the properties important for describing this specific fracture system for groundwater control purposes. The evaluation methods used are therefore those appropriate for this fracture system, but also those possible to use from the data available from the hydraulic tests and geological mapping.

2 Methods for fracture network characterisation

The hydrogeological conditions in the deposition drifts may ultimately determine the feasibility of the KBS-3H repository design. The groundwater flowing into the drifts from intersecting water-conducting fractures may cause design problems and a good knowledge of the hydraulic behaviour of the rock could facilitate the understanding of issues related to groundwater control in the drifts (Antilla et al. 2008). Conceptualisations and thorough characterisations of rock properties are important when making predictions of mechanical and hydraulic behaviour in rock masses. In crystalline rocks characteristics of the fracture network are of particular importance since intact rock is practically impermeable and fluid flow is assigned to discontinuities (Starzec 2001).

This chapter will discuss the components of fracture networks and how conceptual models can be developed to describe their hydraulic behaviour. Hydraulic tests used in tunnel constructions will also be described since they can provide useful information regarding the fracture network.

2.1 Groundwater flow in rock

Rock mass consists, more or less, of a homogenous rock which is separated into blocks of different shapes and sizes by discontinuities (Hernqvist 2009). In crystalline rock, it is reasonable to assume that the intact rock is impermeable and assign all water flow to the fractures. However, a fracture within a rock mass does not necessarily contribute to the groundwater flow in a fracture network, although it contains groundwater, since it could be too tight or unconnected with other fractures.

The ability of a fracture to transmit a fluid is described by its transmissivity, T, which has the unit m^2/s. The definition of transmissivity can be seen in the equation (2.1) below, where Q is the flow of water through a channel with the width B and dh/dl being the hydraulic gradient.

$$Q = -T \cdot B \cdot \left(\frac{dh}{dl} \right) \tag{2.1}$$

The transmissivity can be used to obtain information about the hydraulic fracture apertures. The fracture aperture is a key property when evaluating the hydraulic properties of a fracture system since it describes the open width of a fracture and measures how much water the fracture can conduct. But the physical aperture can vary significantly throughout the fracture and is hard to measure. The aperture can however be represented by the hydraulic aperture, which represents the open width, through which water can flow, in a fracture with plane, parallel walls (Hernqvist 2009). The relation between hydraulic aperture and transmissivity is expressed by the cubic law (Snow 1968, de Marsily 1986):

$$T = \frac{\rho \cdot g \cdot b^3}{12\mu} \tag{2.2}$$

where ρ and μ are the density and viscosity of the fluid, g the acceleration due to gravity and b denotes the hydraulic aperture. For radial flow under saturated and

steady-state conditions, the transmissivity of a fracture may be estimated with the Thiem well equation (Gustafson 2009):

$$T = \frac{Q}{2\pi \cdot dh} \cdot \ln\left(\frac{R_0}{r_w}\right) \tag{2.3}$$

where Q is the flow of water, dh is the overpressure above groundwater pressure, r_w is the borehole radius and R_0 is the radius of influence. The factor Q/dh (flow divided by the change in hydraulic head), also referred to as the specific capacity, can be used to obtain the transmissivity. Fransson (2001) showed that the specific capacity derived from short duration hydraulic test in boreholes, can be used as a reasonable estimation of the transmissivity:

$$T \approx \frac{Q}{dh} \tag{2.4}$$

2.2 Fracture network description

The transport of water in crystalline rock is limited to the fractures. Together, the fractures form a network system, which is connected where the fractures are intersecting each other. The behaviour of the water flow is dependent on the network connectivity and geometry, the applied pressure gradient and the hydro-mechanical properties of individual fractures (Starzec 2001).

According to Hernqvist (2009) are fracture intensity, fracture set orientations, distributions of hydraulic apertures (transmissivity) and fracture lengths the most important parameters to describe a fracture system for grouting-related purposes. This, since these parameters determine flow dimensions (explained in Chapter 2.3) and describe the geometry of the water-conducting fracture system. Properties of the fracture network, such as the connectivity, can be evaluated if these parameters are identified. Important bases for the design process are data received from fracture mapping and hydraulic tests. Parameters such as fracture intensity, fracture orientation, and hydraulic aperture, are properties that can be measured in boreholes (Fransson & Hernqvist 2010).

2.2.1 Fracture intensity

Fracture intensity, also referred to as fracture density or frequency, is a measure of how many fractures there are in a rock mass. It is commonly described with the scale-independent parameter P_{10}, which describes the number of fractures per borehole length (Dershowitz & Herda 1992).

P_{10} is however subjected to bias, which is introduced by the orientation in which a measurement is made relative to the orientation of fractures. A measurement along a borehole will preferentially detect fractures that are orthogonal to the borehole, rather than fractures with an oblique angle. This will bias measures of fracture intensity in favour of fracture sets orthogonal to the borehole. An accumulation of the calculations of fracture intensity in terms of a weighted sum can be used to compensate for this bias. The process is called Terzaghi correction and can be used to calculate the corrected linear fracture intensity, $P_{10,corr}$ (Follin et al. 2007).

Fracture intensity can also be specified with the parameters P_{21} and P_{32}. P_{21} describes the total length of fracture traces per unit area and has the unit m/m^2. P_{10} and P_{21} should be the same after Terzaghi correction (Hernqvist 2009). The P_{32} parameter is a volumetric intensity measure, which is the fracture surface area per unit volume of rock (m^2/m^3). It cannot be observed directly, but can be estimated from $P_{10,corr}$ with numerical simulations.

A statistical distribution that describes the number N of fractures in intervals along boreholes reasonably well is the negative binomial (NB) distribution (Gustafson 2009). The NB distribution has two characteristic parameters, p and r where

$$p = \frac{\mu}{\sigma^2} \text{ and } r = \frac{\mu^2}{\sigma^2 - \mu} \tag{2.5}$$

and μ and σ are the mean and standard deviation. The probability mass function (which gives the probability that a random variable is exactly equal to some value) of the NB distribution is given by:

$$p(n_i = n) = \frac{\Gamma(r+n)}{\Gamma(r)n!} p^r (1-p)^n \quad n = 1, 2, \ldots \tag{2.6}$$

where Γ is the standard gamma function, $r>0$, and $0<p<1$. In this thesis, the NB distribution is used to describe the number of fractures in an interval, and the random NB variables represent the number of fractures in each borehole section.

2.2.2 Fracture set orientations

The orientation of a fracture is commonly defined by its inclination to the horizontal (dip) and its orientation with respect to north (strike) (Hoek & Brown 1990). Fractures are rarely randomly oriented in the rock mass. They frequently occur in fracture sets, which consist of groups of fractures with similar orientations, hydraulic apertures and similar aperture distributions (Hernqvist 2009). Fracture orientations can be graphically presented in stereographic projections. The most commonly used tool is according to Munier (2004) the stereonet (sometimes referred to as Schmidt net) where each strike/dip is represented as a point (pole) on a hemisphere stereogram, see Figure 2.1. Fracture sets can be identified as clusters of points in stereonets. Different contouring methods are used to facilitate the visual identification of fracture sets. One of the standard methods is the Kamb contouring method, which is based on the early work of Kamb (1959), e.g. Robin and Jowett (1986).

Information of the properties for different fracture sets can be obtained if fracture orientation and transmissivities are linked, for example by combining hydraulic tests in short sections with borehole mapping (Hernqvist 2009). Useful information about the fracture network can also be obtained if the fracture set orientations are linked to the fracture intensity, which gives separated fracture intensities for the existing fracture sets.

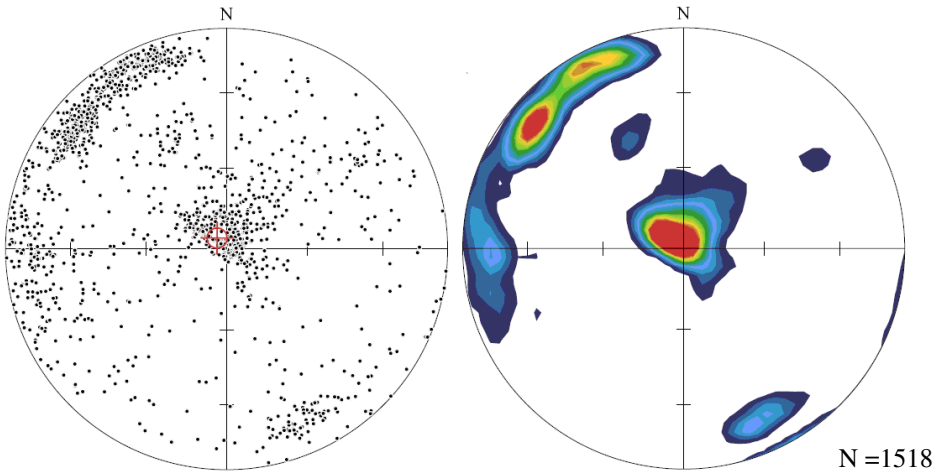

Figure 2.1 *Fracture data from the Forsmark site investigation visualized in a lower hemisphere stereogram (Munier 2004). Left: Projections of poles to fracture planes. Right: The same stereogram contoured according to the Kamb method.*

2.2.3 Fracture transmissivity distribution

The transmissivity of all fractures intersecting a borehole typically stretches over several orders of magnitudes, and normal measurement techniques are not able to identify the tightest fractures (Gustafson & Fransson 2005). Furthermore a measurement often straddles several fractures and this makes the assessments of individual fractures even more difficult. But the transmissivity of an interval is most likely dominated by its largest fracture, and this is used when estimating transmissivities. An approximate transmissivity distribution of individual fractures intersecting a borehole can be derived if section transmissivity data and the number of fractures per section are known.

In this thesis, two probability distributions are used to describe the distribution of transmissivities; the *lognormal distribution* and the *Pareto distribution*. The log-normal distribution is a probability distribution of a random variable whose logarithm is normally distributed. It usually gives a reasonable fit to the main part of the data, though there are large deviations for the largest transmissivity values (Gustafson 2009). The probability density function (PDF) of a lognormal distribution is:

$$F_x(x;\mu,\sigma) = \frac{1}{x\sigma\sqrt{2\pi}} e^{-\frac{(\ln x-\mu)^2}{2\sigma^2}}, \quad x > 0 \tag{2.7}$$

where μ and σ are the mean and standard deviation. The distribution is often presented as a cumulative distribution function, which expresses the probability that a measured value is less than or equivalent to a certain value:

$$p(T \le T_i) = \frac{n_i}{N+1} \tag{2.8}$$

If the data is truncated, i.e. values in the lower measurement interval are missing because of measurement limitations, some assumptions have to be made when

determining the distribution parameters. The first is that the geometric mean of the transmissivity is approximated to the median, $\mu_{geom} \approx T_{50}$. The second is that the standard deviation of the logarithm of T is calculated only using the upper interval; $\sigma_{lnT} \approx \ln(T_{84}/T_{50})$.

The other probability distribution used in the thesis is the Pareto statistical distribution. Gustafson and Fransson (2005) showed that estimated transmissivities obtained in the pre-investigation stage could be well described with the Pareto distribution. It is a feasible distribution because it describes sets of data with many small values and a few high values, and the majority of the fractures in crystalline rock have low transmissivities and only a small number of fractures have quite large transmissivities. The distribution parameters can be assessed with incomplete data. The Pareto distribution determines the probability that a transmissivity is below a certain transmissivity, based on the maximum fracture transmissivity value, T_{max}, according to equation (2.9):

$$P(T_n) = P[T < T_n] = 1 - \frac{(T_{\max} / T_n)^k}{N+1} \tag{2.9}$$

where T_n is the transmissivity with number n in sized-sorted sample of a total number of fractures, N. The parameters used in the distribution can for example be evaluated from detailed inflow measurements or fixed-interval water pressure tests. When rearranging and taking the log of equation (2.9), it gives:

$$\log[1 - P(T_n)] = \log[T_{\max}^k /(N+1)] - k \log(T_n) \tag{2.10}$$

The Pareto distribution is recognised as a straight line in a log-log plot with a slope, $-k$, which represents the coefficient of distribution. Fitting a linear trend-line to the dataset in a log-log plot by the least square method thus gives $-k$, see example in Figure 2.2.

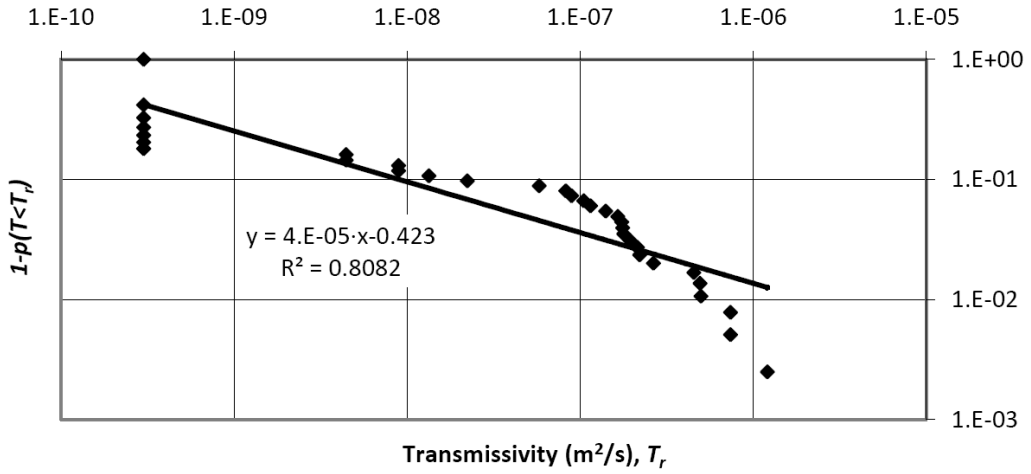

Figure 2.2 Example of an evaluation of Pareto distribution from fracture transmissivity data. From Butrón et al. (2009).

Then the transmissivity value, T_n, for each fracture in an interval can be generated as:

$$T_n = \frac{T_{\max}}{r^{(1/k)}} \tag{2.11}$$

where T_{max} represents the transmissivity of the largest fracture and r is the rank of a value in an ordered sample. The obtained distribution can also be used to evaluate the hydraulic aperture distribution. The hydraulic aperture is estimated with the cubic law, equation (2.2), and the aperture b_r of the fracture with rank r is then given as:

$$b_r = b_{\max} / r^{1/3 \cdot k} \tag{2.12}$$

Here, b_{max} is the hydraulic aperture of the largest fracture, which corresponds to the highest transmissivity observed.

2.2.4 Fracture length

The fracture length is of importance for the connectivity of the fracture network; if the fracture length is short in relation to the distance between the fractures, the network will not be well connected (Hernqvist 2009). Fracture length distributions are hard to determine, because it is not possible to directly measure fracture length in boreholes. But there is a relationship between the size of a fracture and its hydraulic aperture, see Vidstrand and Ericsson (2008), implying that dry fractures are generally short and fractures transmitting lots of water are long, see Figure 2.3. In-direct measurements of the fracture length can therefore be made from hydraulic tests.

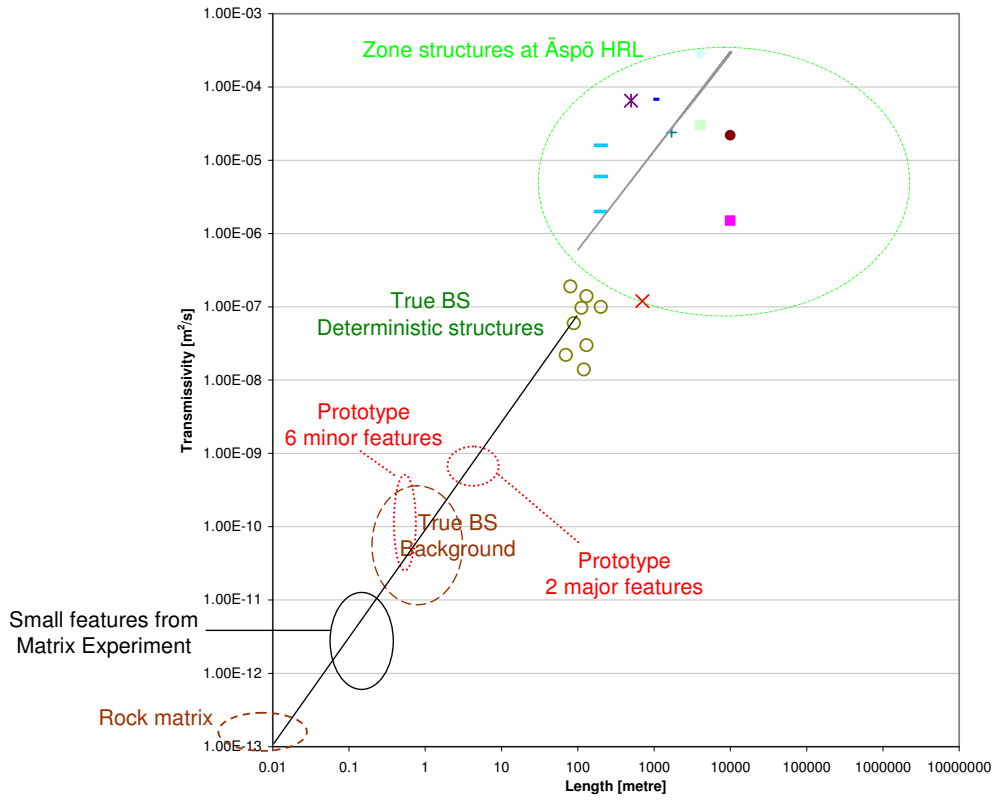

Figure 2.3 Proposed relationship between transmissivity and length for features at Äspö HRL. From Vidstrand and Ericsson (2008).

2.3 Flow dimensions

If there are few connected fractures in a rock mass, and most fractures are parallel to each other, the spread between fractures are small and flow is possible mainly in the dominating direction. But if the fractures have many different orientations and are well connected, there may be a substantial amount of spreading within the fracture network with flow in several directions. Two aspects of flow in rock fractures, also referred to as dimensionality, have been described by Hernqvist (2009). One aspect is the flow dimension, which relates to the flow within the fractures (e.g. channel flow or radial flow). Channel (1D) flow can be described as water moving linearly through fractures, along narrow channels. With radial (2D) flow, water spreads radially in a fracture plane, see Figure 2.4. If there are constrictions and channels within the fracture, the fracture flow will act as one-dimensional, whereas open wide fractures transmit radial two-dimensional flow.

The other aspect of flow in fractures is the fracture network dimension, which relates to the properties of the fracture network (sparsely connected or well-connected). A fracture system with no connected fractures gives a "no flow" situation. One dominating fracture set and sparsely intersecting fractures leads to a 2D fracture network with flow mainly possible in the dominating direction. At least two fracture sets deviating sufficiently will give a 3D fracture network, where spherical 3D flow is possible, with water spreading in several fractures connected in a network, illustrated in Figure 2.4.

Hernqvist (2009) concludes that there is a 3D fracture network if there are two or three deviating fracture sets in a rock mass (unless their fracture frequencies are too low), and a 2D fracture network if there is only one dominating fracture set and a few connecting fractures. But a 3D fracture network does not necessarily lead to 3D flow. The fracture intensity data need to be combined with information on transmissivity and hydraulic aperture, since if the connecting fractures are too tight to transmit water,

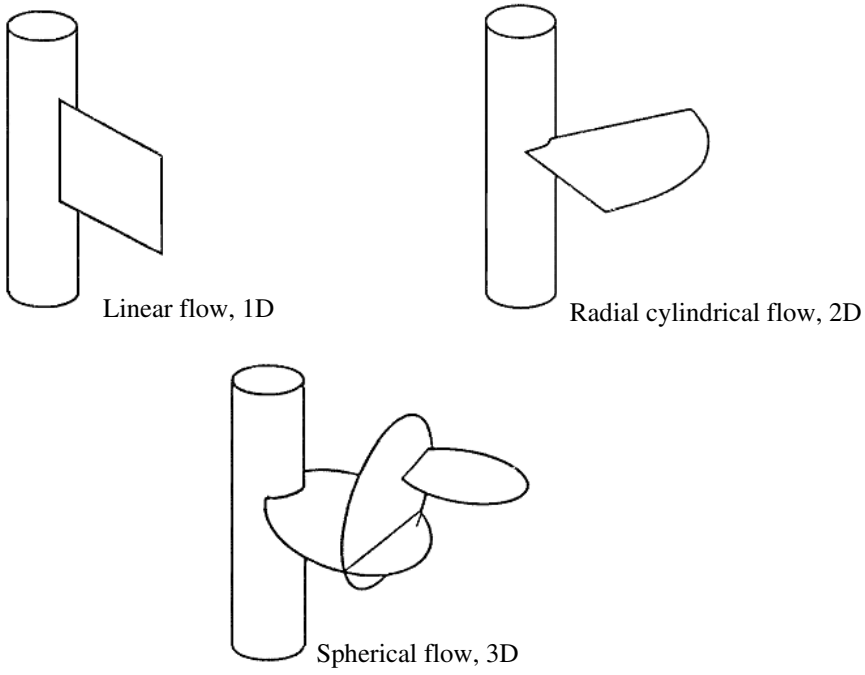

Figure 2.4 Spatial flow dimensions with flow in fracture(s) in each figure. Modified from Doe and Geier (1991).

the result will be 2D flow, irrespective of the fracture intensity. The fracture length is also of importance; fractures too short to intersect will contribute to low connectivity.

Fransson and Hernqvist (2010) suggest that the rock and its fracture zones can be described as Type I (2D flow) or Type II (3D flow) permeability structures. The suggested host rock of a Type I permeability structure mainly consists of one conductive fracture set with a fracture network that is not well connected. Here, a higher fracture frequency describes a fracture zone. Sealing of the zone could limit the flow in connected fractures and reduce the inflow more than estimated from inflow prognosis based on individual fracture apertures along boreholes. The host rock in a Type II permeability structure typically has more than one conductive fracture set and a well-connected fracture network (low RQD compared to a Type I rock). Also here the fracture zones are indicated by locally increased fracture frequency, but systematic grouting is probably required in order to achieve a desirable sealing of the fracture system.

2.4 Hydraulic tests

Hydraulic tests can be used to characterise the fracture system, though it requires a suitable performance, and interpretation (Fransson 2001). Short duration test represents local conditions, long duration tests are required for obtaining information on remote parts of the fracture network (Hernqvist 2009). The hydraulic tests described below are those used in the KBS-3H project: pressure build-up test, water pressure tests and water inflow measurements.

2.4.1 Pressure build-up test

A pressure build-up test can be used to determine the groundwater pressure, evaluate transmissivities and to estimate flow dimensions. A pressure build-up test consists of a flow phase with the duration t_p, and a recovery phase with duration t'. During the flow phase the tested borehole is kept open and undisturbed, and when the hole is closed, the recovery phase starts and the pressure build-up is measured.

The transmissivity can be evaluated from the recovery phase using Jacob's method. The method consists of plotting the pressure against the adjusted time, t_e, in a linear-logarithmic diagram. The adjusted time is estimated from the flow time, t_p, and the recovery time, t'. However, for very short recovery times ($t' << t_p$), the adjusted time can be approximated to the recovery time, $t_e \approx t'$ (Gustafson 2009). After plotting the data, a straight recovery line is fitted to the late time data points. The transmissivity is then evaluated using the following equation:

$$T = \frac{0.183Q}{\Delta s} \tag{2.13}$$

where Q is the inflow measured before the closure of the hole and Δs is the pressure increase, measured in metres, from time t to $10t$, represented by the slope of the recovery line in the lin-log diagram. From the diagram, the resting hydraulic head can be estimated by extrapolating the recovery line to the flow time, t_p (Gustafson 2009). By studying the shape of log-log plots of the recovery sequence, flow dimension of the test can be evaluated (Hernqvist 2009), see Figure 2.5.

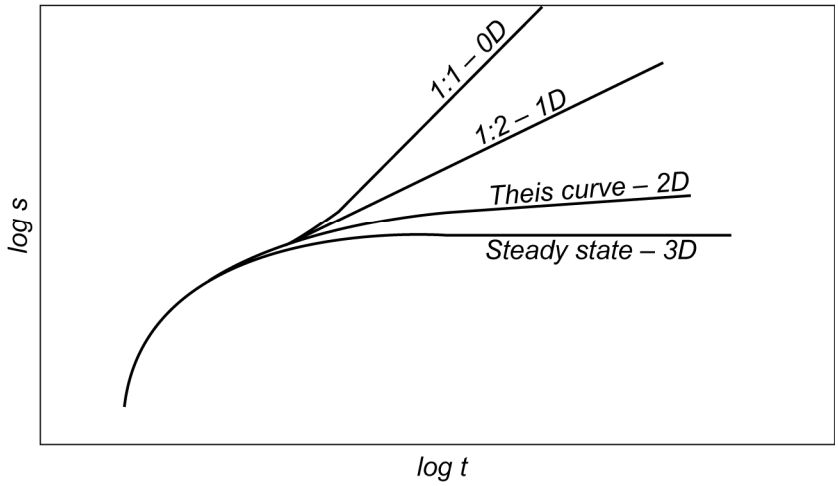

Figure 2.5 *Evaluation of flow dimensions. The pressure, s, during the recovery phase is plotted against time in a log-log diagram, and the shape of the curve determines the dimensionality. From Hernqvist (2009).*

2.4.2 Water pressure test and water inflow measurements

A water pressure test (also referred to as water loss measurement) is a short duration test, which is performed by injecting water into a section of a borehole. If the section used for the measurement is short compared to the fracture intensity, it is reasonable to assume one dominating fracture within the measured interval. The transmissivity from the water pressure test can then be evaluated using the Thiem well equation (2.3).

A water inflow measurement is also a short duration test where the flow of water from a borehole into the tunnel is measured. This will provide information about the fractures close to their intersection with the borehole (Hernqvist 2009). The transmissivity of the fractures, based on the measured inflow, can be estimated using a modified Thiems equation:

$$Q = \frac{2\pi \cdot T \cdot h}{\ln\left(\frac{2h}{r_w}\right)} \tag{2.14}$$

where Q is the water inflow, T is the transmissivity, h is the groundwater pressure head and r_w is the radius of the borehole (Eriksson & Stille 2005).

2.5 Grouting

Grouting, which is a method of sealing rock fractures by injecting grout into them, is used to control groundwater and reduce water inflow to underground structures. A successful grouting session is distinguished by a zone of sealed rock mass through which the groundwater flow is significantly reduced. The performance of the sealing is depending on properties of the fracture system, properties of the grout and the procedure of grouting (Fransson 2001). In practice, grouting is often performed by

drilling boreholes into the rock mass and inject grout under pressure until the fractures around the borehole are filled (Butrón et al. 2009). Most cement-based grouts can penetrate fractures with a hydraulic aperture down to 50-100 μm. If fractures with smaller hydraulic aperture are to be sealed, noncementitious grouts, such as silica sol, may be required.

Silica sol is a colloidal silica mixture, e.g. described in Funehag (2007). It is mixed with a saline solution prior to the injection to initiate a gelling process, which hardens the solution to a gel. The salt causes the particles to collide and form aggregates, which raises the viscosity of the grout. After a certain time, typically within a time range of ten minutes, the viscosity of the grout start to rise rapidly and the grout will stop spreading further.

2.5.1 Penetration of grout

As grout is injected into a borehole, it will spread through the fractures, see Figure 2.6. After a time t, it will have spread a distance, a penetration length I from the borehole, which is individual for each fracture (Gustafson & Stille 2005). Grout penetration lengths can not be exactly predicted, but estimations with analytical solutions can be made. The penetration length is an important parameter when making grouting designs to obtain sealing of intersecting fractures and achieve a grouted zone around a tunnel. The penetration in the smallest fracture necessary to seal should be sufficient, while the spread in the largest fracture should be acceptable.

The rheological properties of a grout, such as the viscosity and yield stress, governs its flow behaviour and hence its penetrability. In general grouting materials are described either as Bingham- or Newtonian fluids. A cementitious grout can be described as a Bingham fluid, where the cement particles have a significant influence on the rheology, and silica sol is characterised as a Newtonian fluid before gelling. The penetration of a Bingham fluid, such as cementitious grout, into a fracture with a hydraulic aperture b are related to the applied pressure difference, Δp, and the initial yield strength of the grout, τ_0 (Gustafson & Stille 2005).

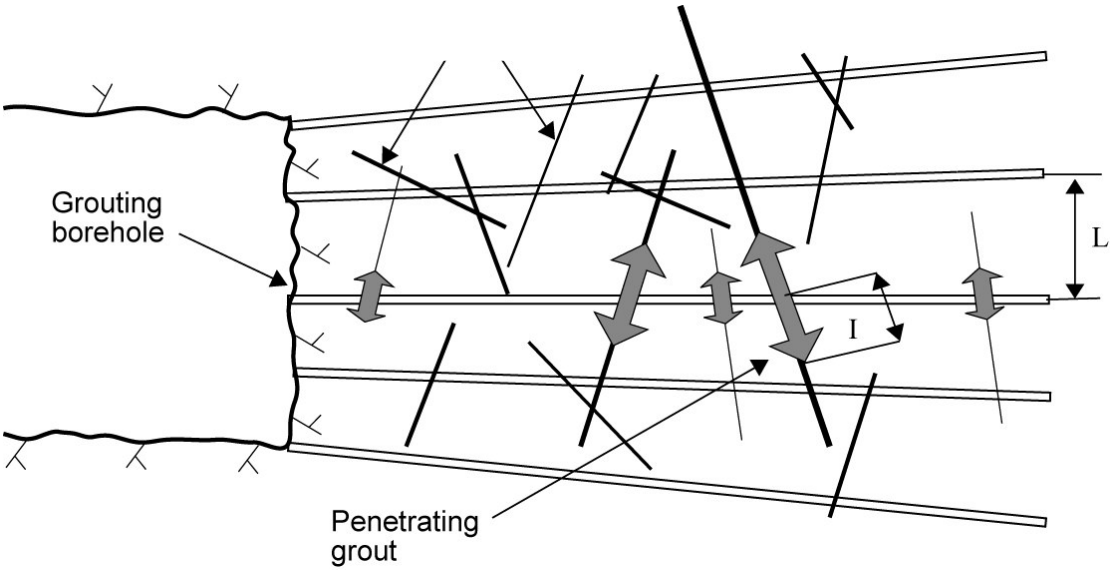

Figure 2.6 Grouting penetration with borehole distance L and penetration distance I. Figure after Gustafson and Stille (2005).

The maximum penetration length at steady state can be calculated as:

$$I_{\max} = \left(\frac{\Delta p}{2\tau_0} \right) \cdot b \tag{2.15}$$

But it takes in principle an infinite time to reach the maximum penetration and the relative penetration, I_D, which is dependent on the time spent grouting is more interesting. I_D is the same in all fractures cut by a borehole and can be expressed as a function $I_D(t_D)$ of the relative grouting time $t_D=t/t_0$, where t_0 is the characteristic grouting time (Gustafson & Stille 2005, Stille et al. 2009):

$$t_0 = \frac{6\Delta p \cdot \mu}{\tau_0^2} \tag{2.16}$$

The relative penetration can then be expressed as:

$$I_D = \sqrt{\theta^2 + 4\theta} - \theta \tag{2.17}$$

where θ are given for the 1D and 2D cases respectively as:

$$\theta_{1D} = \frac{t_D}{2(0.6 + t_D)} \tag{2.18}$$

$$\theta_{2D} = \frac{t_D}{2(3 + t_D + 0.23\ln(t_D))} \tag{2.19}$$

Finally, the actual penetration length is given by:

$$I = I_D \cdot I_{\max} \tag{2.20}$$

The penetration of a Newtonian fluid such as silica sol into a fracture is dependent on the gel induction time, t_G, defined as the time taken for the initial viscosity to double, the applied pressure difference, Δp, and the initial viscosity, μ_0 (Funehag 2007). The maximum penetration length will be obtained after approximately $1.5 \cdot t_G$. The maximal radial penetration length of silica sol in a fracture can be described by equation (2.21) and the maximal linear penetration with equation (2.22).

$$I_{2D} = 0.45 \cdot b \cdot \sqrt{\frac{\Delta p \cdot t_G}{6 \cdot \mu_0}} \tag{2.21}$$

$$I_{1D} = b \cdot \sqrt{\frac{\Delta p \cdot t_G}{6 \cdot \mu_0}} \tag{2.22}$$

2.5.2 Use of grouting data for dimensionality analysis

The spread of grout is governed by several complex relations, and the sealing of fractures can not be directly measured during grouting (Gustafson & Stille 2005). But data from the grouting can, with semi-empirical relations, be used to interpret the penetration and the dimension of flow in the fracture system, and thus give a better understanding of the water-conducting structures in the rock mass. Gustafson and Stille (2005) developed a dimensionality analysis in which flow dimensions (1D or 2D) during grouting can be evaluated. A 1D (channel) or 2D (radial) flow system gives two different scenarios of grout volume penetration. The slope value of a curve describing the relative volume of grout as a function of relative grouting time can thus be used to determine the flow regime. No assumptions of fracture apertures or the number of fractures are required in order to make an analysis of the dimensionality of the flow system. By using data of pressure, volume and time (PVT) recorded by the grouting equipment, the slope value can be described as:

$$\frac{d\log V}{d\log t} = \frac{Q \cdot t}{V} \tag{2.23}$$

where Q is the momentaneous grout flow, t is the time and V is the accumulated grout volume. If $Q \cdot t/V$ is plotted against t_D, which is the relative grouting time, flow dimensionality can be determined according to Table 2.1 (Butrón et al. 2009). The slope values for 1D and 2D are approximately the same for cement grout and silica sol.

Table 2.1 Slope value from dimensionality analysis and corresponding flow regime. From Butrón et al. (2009).

***(Q·t)/V* (approximate value)**	**Flow regime**	**Denotes**
0.45	1D	Channelled fracture system
0.8	2D	Radial flow, planar fractures
1 or higher	3D	Spherical flow, fracture network system

2.6 Fracture network modelling

The purpose with fracture network modelling is to create a representative description of the fracture network within a specified rock mass. Fracture network modelling often starts with estimations of the fracture network geometry, based on observed field data, in order to generate a Discrete Fracture Network (DFN) model that reproduces the observed geometry properties. A DFN model is a discontinuum model, where the rock mass is represented by a set of rock blocks separated by fractures (Starzec 2001). Fractures can be divided into sealed fractures, open fractures or partly open fractures. It is assumed that open (and partly open) fractures form potential conduits for groundwater flow, but their connectivity and transmissivity determines if it is actually possible.

Generally, it is not practically possible to determine all properties of each fracture. Then conceptualization and a statistical approach are needed to provide a bridge between measurement results and the representation of the fractures. In DFN-models,

it is possible to combine deterministic fractures with statistically generated fractures (Cox et al. 2005). In this thesis a deterministic approach was applied, and the obtained geometrical model only contains deterministic fractures which are based on field data, such as borehole logging, fracture mapping and hydraulic tests. With information of fracture orientations from drill cores and tunnel mapping, the position of fractures along the tunnel can be determined and visualised in a visualisation programme, for example RVS (Rock Visualization System).

3 The horizontal drifts at Äspö HRL

The Äspö Hard Rock Laboratory is located on the Äspö Island, near the Simpevarp nuclear site in the province of Småland, see Figure 3.1. The underground part of the laboratory consist of a 3600 m long tunnel, which goes from the Simpevarp peninsula to the southern part of Äspö where it continues in a spiral down to a depth of 450 m.

The study area is located in the Precambrian Fennoscandian Shield. The bedrock in the Äspö-Simpevarp region is dominated by intrusive rocks from the Transscandinavian Igneous Belt (TIB), comprising gabbroid-dioritoid-syenitioid-granite rocks, formed approximately 1800 million years ago (Forssberg et al. 2005). Younger rocks, such as dolerite dikes and granitic plutons are also encountered within the region. The dominant rock types at Äspö are Ävrö granite and Äspö diorite. The Ävrö granite is a grey to greyish red, finely medium-grained granite and Äspö diorite is a dark grey to greyish red, fine medium-grained granodiorite (to quartz monzodiorite), generally with megacrysts of microcline (Berglund et al. 2003). Fine-grained granitic or aplitic dykes are locally occurring quite frequently, as well as mafic rocks.

The KBS-3H demonstration project is located at the –220 m level at Äspö HRL. The niche at the level, NASA1623A was enlarged to about 25×15×7.5 metres (length×width×height) in 2003 and exploration drilling for the horizontal drifts was performed. Grouting of the core boreholes was carried out during the first part of 2004. The two horizontal demonstration drifts, with a diameter of 1.85 m and 15 m respectively 95 metres long, were excavated in 2004 and 2005. The longer drift was post-grouted in five positions in 2007 and 2008 using Mega-Packer equipment and silica sol as grouting material. The different steps of the KBS-3H project at Äspö HRL is presented in detail on the following pages.

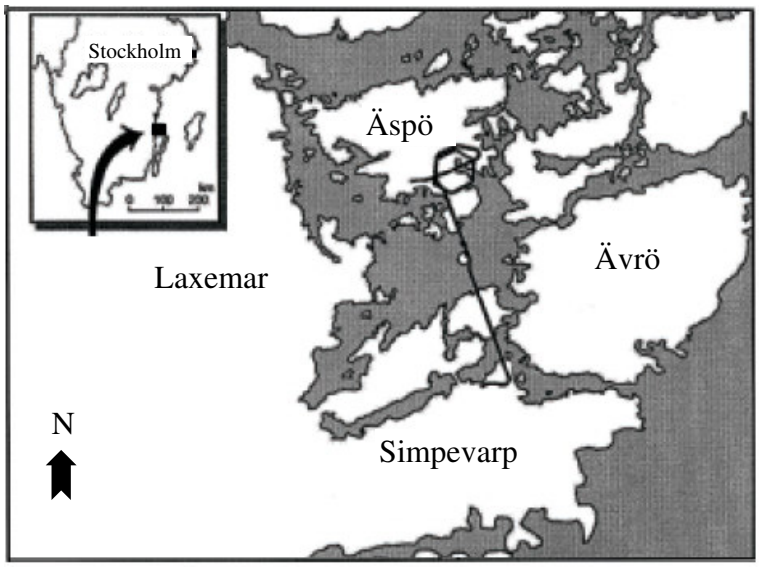

Figure 3.1 Location of the Äspö Island and the Hard Rock Laboratory. Modified from Rönnback (2005).

3.1 Site pre-investigation with core-drilled boreholes

The site investigation prior to the excavation of the demonstrations drifts included core drilling of three boreholes. Two of them were 30 m long and 56 mm in diameter (KA16*16*A01 and KA16*21*A01) and the third one was 100 m long with a diameter of 76 mm (KA16*19*A01), see Figure 3.2. The bearing of the boreholes are 254.9°, 270° and 284.4°. These boreholes have been mapped with respect to lithology, structures and fractures, and hydraulic testing was performed to characterise water-conducting zones at the site. The three boreholes were grouted and a control hole, KA16*19*A02 was drilled to evaluate the performance of the grouting sessions. The purpose of the grouting was to seal larger water-conducting fractures before excavating the horizontal deposition drifts (Johansson 2005).

The site investigation scheme with hydraulic testing was as follows:

1. Core drilling of KA16*16*A01, KA16*21*A01 (∅56 mm, 30 m long) and KA16*19*A01 (∅76 mm, 100 m long).

2. Inflow measurements in all boreholes, taken every third meter during core drilling. A total of 7 large inflow sections were found in the holes, ranging from 0.45 to 30 l/min per 3 m-section.

3. Water pressure tests in five-meter sections, carried out with a pressure of 1.0 MPa over the groundwater pressure, which was 1.55 MPa. Measurements in the two 30-metres boreholes were carried through without complications, but the choice of packer for the larger 100-metres hole was incorrect and the testing was stopped without a complete hydraulic testing of KA16*19*A01.

4. Grouting of the boreholes, using a cementious grout. The two shorter boreholes were grouted in full length (30 m) and the longer hole was grouted in three sections; 70-100 m, 35-70 m and 0-35 m.

5. Drilling of control hole KA16*19*A02 (∅76 mm, 96 m long) close to KA16*19*A01.

6. Water pressure tests in five-meter sections along the control hole.

7. Grouting of control hole KA16*19*A02 with a cementious grout in three sections; 70-100 m, 35-70 m and 0-35 m.

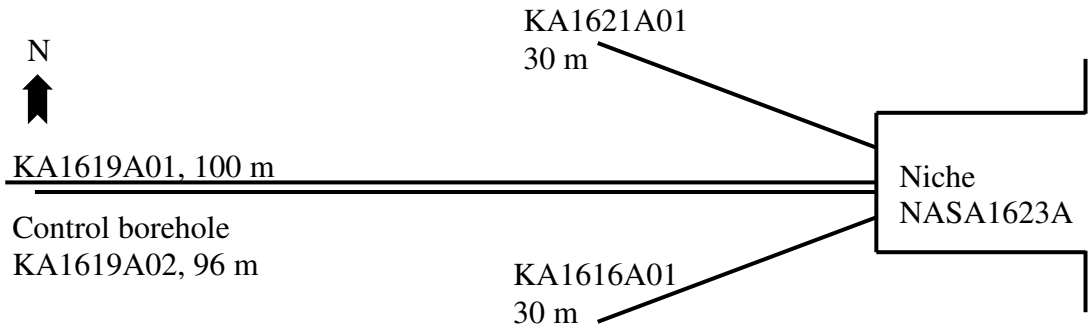

Figure 3.2 Top view of boreholes. Modified from Nordman (2003).

3.2 Pilot hole drilling and reaming of drifts

The excavation of the full-size, 1.85 m horizontal drifts was carried out by horizontal push-reaming, which included an excavation of a pilot hole, followed by reaming to full diameter with quite conventional raise-drilling equipment (Bäckblom & Lindgren, 2005). Two drifts were excavated, (see positions in Figure 3.3) one for demonstration of the emplacement process and evaluation of the deposition equipment and one for the testing of low-pH shotcrete plugs. The longer drift, DA1619A02, is 94.45 metres long and the shorter drift, DA1622A01, is 15.85 metres long. The longer drift was planned to be 100 metres long, but during the preceding core drilling, a significant water inflow of 30 litres per minute occurred at about the length 100 m and to avoid high water inflow, it was decided to only excavate 95 metres.

Two different hole diameters were used for the pilot drilling, 152 mm and 279 mm. The pilot hole for the 15 m drift had a diameter of 279 mm. The excavation of the 95 m drift started with the drilling of a 152 mm pilot hole, which was going to be reamed to 279 mm before excavating the 1.85 m drift. But the 152 mm hole failed and was abandoned after 19 meters. A new pilot hole, ∅ 279 mm, was drilled instead. Full-length inflow measurements were performed in the pilot holes and after reaming the drifts.

The drift excavation sequence, including the hydraulic tests, was as follows:

1. Drilling pilot hole (∅279 mm) for the 15 m drift.

2. Reaming of the 15 m drift (∅1.85 m), followed by inflow measurements.

3. Drilling of pilot hole (∅152 mm) for the 95 m drift that was abandoned after 19 m.

4. Drilling of a new pilot hole (∅279 mm) for the 95 m drift, full-length inflow measurements in the new pilot hole.

5. Reaming of the 95 m drift (∅1.85 m), inflow measurements.

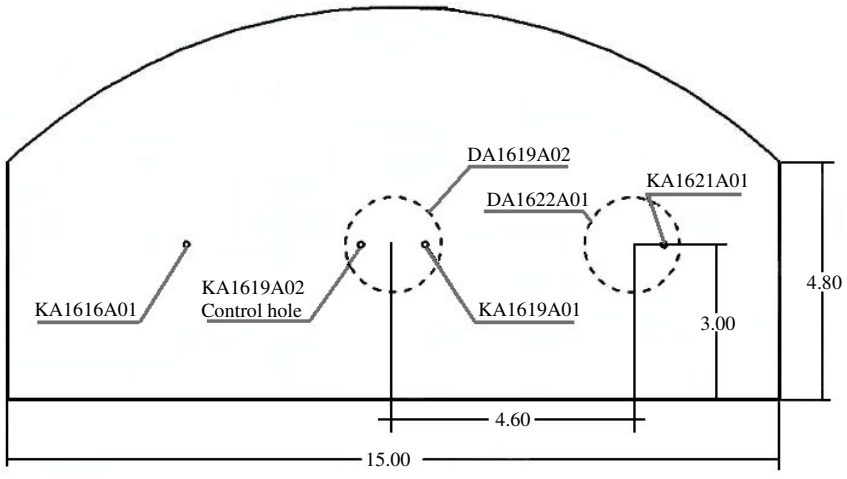

Figure 3.3 Section showing the emplacement of core boreholes, control hole and drifts in the niche at the 220 m level at Äspö HRL.

3.3 Mega-Packer post-grouting project

The Mega-Packer post-grouting project was performed to validate Mega-Packer as a potential grouting method and to fulfil the requirements set up regarding water leakage after grouting (Eriksson & Lindström, 2008). The longer drift, DA1619A02 was used in the post-grouting test and the shorter drift, DA1622A01 was used for studying changes in groundwater inflow when the longer drift was grouted. The Mega-Packer can be seen in Figure 3.4, the construction is in detail described in Eriksson and Lindström (2008).

A total of five inflow positions relevant for the post-grouting study were identified. The drift was hydraulically characterised in order to create a base for the grouting design and to be able to evaluate the grouting effect. The characterisation included hydraulic testing of the five selected positions in the drift, before and after grouting (pre- and post-characterisation) and the test programme included water pressure build-up test, water inflow measurement and water pressure test. The post-characterisation consisted of measurements of water inflow after the grouting was performed in all positions.

The grouting of the five positions in the drift was performed in two stages, with a total of seven grouting sessions. Grouting was done with silica sol in all sessions. A principal sketch of the drift and the arrangement of the grouting sessions are shown in Figure 3.5. The first stage, in which position 3 and then position 1 was grouted, was carried out in November 2007. Position 3 was grouted twice, due to problems in the first session. After grouting these two positions, a break was taken. Positions 2, 4 and 5 had new pre-characterisations in March 2008, during the continuation of the grouting sessions. The second grouting stage started at position 5, but due to miscalculations of time and pressure, the grouting was unsuccessful. It took longer time to fill the hoses and the gap than calculated and the gelling had proceeded too far when the actual penetration into the rock could start. The next grouting session was position 4 followed by position 2. Before making a second grouting session of position 5, another hydraulic pre-characterisation was made.

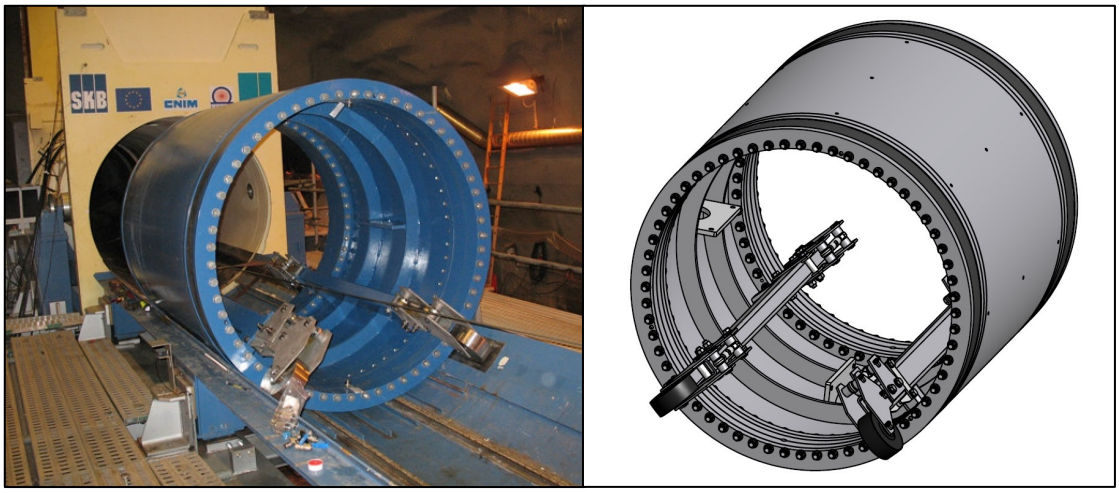

Figure 3.4 The Mega-Packer and a sketch of it (Eriksson & Lindström 2008).

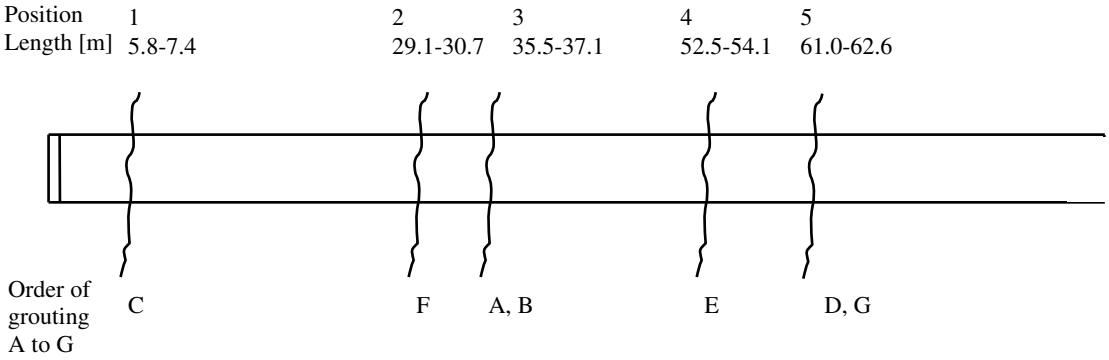

Figure 3.5 Principal sketch of drift DA1619A02 and the order of the seven grouting sessions. After Eriksson and Lindström (2008).

The different stages in the grouting project with its hydraulic tests are presented below:

1. Measurements of the total inflow to the drift.
2. Hydraulic pre-characterisation of the five selected positions.
3. Grouting of position 1 and 3.
4. New measurement of the total inflow to the drift.
5. Pre-characterisation of position 5 followed by an unsuccessful grouting.
6. Pre-characterisation of position 4 followed by grouting.
7. Measurement of the total inflow to the drift.
8. Pre-characterisation of position 2 followed by grouting.
9. Measurement of the total inflow to the drift.
10. A new pre-characterisation of position 5 followed by the last grouting session.
11. Inflow measurements in all positions, and in the whole drift.

3.4 Characterisation of the fracture network

This characterisation aims at describing the local hydrogeological conditions of the rock surrounding the horizontal drifts, based on the investigations performed at the different stages of the KBS-3H project in Äspö HRL at level 220. The characterisation thus considers data from the pre-investigation, the reaming of drifts and from the post-grouting project. It will mainly consist of new evaluations of data, but compilations of previously performed evaluations have also been made.

The main focus of the characterisation is to achieve a better understanding of the fracture network with investigations of fracture properties and flow dimensions in the fractures. The parameters evaluated are:

- Transmissivity and hydraulic aperture, which describes the ability for a fracture to transmit water. T and b are obtained from hydraulic tests.

- Fracture intensity (P_{10} and P_{21}), which is important for the connectivity between fractures. P_{10} is determined from the core mapping and P_{21} from the mapping of the drift where there are fracture length data.

- Fracture orientations, which are important for the geometry of the fracture network. The orientations are determined from the fracture mapping.

- Flow dimensions in fractures, which is related to the contact areas within the fractures. The flow dimension is determined from pressure build-up tests and flow/time/volume relationships during injection of water and grout.

The analysis of the pre-investigation data are based on core mapping, inflow measurements and water pressure tests conducted in the boreholes at the site, presented in Nordman (2003) and an unpublished report by Johansson (2005). The analysis includes evaluations of open fracture frequencies, fracture orientations, transmissivities, hydraulic apertures and the distributions of these.

The analysis of the drifts have been based on mapping of the drifts, full-length inflow measurements, and the hydraulic characterisation of five positions in the long drift, performed during the post-grouting project. It considers fracture frequencies and locations of water-conducting fractures, transmissivities, apertures and flow dimensions. The hydraulic tests used were all short duration tests and they provided information about the fractures close to their intersection with the borehole.

3.4.1 Geological conditions

The cored boreholes were examined with the Boremap method, which combines information taken from the cores with information from BIPS (Borehole Image Processing System) images. All orientations are given in coordinate system Äspö96. A conclusion made from the core mapping was that the rock in the area is sound with what Nordman (2003) describes as few open fractures. The rock surrounding the horizontal drifts has been characterised as typically homogenous with generally hard rock, some zones of extremely hard rock, and parts with layers of narrow weak zones. About 90% of the rock mass is identified as sparsely fractured (with a RQD of 100), the rest has a RQD ranging from 65 to 99.

The most common rock type in the drift is the Äspö diorite, which is intruded by several dykes or veins of red, fine-grained granites and coarse-grained pegmatite showing same sets of orientations: 235/85-90° and 335/60°. Also occurring is the Ävrö granite and several small xenoliths of greenstone (Bäckblom & Lindgren 2005). The drifts were mapped in the spring of 2005 with focus on rock types, fracturing and water inflow. The results from the mapping of rock types in the drifts were mainly consistent with the mapping of the cored holes. The Ävrö granite occurs in the 95 m drift as large, irregular bodies or as small fragments. Two large bodies occur between 36-49 m and between 61-79 m. The latter is strongly faulted by traversing fractures at 62, 71 and 75 m.

3.4.2 Fractures and fracture intensity

There were no observations of crushed zones in any of the boreholes, though two sections with higher frequency of open fractures were observed in KA16*19*A01 (at 29 m with 8.2 fr/m and 35 m with 14 fr/m). The boreholes had relatively few natural open fractures; the intensities of open fractures along the whole lengths of the three boreholes have been calculated to 1.1, 0.7 and 0.7 fr/m for KA16*19*A01, KA16*16*A01 and KA16*21*A01 respectively (see Table 3.1). The total fracture intensity, P_{10}, is 1.8 fr/m (not Terzhagi corrected data). This can be compared with an observed intensity of natural fractures of 2.3 fr/m in KLX 02 (Andersson et al. 2002). KLX 02 is a 1,700 metre deep subvertical borehole, located in the Laxemar area, to the west of the Island of Äspö.

Table 3.1 Fracture intensity (P_{10}) of the cored boreholes. Based on core mapping in 2003.

Borehole	Total: all fractures	P_{10} [fr/m]	Total: open fractures	$P_{10,open}$ [fr/m]
KA16*19*A01(100 m)	190	1.9	114	1.1
KA16*16*A01 (30 m)	52	1.7	22	0.7
KA16*21*A01 (30 m)	44	1.5	20	0.7

A fracture frequency diagram presenting the frequency of fractures along all 3 m-sections in the core boreholes is shown in Figure 3.6. The calculated average is 5.4 fractures per each 3 m long section, but the variance for the data set is high, over 24. A negative binomial distribution is fitted to these data with the maximum-likelyhood-method (see Gustafson 2009), which is represented by the black line, all illustrated in Figure 3.6. In Figure 3.6 also borehole KLX 02 is shown, whose fracture frequency was evaluated in Kozubowski, Meerschaert and Gustafson (2008). It had a total of 45 3 m-sections. As can be seen below the fracture frequency from the two data sets are following a reasonably similar NB-distribution, with the parameters being $p = 0.22$ and $r = 1.5$ for the boreholes at the KBS-3H site and $p = 0.25$ and $r = 1.9$ for KLX 02.

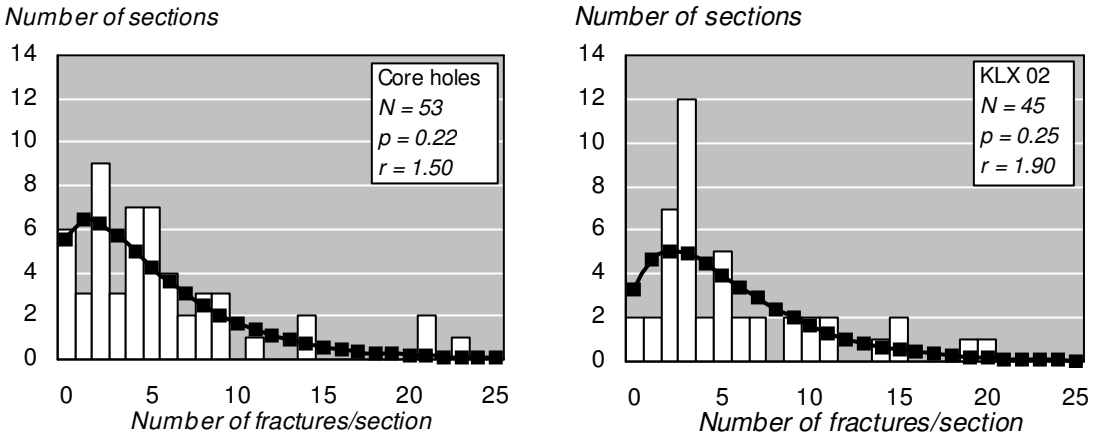

Figure 3.6 Frequency diagrams with negative binomial distributions fitted to the data (black line). Left: Frequency of fractures in 53 3 m-sections from the three core boreholes at the KBS-3H site. Right: Frequency of fractures in 45 3 m-sections from the KLX 02 borehole at Äspö.

The mapping of the drifts showed that the rock mass is generally sparsely fractured, with in average six fractures per meter. A thin shear zone with closed fractures occurs 7 m into the 15 m drift. The zone is sealed, but open water-conducting fractures are present in the proximity. These fractures have the same orientation as the water-conducting fractures found 6 m into long drift (about 340/60-70º). Since the distance is around five meters between the two drifts, it is probable that these fractures belong to the same fracture planes. Other weak zones with quite steep fractures that traverses the 95 m-drift perpendicular or in steep angles have been identified at 29 m, 62 m, 86 m, 88 m and 90 m. The two other prominent groups of fractures are sub-horizontal fractures, and short fractures in several directions.

There is no information about open fractures in the drift, but water-conducting fractures were mapped after the excavation in 2005, with appearance ranging from occasional drops or patches of moisture to flow. A total of 92 fractures were found to be water-conducting in the long drift (15 %), of these seven fractures were noted to have seepage or flow (1 %). Five of these were later post-grouted in the Mega-Packer-project. In borehole KLX 02 was, as a comparison, the observed intensity of water-conducting fractures 14 % (Andersson et al. 2002).

The water conducting fractures were also divided into 3 m-sections from which fracture frequency per section was derived, see Appendix B. The calculated average is 3.4 water-conducting fractures per 3 m-section, but also here the variance is large, with clustering of water-conducting fractures around zones. Since the length of the majority of the fractures are mapped, the fracture intensity P_{21} (total length of fracture trace per unit area) is evaluated for the drifts, see Table 3.2. P_{21} and P_{10} are both scale-independent and should be the same after Terzhagi correction according to Hernqvist (2009). The P_{10} data is however not Terzhagi corrected. The P_{21}-value for the long drift is though close to the P_{10} observed in KLX 02 (Andersson et al. 2002).

Table 3.2 Surface intensity (P_{21}) of the drifts. Based on the drift mapping in 2005.

Drift	Area [m^2]	All fractures	Tot. length all fr. [m]	P_{21} [m/m^2]	Water-cond. fractures	Total water fr length [m]	$P_{21,water}$ [m/m^2]
Long drift (95 m)	550	591	1301	2.4	92	306	0.6
Short drift (15 m)	90	101	189	2.1	33	52	0.6

3.4.3 Fracture set orientations

The oriented fractures along the core boreholes have been visualized in stereographic equal-area projections (stereonets), created in the software GeoPlot. A stereonet showing the open fractures can be found in Figure 3.7. Nordman (2003) observed two fracture sets in the mapping data, 310/80-90˚ and 025/80˚. The main direction of open fractures is 310/80-90˚ which also is almost the same direction as the main stress direction at Äspö HRL. There are also indications of a set with almost horizontal fractures, these are probably underrepresented due to the orientation of the boreholes (the data set is not Terzaghi corrected).

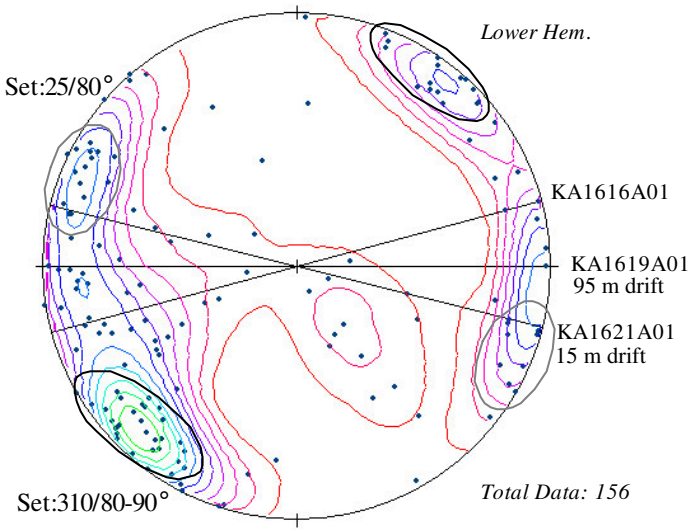

Figure 3.7 Fracture orientation of the open fractures mapped in the cored boreholes in 2003. (N=156)

The fractures belonging to the interpreted fracture sets have a tendency of occuring in clusters along the boreholes. The correlation between the fracture sets were calculated to investigate if there are any tendencies that the two fracture sets occur at the same positions. To determine the correlation, the holes were divided into 5 m-sections, and the number of fractures from each fracture set, observed within these 5 m-intervals were calculated. Then the correlation coefficient ρ was calculated. The correlation coefficient can vary between -1 and 1, describing a complete negative or positive linear relationship. If the sets are completely independent, the coefficient is 0. The resulting correlation coefficient for the two sets are -0.21, which is a quite weak relationship with a tendency that the sets does not occur in the same sections.

The fractures mapped in the drifts have also been visualized in stereographic projections, see Figure 3.9. Generally the vertical fracture sets found in the core boreholes are also represented in the drift, the sub horizontal set is though much more distinct in the drift because of a larger part of the rock is exposed. From the stereonet, it can also be noted that most fractures fall into sets which are in line with the mapping performed in the whole Äspö HRL (Rhén et al. 1997), see Figure 3.8.

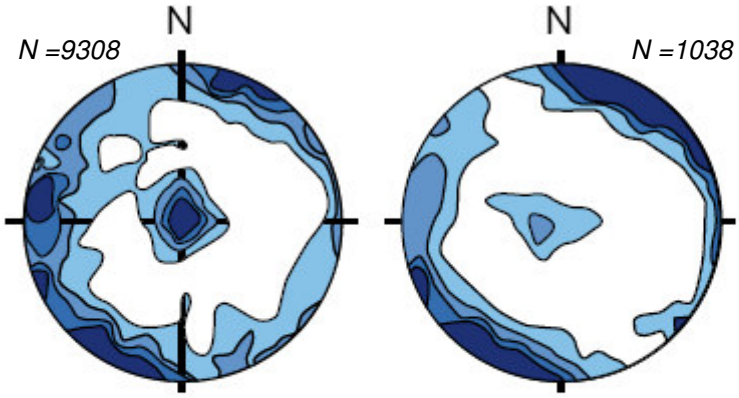

Figure 3.8 Stereoplots of left: all fractures; right: water-conducting fractures. Data from the access tunnel at Äspö HRL (Rhén et al. 1997)

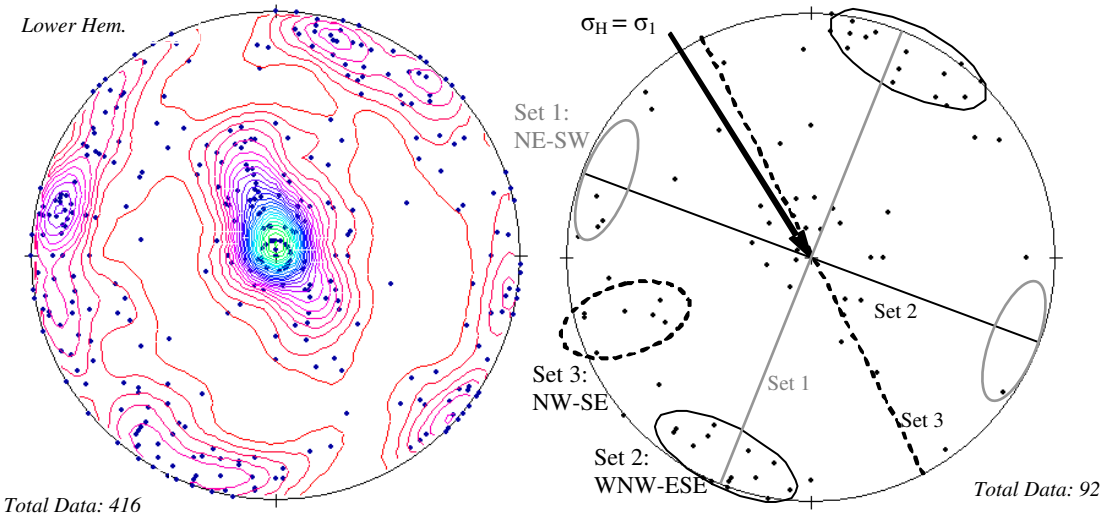

Figure 3.9 *Stereo plots showing the orientation of fractures along the two drifts. Left: All mapped fractures with orientation (N=416). Right: Water-conducting fractures (N=90), with interpretation of fracture sets and orientation of maximum principal stress at Äspö HRL.*

However, not all of the distinct fracture sets from the plotting of all fractures are well represented in the plot with only water-conducting fractures. There are a limited number of fractures mapped, but it could be that some fracture sets are generally not conductive. For example three of the inflow section post-grouted in the drift (position 1, 2 and 4) are belonging to a NW-SE set (Set 3 in Figure 3.9), and the major inflow position at 99 m in the core borehole was also from fractures belonging to this set. This coincides with the mapping performed of fractures at Äspö HRL. There is according to Talbot and Sirat (2001) an anisotropic hydraulic conductivity in the Äspö rock mass, which causes some fracture set to be active groundwater flow pathways; whereas some fracture sets are much less conductive. This is assumed to be a result of the in situ stress field at Äspö, where the horizontal maximum stress is orientated NW. The fractures that are water-conducting are mainly those held open by the current stress field. Set 3 in Figure 3.9 are most likely dilated by the current stresses, and fractures belonging to set 2 are reactivated as shear fractures (Figure 3.10). The same stresses reduce and close the apertures of fractures belonging to unfavourable orientations, such as fractures belonging to the NE-SW oriented Set 1. This anisotrophic conductivity at Äspö is further described by Rhén et al. (1997).

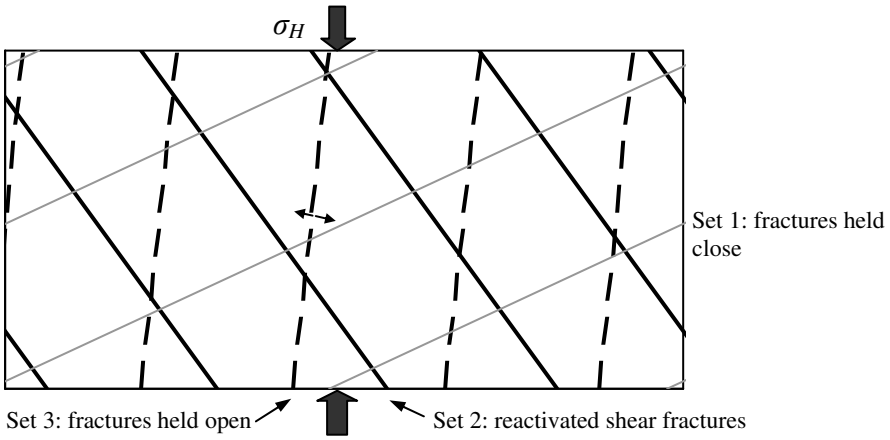

Figure 3.10 *Orientation of the largest horizontal stress, together with fracture sets.*

3.4.4 Transmissivity distribution based on the pre-investigation

The water pressure tests (WPTs) conducted in the boreholes consisted of pressuring water in five meters long sections at 1 MPa of constant over-pressure. The measurement limit for the WPT test equipment is unknown, but the smallest measured value was around 0.04 Lugeon per five meter section, which corresponds to a fracture with a transmissivity of $2 \cdot 10^{-8}$ m^2/s. The inflow measurement was performed every third meter during the drilling, and the smallest recorded inflow was around 0.4 l/min, which corresponds to a section with a transmissivity of $6 \cdot 10^{-8}$ m^2/s.

The results from the inflow- and water pressure tests have been used to estimate the transmissivity of sections in the boreholes, and further on evaluate hydraulic apertures. For estimations based on inflow measurements, equation (2.14) was used and for the water pressure tests, Thiem's equation was applied (2.3). The specific capacity, *Q/dh*, was also evaluated from the inflow measurements. The hydraulic apertures were estimated with the cubic law, equation (2.2). Table 3.3 presents the resulting transmissivities and apertures based on inflow measurements, the estimated values based on the water pressure tests can be found in Table 3.4.

Table 3.3 Resulting transmissivities and hydraulic apertures based on inflow measurements in 3 m-sections.

Borehole [-]	**Section [m]**	**Flow [l/min]**	***T* (Eq. 2.14) [m^2/s]**	***b* (T) [μm]**	***Q/dh* [m^2/s]**	***b* (*Q/dh*) [μm]**
KA162*1*A01	21-24	1.3	$2.04 \cdot 10^{-7}$	69	$1.37 \cdot 10^{-7}$	60
KA16*16*A01	3-6	11	$1.72 \cdot 10^{-6}$	140	$1.16 \cdot 10^{-6}$	123
KA16*19*A01	6-9	0.65	$9.85 \cdot 10^{-8}$	54	$6.85 \cdot 10^{-8}$	48
	45-48	0.45	$6.82 \cdot 10^{-8}$	48	$4.75 \cdot 10^{-8}$	42
	57-60	24	$3.64 \cdot 10^{-6}$	180	$2.53 \cdot 10^{-6}$	159
	84-87	5	$7.57 \cdot 10^{-7}$	107	$5.27 \cdot 10^{-7}$	95
	96-100	30	$4.54 \cdot 10^{-6}$	194	$3.16 \cdot 10^{-6}$	172

Table 3.4 Resulting transmissivities and hydraulic apertures based on water pressure tests in 5 m-sections.

Borehole [-]	**Section [m]**	***Q* [l/min]**	***T* (Eq. 2.3) [m^2/s]**	***b* (T) [μm]**
KA162*1*A01	20-25	1.2	$1.49 \cdot 10^{-7}$	62
KA16*16*A01	0.5-5	0.4	$4.98 \cdot 10^{-8}$	43
	5-10	0.8	$9.96 \cdot 10^{-8}$	54
	20-25	2.2	$2.74 \cdot 10^{-7}$	76
	25-30	1.8	$2.24 \cdot 10^{-7}$	71
KA16*19*A01*	90-95	0.2	$2.49 \cdot 10^{-8}$	34
	95-100	19.2	$2.39 \cdot 10^{-6}$	157

*No water-water pressure tests were performed between 0 and 90 m

The correlation between the aperture based on inflow measurements and the aperture based on WPTs is somewhat weak. In Figure 3.11, the two series of apertures from the corresponding sections are compared. The main reason for the weak correlation is the fact that some sections had fractures with no inflow, but it was possible to inject water into them. This could be an indication of open fractures with no connections to the water-conducting fracture network. In the three sections with inflow there are though fairly good agreements in the magnitude of the apertures based on WPT and inflow. This even though different measurement techniques, section lengths and evaluation techniques were used.

The fracture intensity of open fractures along 3 m-sections in borehole KA16*19*A01 and the evaluated transmissivities based on inflow measurements from the tested intervals are compared in Figure 3.12. From this comparison, it can be noted that high fracture intensity does not always generate an inflow, although the possibility of an inflow increases in sections with a larger number of fractures.

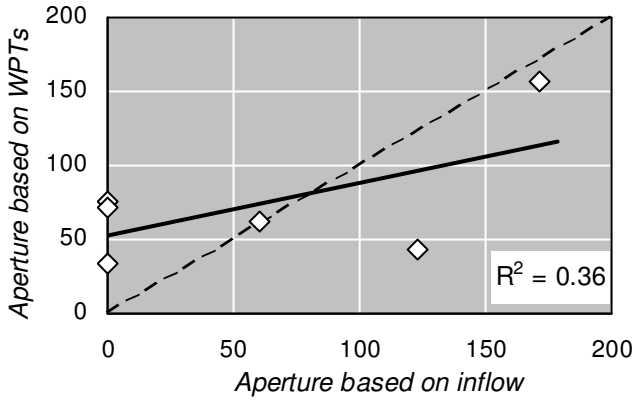

Figure 3.11 Comparison of the hydraulic apertures [µm] evaluated from WPTs and inflow measurements in the core boreholes (see the compared sections in Appendix A).

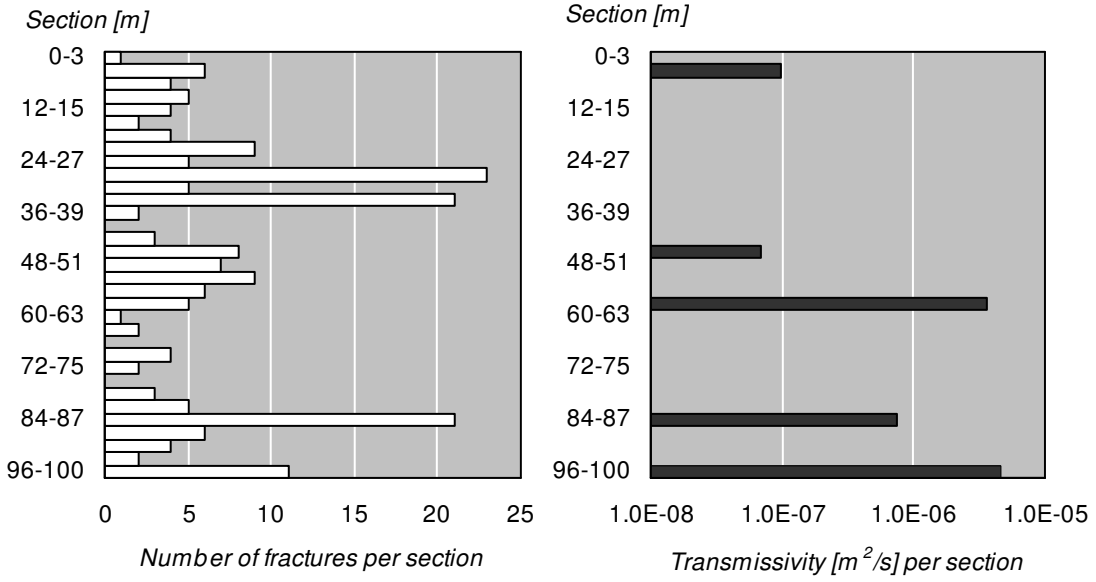

Figure 3.12 Fracture frequencies (open fractures) and their calculated transmissivities based on inflow measurements along borehole KA1619A01.

The measured interval transmissivity values, based on 14 sections of water pressure tests, have been plotted as a cumulative distribution, presented in Figure 3.13. A lognormal function has been fitted to these values in order to estimate the distribution of transmissivity values below the measurement limit. The distribution has been adjusted after the upper data interval since the lower values are unknown. The interval transmissivity values from the inflow measurements are not evaluated since a majority (85 %) of the 3 m-sections had water inflows that were lower than the measurement limit and this would influence a lognormal distribution to a great extent.

The lognormal distribution fitted to the 14 WPT sections gave simulated transmissivity values. To verify the accuracy of this distribution the inflow from the sections was analysed from the simulated transmissivities, see Appendix A. The simulation of total inflow from these sections was around 5 l/min, which is considerable lower than the 42 l/min that were actually measured in these 14 sections.

The Pareto distribution is another statistical distribution fitted to the inflow fracture transmissivity data. Based on the maximum fracture transmissivity value, the Pareto distribution describes the probability that a transmissivity is below a certain transmissivity. The Pareto distributions was approximated to a straight line in a log-log plot (Figure 3.14a) and the coefficient of the distribution, *k*, for the inflow data was determined to 0.370. This coefficient was used to evaluate the hydraulic aperture distribution for the 114 open fractures found in the mapping of the 100 m long core borehole, also Figure 3.14b.

As can be seen in Figure 3.14b, around 99 % of the fractures have an aperture of less than 0.1 mm and 77 % have apertures of less than 0.01 mm. A simulation of inflow can be made also from these transmissivity values. The result of the simulation corresponds to a total inflow of 41 l/min, and this from all open fractures in the three core boreholes. The actual inflow from the core holes was 72 l/min, which makes the simulation an underestimation. But since the three boreholes are parallel is there a substantial risk that inflow from the same fracture was measured more than once. The statistical model is based on individual fractures, which are not connected to other fractures.

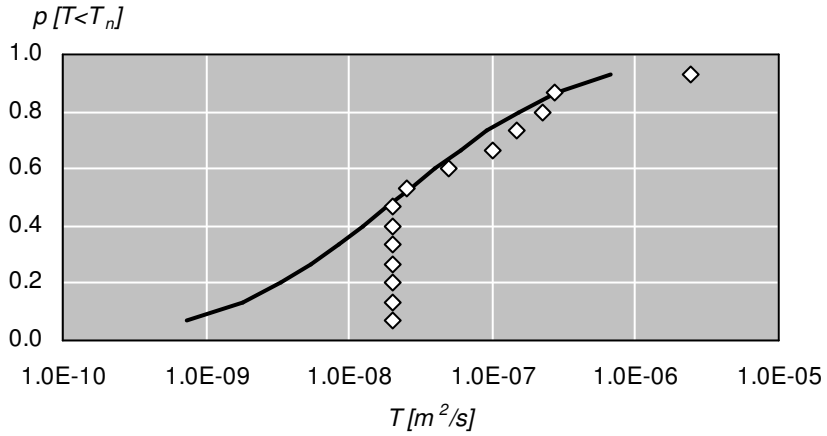

Figure 3.13 Cumulative distribution of transmissivities and corresponding lognormal distribution (black line) for 5 m-intervals in the core boreholes based on WPTs (sections = 14).

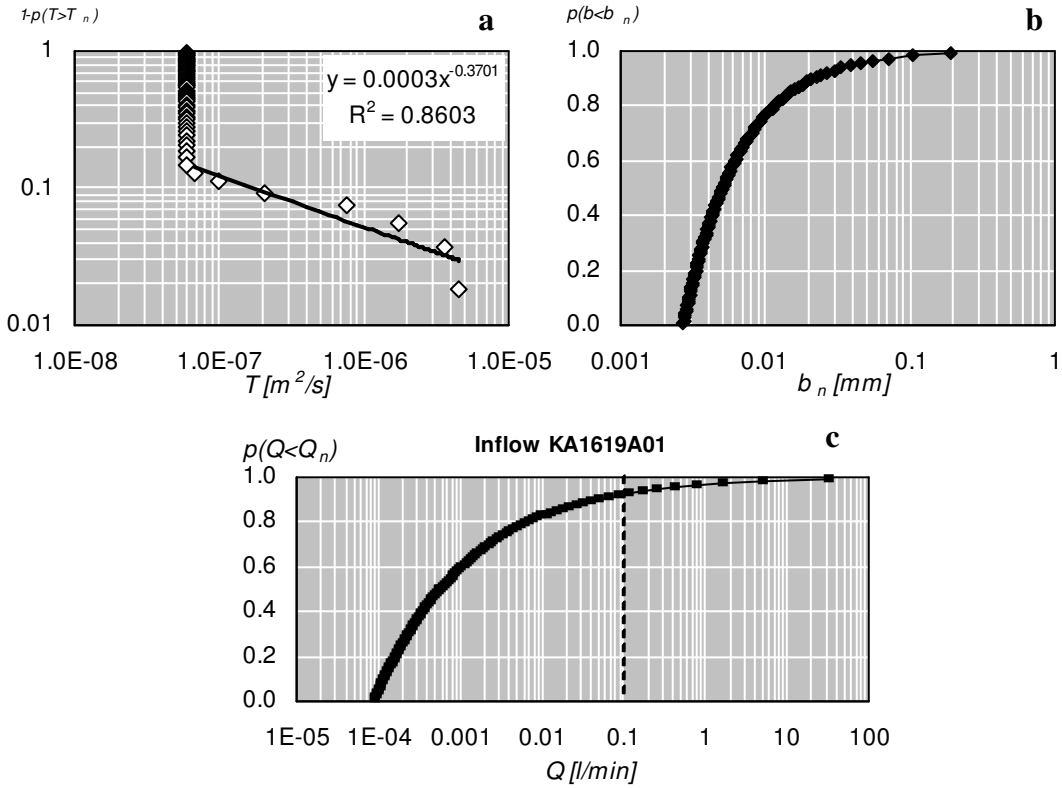

Figure 3.14 **a***: Evaluated Pareto distribution from fracture transmissivity data from inflow measurements.* ***b****: Cumulative distribution plot of simulated hydraulic apertures.* ***c****: Inflow simulation for KA1619A01 based on the Pareto distribution in* ***a****, giving a total inflow of 41 l/min.*

If only the inflow from the 114 open fractures in the 100 m borehole is regarded the simulation of inflow (Figure 3.14c) gives a better fit to the measured inflow of 60 l/min. The inflow simulations are further discussed in Chapter 4.1.

3.4.5 Pre-grouting and penetration of cement

The three core-drilled boreholes were grouted using a cement-based grout; a more detailed description of the procedure is given in Johansson (2005). The used up quantity of grout indicated that the grouting in the two shorter boreholes only filled the holes, and only a limited amount of grout penetrated the rock mass. In KA16*19*A01 however, grout penetrated the rock mass in all three sections where grouting was performed.

A 96 m long control borehole, KA16*19*A02, was drilled in the close proximity (around 1 m) to KA16*19*A01, and water pressure tests in 5 m-sections were performed in this control hole to be able to evaluate the grouting performance. Estimations of transmissivities and apertures in the control hole, based on these WPTs, are presented in Table 3.5. It can be seen that there was a larger number of water-loss positions than inflow-positions identified, probably due to the fact that open but not water-conducting fractures were included in the WPT.

Table 3.5 Estimated hydraulic apertures after grouting, based on water pressure tests in the 96 m control borehole, compared with apertures in these sections in KA1619A01 based on inflows before grouting.

	After grouting, control hole		Before grouting, 100 m core hole	
Section [m]	***Q*** **[l/min]**	***b*** **[µm]**	***Q*** **[l/min]**	***b*** **[µm]**
6-11	1.0	58	0.65	54
16-21	1.0	58	-	-
36-41	0.6	49	-	-
41-46	0.2	34	-	-
46-51	0.2	34	0.45	48
51-56	0.8	54	-	-
56-61	0.4	43	24.0	180
61-66	0.6	49	-	-
66-71	4.2	94	-	-
71-76	5.0	100	-	-
76-81	0.6	49	-	-
81-86	0.4	43	5.0	107

When comparing the hydraulic measurements before and after grouting it can be seen that the largest hydraulic apertures are reduced; at section 56-61 m from 180 to 43 µm and at 81-86 m from 107 to 43 µm, which indicates that the larger fractures in these sections are partially or completely sealed. The two other inflow sections at 7 and 46 m, with apertures around 50 µm seem unaffected by the grouting. The large inflow position at 99 m is not possible to evaluate since the control hole only was 96 m long. All fractures with apertures larger than 100 µm were probably completely or partially sealed since all evaluated hydraulic apertures after grouting was in the range of 50-100 µm, which is the limiting penetrability for cement grout.

The grouting also affected the groundwater pressure around the boreholes; the measured pressure before grouting was 1.55 MPa and it had increased to 1.7 MPa after grouting (Johansson 2005). No inflow measurement was performed in the control borehole, but it seems like the larger inflows stopped with the grouting, leaving fractures with apertures around 50-100 µm open (corresponding to an inflow of about 0.5 l/min to 3 l/min).

A Pareto simulation of hydraulic apertures of fractures still open after the grouting has been made, using results from the WPT evaluated transmissivities of the 19 sections along the control hole (Figure 3.15a and Appendix A). In this simulation about 16 % of the fractures exceeded 0.1 l/min, but no fracture exceeded 5 l/min since all fractures larger than 100 µm were sealed. The total inflow from the control borehole was simulated to 13.7 l/min (Figure 3.15b).

The penetration of cement grout into the fractures intersected by the 100 m core borehole has been analysed. The 100 m core hole was grouted in three sessions; 0-35 m, 35-70 m and 70-100 m (Johansson 2005). In the first two sections, one grout mixture with w/c ratio of 1.0 was used, but in the last section, 70-100 m, two grout

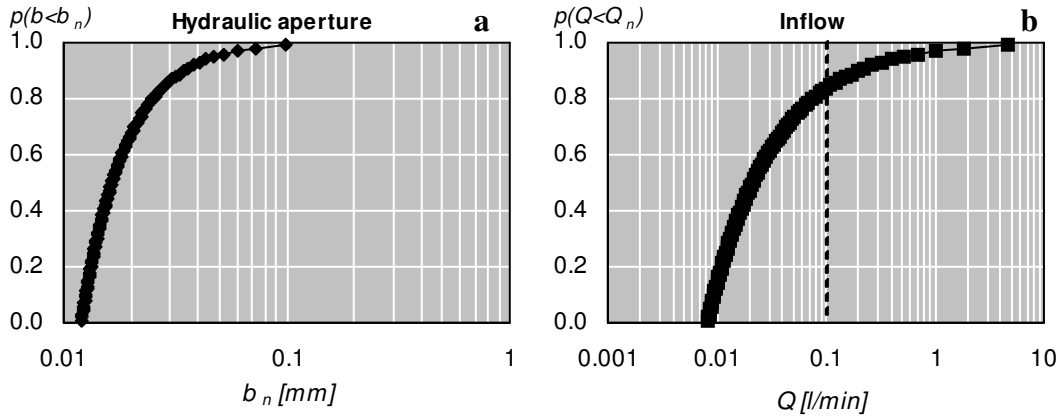

Figure 3.15 ***a****: Pareto distribution of hydraulic apertures based on WPTs in the control borehole.* ***b****: Inflow distribution based on a the Pareto simulated hydraulic apertures in* ***a****.*

mixtures with different w/c-ratios were used. Three of the water-conducting sections had an aperture larger than 100 µm (at 60, 86 and 99 m, according to Table 3.3), and those are the fractures regarded in the penetration analysis.

The material properties of the grouts used in the 100 m core borehole are not clearly presented in the report (Johansson 2005) or in the protocols from the grouting in March 2004. But there are some information that can be used to at least make estimations of properties such as yield strength and initial viscosity. The grout used was an INJ30 with 1 % of additives. The w/c-ratios for the two grout mixtures used in the grouting aimed at 1.0 and 0.8, but tests of the actual mixtures showed results of w/c-ratios of 1.47 and 1.55 (!), which are rather high ratios. By using information from laboratory testing of cement grout used in the Citybanan project (Draganovic 2009), the yield strength of the grout was estimated to 1 Pa and the viscosity to 10 mPas for both mixtures.

The grouts are assumed to spread radially and fill fracture planes circular around the borehole, thus obtain 2D penetration. The results from the calculation of 2D penetration length in the three fractures, using equation (2.15) to (2.20), are presented in Table 3.6 (see calculation in Appendix A). The time spent grouting in the borehole was long, and estimations show that the cement grout could have spread as far as 35-40 meters out from the borehole in these fractures. The reaming of the drifts in 2005 did therefore probably not have any large influence on the conductivity of these fractures; the grout had likely spread further out in the rock than the diameter of the drifts.

Table 3.6 Penetration length, I_{2D}, of cementious grout in three fractures based on information from grouting of the core boreholes in March 2004.

Inflow section	b [µm]	w/c-ratio	Grouting time, [min]	I_{2D} [m]
60 m	180	1.47	82	32
86 m (grout I)	107	1.47	101	21
86 m (grout II)	107	1.55	66	18
99 m (grout I)	194	1.47	101	38
99 m (grout II)	194	1.55	66	32

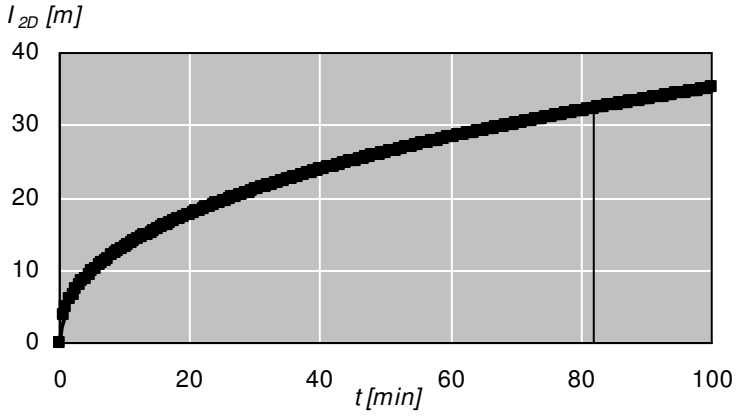

Figure 3.16 Penetration of cementious grout in the fracture at 60 m (180 µm) plotted against time. The narrow black line represent the stop time for the grouting session.

The calculated penetration plotted against time for the 180 µm fracture at 60 m is shown in Figure 3.16. It can be seen that the grouting time required to get a penetration of 10 m is about 10 minutes. A grouting time of 82 minutes was therefore probably not necessary for obtaining a satisfactory penetration into the fractures possible to grout with cementious grout.

3.4.6 Hydraulic testing in the post-grouting project

The drifts were excavated in 2005, and five inflow positions in the long drift were hydraulically characterised in the post-grouting project in 2007-2008. This included hydraulic testing before and after grouting (pre- and post-characterisation). The test programme consisted of water pressure build-up tests, water inflow measurements and water pressure tests.

The equipment used for the water pressure test in the drift consisted of a pump and a logging computer, which logged the pressure and the instant water loss every other second. Water was pumped into the Mega-Packer at a pressure of 1 MPa over the groundwater pressure and each water pressure test lasted for 15 minutes. The transmissivity from the water pressure test was evaluated using Thiem's equation (2.3) and the radius of influence was assumed to be 100 times the drift radius in all inflow positions.

The inflow measurements were performed before, during and after the grouting sessions were completed. The gap was filled with water, and the water leaking into the gap from the fracture overfilled the gap and leaked out of the top valve of the Mega-Packer. The leaking water was measured with a graded cylinder in three sessions, during one minute each, and a mean value of these inflows was calculated. To get a stable flow, measurements started after about 30 minutes with open valve and leaking water (Eriksson & Lindström 2008). The transmissivity of the fractures, based on the measured inflow, was estimated using equation (2.14).

The pressure build-up tests were performed using the Mega-Packer and logging equipment. The gap between the packer and the drift wall was filled with water leaking from the position, and the top valve was closed, enabling the groundwater

pressure to be built up. A sensor was connected to one of the valves in the packer, and the pressure could be logged with the logging equipment. The Mega-Packer only could seal off a small part of the drift, which resulted in rather unstable groundwater pressures. The time for measurement was set to about 30 minutes, but several of the measurement sessions lasted more than 30 minutes since the pressure still was increasing after 30 minutes.

The groundwater pressure build-up tests were used in the pre-characterisation to determine the groundwater pressure and the transmissivity of the positions, using Jacob's method, equation (2.13). This evaluation was remade in this thesis since incorrect units were used in the evaluations in the Mega-Packer project. The recovery time was short in comparison with the flow time, and the adjusted time was therefore approximated to the recovery time (Eriksson & Lindström 2008). The groundwater pressure build-up test gave no stable values in position 1 and 2, and could not be used for evaluation of transmissivities.

A presentation of the evaluated transmissivities and hydraulic apertures in the long drift, based on the different characterisation methods, can be found in Table 3.7. The values based on the pressure build-up tests are re-evaluated in this thesis (see Appendix B); the others are taken from the Eriksson and Lindström (2008). The correlations between the different evaluation methods are good.

The evaluated transmissivity values can as previously calculated transmissivities be used for a Pareto-based transmissivity distribution, here of the 92 fractures mapped as water-conducting in the drift. The transmissivities evaluated from the inflow measurements were used, giving a coefficient of distribution, k, of 0.36, see Figure 3.17a. The simulated inflow was performed with a hydraulic head set to 0.8 MPa, the total inflow became 6.0 l/min with the largest inflow corresponding to 4.7 l/min followed by 0.7 and 0.2 l/min (compared to actual largest values; 2.4 l/min, 1.5 l/min and 0.5 l/min).

Table 3.7 *Evaluated transmissivities and hydraulic apertures for the positions in the long drift, performed with the Mega-Packer. Inflow and WPT based results are taken from Eriksson and Lindström (2008) and pressure build-up test evaluated in this thesis (see Appendix B).*

Position	Location [m]	November 2007 Inflow [l/min]	Water pressure tests		Pressure build-up tests		Water inflow measurements	
			T [m^2/s]	b [µm]	T [m^2/s]	b [µm]	T [m^2/s]	b [µm]
1	5.5-7.5	2.400	$1.71 \cdot 10^{-6}$	133	-	-	$1.20 \cdot 10^{-6}$	124
2	28.5-31	0.025	$2.57 \cdot 10^{-8}$	33	-	-	$1.25 \cdot 10^{-8}$	27
3	35.5-37.5	0.490	$1.23 \cdot 10^{-8}$	55	$1.22 \cdot 10^{-7}$	58	$7.97 \cdot 10^{-8}$	50
4	52.4-54.5	1.470	$3.21 \cdot 10^{-7}$	76	$1.15 \cdot 10^{-7}$	57	$2.39 \cdot 10^{-7}$	72
5	60.7-64.3	0.148	$5.42 \cdot 10^{-8}$	42	$4.70 \cdot 10^{-8}$	42	$2.99 \cdot 10^{-8}$	36

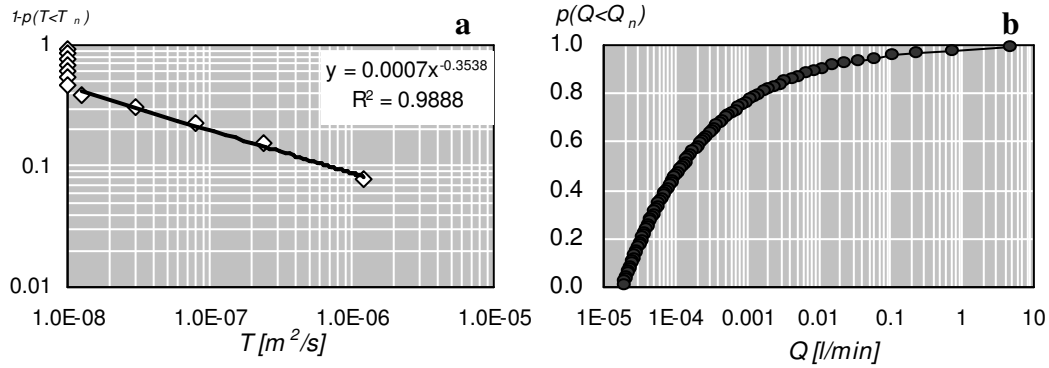

Figure 3.17 ***a****: Evaluated Pareto distribution from inflow measurements in the long drift.* ***b****: Simulated distribution of inflow for 92 water-conducting fractures, with a hydraulic head of 0.8 MPa. Total flow is 6 l/min.*

3.4.7 Flow dimensionality analysis

The flow dimension of the water in fractures can be evaluated from the shape of a pressure build-up curve, see Figure 2.5. A total of six curves obtained from the PBTs before grouting, based on data from Eriksson and Lindström (2008), were evaluated (see Appendix B) and two of them are presented in Figure 3.18. It can be seen that these positions follow the Theis curve, which indicates a 2D flow dimensionality in the fractures. The curve for position 4 in November does not show an explicit flow dimension, an interpretation of the curve is that it starts with 1D flow, and changes to 2D flow. In March, when the nearby situated position 5 had been grouted, the shape of the PBT curve in position 4 was only describing a 2D flow.

Pressure, volume and time recordings from the WPTs performed in autumn 2007, before grouting, have been used in the dimensionality analysis described for grouting in Chapter 2.5.2. Water has approximately the same rheological properties as silica sol has before gelling, and the resulting values of $Q \cdot t/V$ are evaluated according to Table 2.1. Figure 3.19 shows the dimensionality evaluation curves for the five positions. The first couple of minutes were used to fill the space between the Mega-Packer and the rock wall with water. The dimension curves, which represents the injected water volume as function of time according to equation (2.23), starts when the Mega-Packer space is filled.

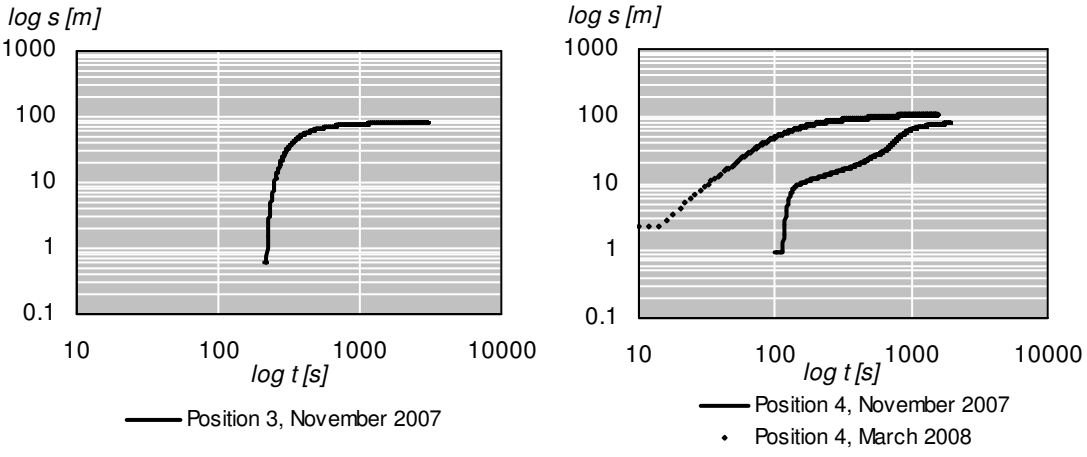

Figure 3.18 Log-log plots of position 3 and 4 from pressure build-up tests.

The resulting values of $Q \cdot t/V$ for position 1, 3 and 4 are approximately equal to 0.8, which corresponds to a 2D flow regime. In position 3, the starting flow regime can be interpreted as 3D, which is after a couple of minutes changes to 2D. The dimension curve values for position 2 is difficult to interpret, because of the spread of calculated values. The average value for the index parameter, $Q \cdot t/V_{average}$, is 0.34, which indicates a 1D flow rather than a 2D flow regime. However, it could be a result of a low accuracy of the measurement in this section; the flow was below 1 l/min (less than 4 litres were lost during 10 minutes of testing). Position 5 had a value very close to 1, which would indicate a 3D flow, but also here is an uncertainty of the accuracy since only 6 litres were lost during 15 minutes of testing.

The pressure, volume and time recordings obtained from the grouting of the positions have also been used for a dimensionality analysis based on the concept in Chapter 2.5.2. Here, the first five minutes of the grouting in the positions were assumed to be used to fill the Mega-Packer void. This can be verified by the flow curves (Appendix B); the grout flow was around 20-40 l/min during the filling of the packer. The start of the dimension curve evaluation is approximately when the Mega-Packer space was filled and continues during the grouting of the rock mass.

There were some difficulties in determining the duration of the pure fracture filling, since the pressure, momentaneous flow and volume varied a lot during the recordings. Position 1 was not possible to evaluate at all, due to problems in the recordings, and position 3 is not reliable, since the same equipment were used there. The average values of $Q \cdot t/V_{average}$ for position 2, 4, 5a and 5b are 0.92, 1.37, 0.80 and 2.05, but the shapes of the curves were hard to interpret, see appendix B. The main reason for the

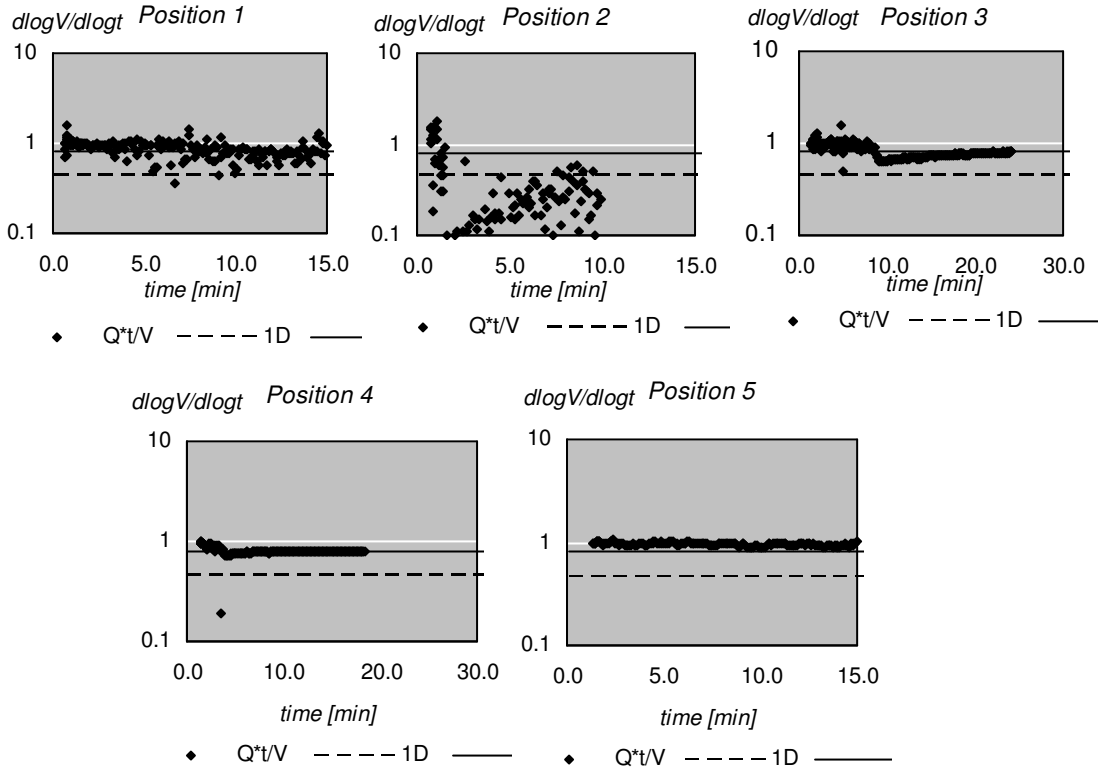

Figure 3.19 Flow dimension curves based on water pressure tests. Q represents the momentaneous flow, t is the accumulated time and V is the accumulated volume.

uncertainties is probably the low recorded flow during grouting. The flow was around 1 to 5 litres/minute, and the measurement accuracy for the grouting equipment (pressure, flow and volume recordings) is low for these magnitudes. Presentations of the interpreted flow dimensions, which are mainly interpreted from the WPTs dimensionality analysis, are given in Table 3.8.

Table 3.8 Interpreted flow dimensions for the five inflow positions in the long drift.

Position	Location [m]	November 2007 Inflow [l/min]	Flow dimension
1	5.5-7.5	2.400	2D
2	28.5-31	0.025	1D
3	35.5-37.5	0.490	2D
4	52.4-54.5	1.470	2D
5	60.7-64.3	0.148	2D

3.4.8 Post-grouting and penetration of silica sol

The post-grouting was performed, as previously mentioned, with the almost 2 m long Mega-Packer in five positions with silica sol as grout. The design of the grouting was performed to ensure reaching the target of maximum 0.1 l/min in each inflow position. All grouting rounds were planned using a grouting time to fulfil a theoretical penetration length of 5 m.

The grouting of the different positions caused an increased inflow in the positions until then not sealed. An apparent example of this is position 2 where the flow increased from 25 ml/min to 145 ml/min due to the grouting in position 1 and 3. The increased flow is caused by the increased groundwater pressure head which resulted after the grouting. Two smaller fractures at 11 and 17 m, which had no apparent inflow of water before grouting, started dripping after the sealing of the five positions. The inflow to the short drift also increased as the long drift was grouted. More details about the water inflow changes over time are given in Chapter 3.4.9.

The inflow from the five positions in the long drift was reduced from 4.5 l/min to 0.054 l/min after grouting, and the obtained sealing effect ranged from 86.8 to 99.8 % for the five positions (Eriksson & Lindström 2008). The total inflow into the long drift was however only reduced from 4.5 l/min to 0.42 l/min (90.7 %). The five positions, which before post-grouting stood for almost 100 % of the inflow, only contributed with 13 % of the total inflow after grouting. Hence the sealing of the five inflow positions was effective, but the increased groundwater pressure caused an increased inflow in the smaller, not sealed fractures.

The theoretical penetration lengths of silica sol for the grouting in the five positions are calculated using equation (2.21) and (2.22), which describes 1D and 2D penetration. The theoretical penetration length for the positions can be seen in Table 3.9. The evaluation of the flow dimension in the five investigated positions though suggests radial flow in a majority of the inflow positions. The groundwater pressure is assumed to be 0.8 MPa in all positions.

Table 3.9 Data from the post-grouting in the long drift using silica sol, with a calculation of the radial penetration length.

Position	Hydraulic aperture, b [µm]	Grouting overpressure Δp	Gel time, t_G [min]	$I_{max\text{-}2D}$ [m]	$I_{max\text{-}1D}$ [m]
1	133	0.6	40	7.6	16.8
2	33	1.3	43	2.9	6.4
3	55	1	40	4.0	9.0
4	76	1.3	43	6.6	14.7
5	42	0.9	31	2.6	5.7

An illustration of the extent of the grout spread in the shapes of discs is shown in Figure 3.20, assuming radial flow in all positions and a uniform spread. Grout spread to the short drift during grouting of position 1, a distance of around 4 meters. The first observation of penetrating silica sol was noticed in the roof of the short drift after only 1 minute of grouting. A few minutes later grout was also penetrating from the wall closest to the long drift (Eriksson & Lindström 2008). This indicates that the spread of grout seems to be at least 4-5 meters in a rather short time period and it confirms that there is contact between the two drifts. The theoretical penetration length for position 1 is 7.6 m, which seems to be a reasonable estimation.

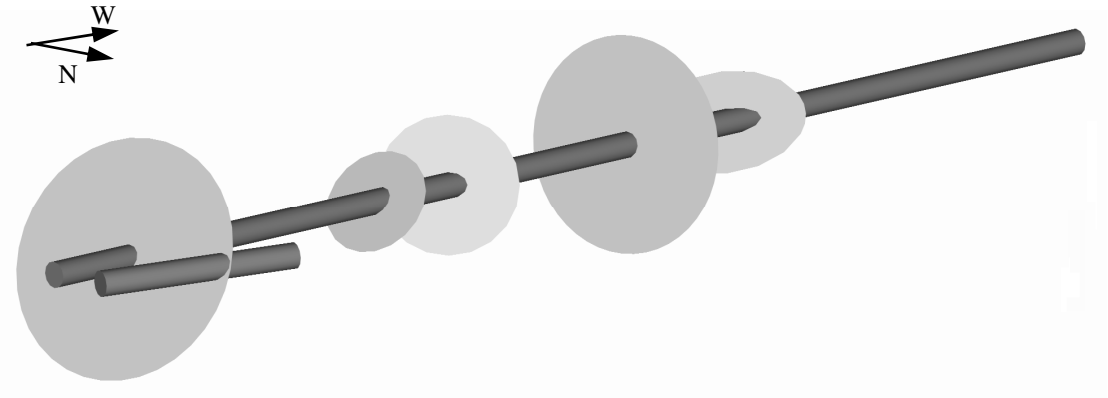

Figure 3.20 3D picture of the theoretical penetration lengths of silica sol in the five grouted positions.

3.4.9 Inflow measurements over time

Full-length water inflow measurements have been performed in boreholes, pilot holes and in drifts at several occasions since the start of the KBS-3H project. The accumulated inflow into the 100 m long pre-investigation borehole was 60 l/min, of which 30 l/min was leaking from section 96-100 m. To avoid this significant inflow, it was decided to only excavate the long drift 95 metres. There was no inflow measurement performed in the control hole drilled after the cement grouting.

Before the reaming of the long drift, the total water inflow to the 95 m long pilot hole was measured to less than 2 l/min. After finishing the reaming of the drift, the total

inflow was around 10 l/min. According to Bäckblom and Lindgren (2005) the inflow was characterised by a high pressure gradient and a channelled flow. This since most of the water was spraying or dripping from spots, and not leaking from the whole fracture trace. The water seepage distribution for the individual seepage spots was in the range of 0.3-1.6 l/min. Most water seepage in the long drift came from fractures and fracture zones at 7 m, 37 m and 53 m, where water sprinkled out or was intensely dripping, see Figure 3.21.

In 2007, five inflow positions were identified in the long drift and the total inflow was measured to around 4.5 litres per minute. The inflows were then visible as drops or as minor streams of water down the rock wall (Lindström & Eriksson 2008), see Figure 3.21 where the character of the inflow in a fracture 2005 are compared with 2007. The total inflow was reduced to 0.42 l/min after the completion of the post-grouting. A compilation of the water inflows measured along the first 95 metres of borehole, pilot hole and long drifts are found in Figure 3.22, together with measured groundwater pressure levels. The groundwater levels are measured and estimated from water pressure tests or pressure build-up tests performed during the KBS-3H project.

The first 15 metres of core borehole KA16*21*A01, which was located where the short drift later was excavated, was considered sealed during the pre-investigation with no water-inflow in the core borehole (Johansson 2005). The inflow to the 15 m-drift was 0.4 l/min short after reaming, with only minor leakages, mainly from the fractures close to the shear zone at 7 m (Bäckblom & Lindgren 2005).

After post-grouting of the five positions in the long drift, the inflow in the short drift increased from 65 to about 290 ml/min, see sequence in Figure 3.23. It can be noted that the grouting of position 1 and 3 had the largest influence on the inflow into the short drift. After these two were grouted, the inflow increased to around 270 ml/min. This implies that the sealing of the long drift also affected the hydrogeological conditions of the short drift, with the sealing of position 1 having the largest influence.

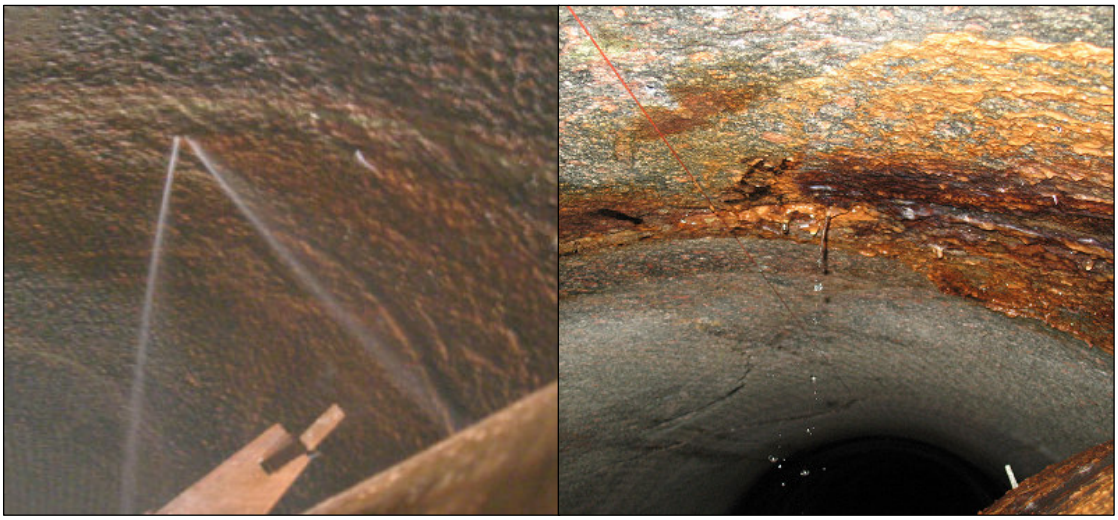

Figure 3.21 Photos from the drift taken in 2005 (left) and in 2007 (right). From Eriksson and Lindström (2008).

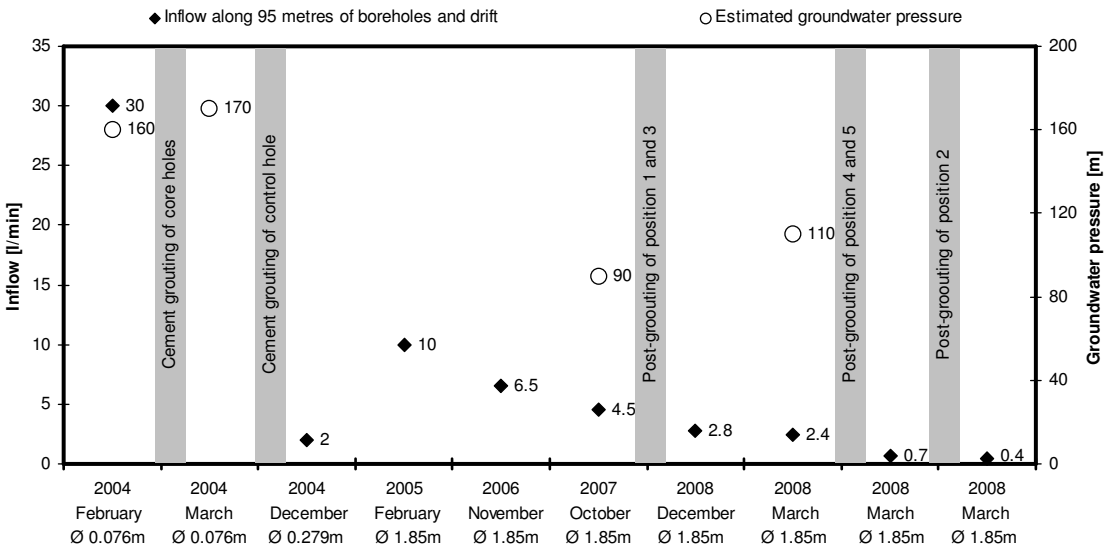

Figure 3.22 Compilation of inflows and pressures along the first 95 m of core hole KA1619A01, control hole KA1619A02 and the 95 m-drift.

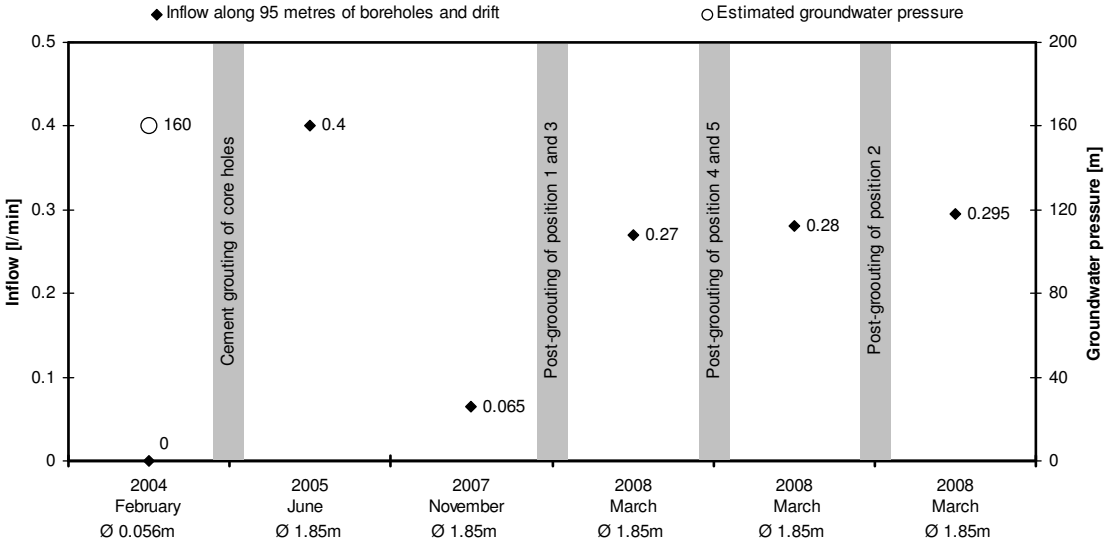

Figure 3.23 Compilation of inflows in the first 15 m of the core hole KA1621A01 and the 15 m-drift.

4 Discussion

The results from the characterisation of the fracture system surrounding the horizontal drifts are used to make a comprehensive description of the fracture network and its flow characteristics, but also to investigate how the two grouting operations has affected the hydrogeological situation.

4.1 Fracture network description

A description of the fracture network is important for the assessment of transport of water in the rock mass. An adequately described network increases the accuracy of predictions concerning water inflows and necessary grouting applications (Fransson 2001). The most important parameters for describing a fracture network are as previously stated; fracture intensity, fracture set orientations, distribution of hydraulic apertures and fracture lengths. Below the results from the evaluation of the fracture network surrounding the two horizontal drifts at Äspö HRL are discussed, focusing on the network geometry (intensities and orientations) and flow characteristics (hydraulic apertures, inflow positions and flow dimensions).

There are some uncertainties related to the results of the evaluations performed in Chapter 3, with elements of uncertainty concerning the extent and performance of hydraulic measurements, as well as measurements of grout properties and grouting performance. The cement grouting, which was performed in between the pre-investigation and reaming of drifts, has made the hydraulic situation more complex and made interpretation of data more difficult. Some results are therefore considered more as approximate values rather than absolute results, for example penetration lengths and flow dimensions.

4.1.1 Network geometry

The two horizontal drifts at Äspö HRL are deep tunnels, located at 220 m depth in crystalline rock, mainly consisting of diorite. About 90% of the rock mass is identified as sparsely fractured with a RQD of 100, and the fracture intensity (P_{10}) was in total 1.8 fractures/m in the core boreholes. The surface intensity of fractures in the two drifts (P_{21}) corresponds to around 2 m/m^2. Water-conducting fractures are not frequently occurring in boreholes or drifts. Only five inflow positions with a flow larger than 0.45 l/min were indentified along the 100 m core borehole. After reaming of the drifts, the fractures could be investigated more in detail, and 92 fractures were mapped as water-conducting (representing 15 %). The absolute majority had a very small seepage; only seven fractures had leakage resembling dripping or flow (1 %).

Several steep fracture sets and a subhorizontal set could be interpreted from the fracture mapping of core holes and drifts, all in line with the general mapping performed at Äspö HRL. The proportion of water-conducting fractures within the fracture sets varied. Some fracture sets had a large proportion of water-conducting fractures, while others almost exclusively had non-conductive fractures. This is assumed to be caused by the current stress field, where favourably orientated fractures, mainly NW-SE orientated, have been shown to be the most active groundwater flow pathways. In Figure 4.1 the orientations of drifts and water-conducting fractures are illustrated in relation to the current stress field at Äspö HRL.

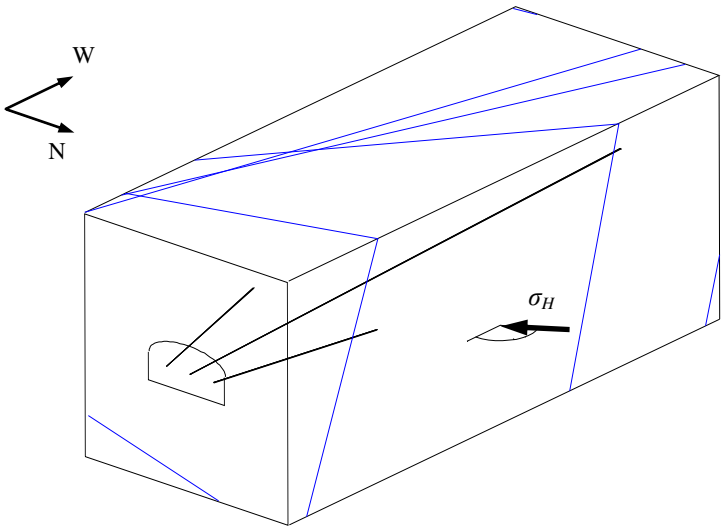

Figure 4.1 *The alignment of the stress field around the boreholes, with the blue lines representing the orientation of the five fractures with a larger inflow reported in the core drilling.*

An evaluation solely concerning fracture lengths has not been performed, due to a lack of suitable data covering this topic. But it was noted in the drifts that the water-conducting fractures, especially the ones with a notable inflow, appeared in the drift walls as larger than the drift perimeter. This coincides with the theoretical relationship between transmissivity and fracture length compiled by Vidstrand and Ericsson (2008), in which fractures with a transmissivity larger than 10^{-8} m^2/s are at least a couple of metres.

The results concerning the so far mentioned network properties (intensities, fracture sets and water-conducting sets) were in line with the overall observed characteristics of the Äspö rock mass. The rock is sparsely fractured with mainly one conductive fracture set and this implies a poorly connected fracture network which can be described as a Type I permeability structure. In a Type I permeability structure fracture zones are indicated by locally increased fracture intensities, and according to Fransson and Hernqvist (2010) grouting only in selected areas (such as these zones) can be sufficient to reach inflow requirements. However, in KBS-3H drifts would probably extensive grouting be necessary anyway, due to the strictly set inflow requirements.

The poor connectivity of the fracture system is also indicated by the fact that there were few fractures contributing to main flow, only five positions in the 100 m long core borehole and in the 95 meter long drift. The total inflow was also significantly reduced as these main water-conductors were sealed. The groundwater did find new ways, but there were only two new inflow positions registered along the whole 95 m-drift after the post-grouting. Several positions with high fracture intensities and water losses but no inflow, not even after grouting of nearby inflow position, also implies that the connectivity of the whole fracture system is fairly low. The fact that the grouting with the Mega-Packer, which only sealed about two meters of the drift, gave no backflow into the drift through closely located fractures is another indication of poor connectivity.

4.1.2 Flow characteristics

The flow characteristics within the fractures and the fracture network surrounding the drifts are investigated mainly with respect to inflow and inflow positions, since the flow of groundwater is a very important consideration in the KBS-3H design.

The flow dimensionality evaluations in the long drift suggest a 2D flow regime possible within a majority of the fractures. The visible inflow to the drift looks though more like point leakage (see Figure 3.21) with groundwater flowing into the drift through channels, which is the case when there is 1D flow within the fractures. An explanation of this behaviour could be that water spreads radially in the fractures surrounding the drift (2D-flow), since there are enough 1D-channels within the fracture to sum up to a 2D network, see example in Figure 4.2. This is also in accordance with the description of a Type I system given by Hernqvist (2009). It is though important to bear in mind that there are uncertainties related to the flow dimension evaluations, with low accuracy of the measurement equipment at the measured flows.

The inflow measurements along the 3 m sections of the core boreholes correspond to estimated hydraulic apertures between 50-190 µm. After reaming the drifts, the apertures varied between 27 and 124 µm. Several attempts of making inflow simulations have been made based on results from the hydraulic tests. The lognormal distribution did not reproduce the highest transmissivity values well enough, and hence this gives an apparent underestimation of the conductivity of the rock.

A Pareto simulation, based on inflow measurements, gave a more accurate representation of the fracture system, with a simulated inflow of 41 l/min in the 100 m core borehole compared to the measured inflow of 60 l/min. The distribution of hydraulic apertures indicated that less than 8 % of the fractures have apertures corresponding to more than 0.1 l/min of inflow (see Chapter 3.4.4), and together these 8 % contribute to 99 % of inflow.

The coefficient of distribution, k, for this Pareto distribution was 0.37. Pareto distributions for other boreholes at Äspö HRL have given relatively stable values of the coefficient of distribution; Gustafson (2009) presents coefficients ranging between 0.39 and 0.48 for three separately located boreholes at Äspö. The k-value evaluated from the inflow in the core boreholes, 0.37, can thus be assumed to give a plausible distribution of transmissivities in the rock mass. The inflow simulation to the control borehole gave a total inflow of 13.7 l/min. It could be a slight overestimation, considering all open fractures, not only water-conducting, are included in a WPT. Since no inflow measurements were performed in the control hole is it not possible to evaluate the accuracy of the simulation. It should though be in these magnitudes,

Figure 4.2 ***a****: Fracture with channelled flow.* ***b****: Fracture where water spread radially.* ***c****: Fracture with enough channels to enable a radial spread of water. Modified from Gustafson (2009).*

considering the largest and most influential WPT transmissivities probably origins from water-conducting sections, and because the maximum inflow after reaming of the drifts actually was 12 l/min. The results from all inflow simulations and the measured inflow are 41 l/min simulated in KA16*19*A01 compared to 60 l/min, 13.7 l/min simulated in the control borehole and 6 l/min simulated in the long drift, compared to 4.5 l/min. These are rather good predictions considering the quality of the input data, with 3 to 5 m long sections and measurement limits of 0.4 l/min for some of the hydraulic tests.

The boreholes in the pre-investigation revealed the largest inflow positions in the rock mass, but there are difficulties when using inflows in core boreholes to interpret the location of all inflow positions in a larger tunnel. The pre-grouting of the boreholes before reaming the drifts created an even more complex situation in this case. There were variations in where the inflow appeared before and after reaming of the long drift.

In Figure 4.3 hydraulic apertures evaluated for positions along the long drift and the long core borehole are shown. The inflow position around 6 m and around 60-61 m were the two sections where inflows were noted both before and after reaming of the drifts. It should though be noted that the drift is only 95 m long and does not include the larger inflow at 96-100 m. The WPT in the control borehole did not include this position either. What can be seen in Figure 4.3 is that the cement grouting of the boreholes affected the inflow positions with a hydraulic aperture larger than 100 µm, which were evaluated at 99 m, 87 m and 60 m. These are also the apertures IC30 cement is expected to penetrate and efficiently seal.

It can also be seen that it can be hard to detect smaller inflow positions in boreholes (such as at 29 m) and to evaluate the full-scale hydraulic aperture of fractures (as in position 1). These differences could be a result of variations in the fracture aperture, caused by contact areas within the fractures. The probability that a 76 mm borehole intersects a tight or low flow part of a water-conducting fracture is higher than for a 1.85 m drift, where a larger part of the fracture is exposed. This could for example be the case at position 2 (29 m) and at 7 meters into the short drift, which both were tight sections giving neither inflow nor water losses in the small boreholes, but caused an inflow to the drifts. These section had an increased fracture intensity, so had also

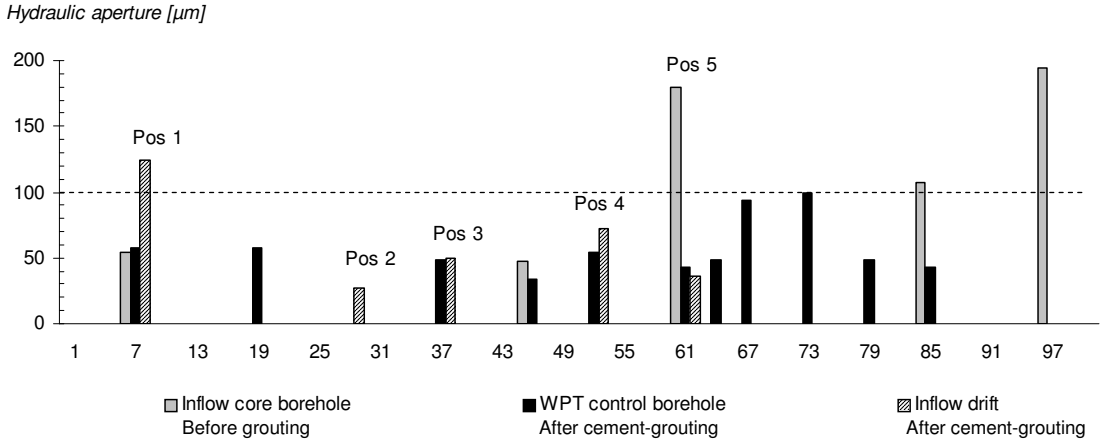

Figure 4.3 Hydraulic apertures evaluated from inflow measurements in the core borehole, WPTs from the control hole after pre-grouting, and inflow measurements into the drift before the post-grouting.

position 3 (36 m) and position 4 (53 m), which gave considerable inflow in the drift, but showed no sign of inflow in the core hole. But these sections had water losses in the control borehole, and the inflow changes at these positions could be related to relocation of groundwater. Position 4 is for example located closely to position 5 which was partly sealed in the pre-grouting.

The relationship between fracture size and transmissivity proposed by Vidstrand and Ericsson (2008) also suggests that fractures with low transmissivity are smaller than high transmissivity fractures. The probability of hitting an open part of a low transmissivity fracture with a borehole is thus lower than hitting an open part of a fracture with a high transmissivity. A larger number of boreholes may therefore be required to make a successful grouting in these low transmissivity fractures.

Another way of detecting inflow positions could be by investigating fracture intensities. An illustration of the fracture intensities along 3 m sections of the 100 m long core hole are shown in Figure 4.4. The calculated average is 5.8 fractures per 3 m- section, and 11 of 33 sections exceed this value. Seven of these exceeding sections had inflow, either in the core borehole or in the drift. Only one inflow position had an intensity lower than average. But increased fracture intensities do not necessarily lead to water-conducting fractures, hence the number of inflow positions will be overestimated if only looking at intensities.

The water-conducting features with a measured inflow determined from hydraulic testing in boreholes and drifts in different phases of the KBS-3H project have been 3D visualized, see Figure 4.5. The inflows at position 1, section 7 m in the short drift and at 5 m into the borehole KA16*16*A01 are probably originating from the same fracture. Position 2 was very much affected by the sealing of position 3, which could be expected considering their relationship to each other. Also Position 4 and 5 could have a hydraulic connection.

The inflow in the area has been affected by grouting and reaming of drifts, but another aspect is the withdrawal of the fracture reservoir. The withdrawal caused by the opening of the holes and drifts have caused a lowering of the pressure head and a lowering of inflows over time, which is obvious both in the short drift and in the long drift (see Chapter 3.4.9).

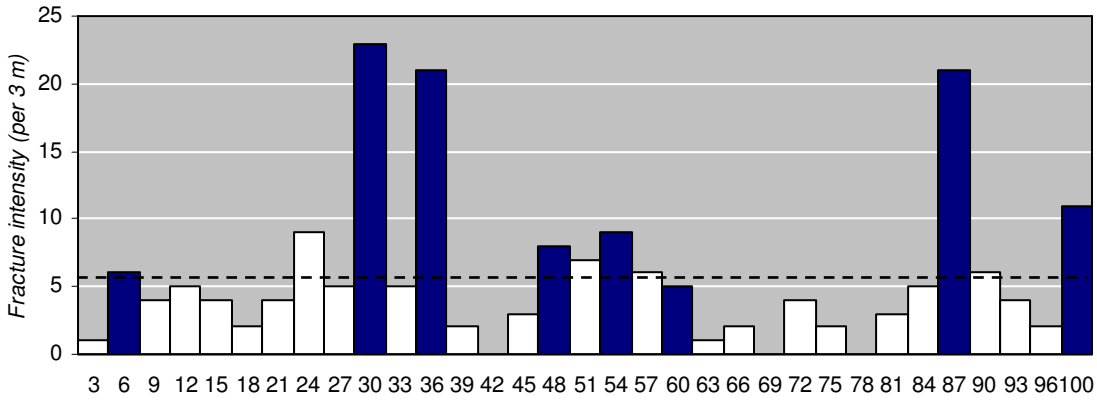

Figure 4.4 *Fracture intensity per 3 m in the 100 m long core borehole. The dashed line represents the average intensity, and the filled sections are those where inflow has been measured, in core hole or in the drift.*

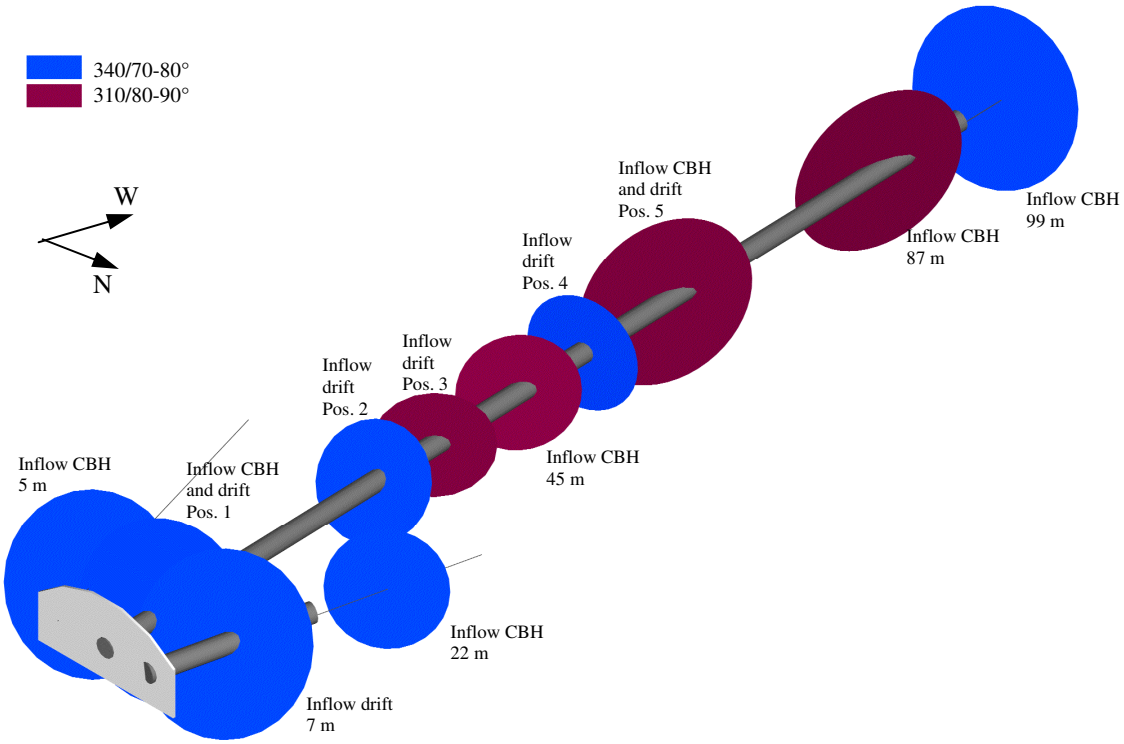

Figure 4.5 *3D-model of conductive fractures along the drifts and core boreholes. The colouring represents fracture sets, and the sizes of the discs represent the extent of the water inflow. The large discs represent fractures with a measured hydraulic aperture larger than 100 µm, the small discs represent fractures with apertures less than 100 µm.*

4.2 Sealing of the fracture system

The fracture system surrounding the two horizontal drifts has been grouted in two grouting rounds. First there was cement-based grouting of the core boreholes, and then the long drift was post-grouted in five positions using silica sol. The cement grouting lowered the total conductivity of the long core hole since three positions with larger inflows were partly or completely sealed (at 60 m, 87 m and 99 m). This reduced the flow, but the extent can only be approximated due to measurement limitations. The maximum inflow in an inflow section should though have been around 4-5 l/min. The sealing around 87 m was successful since it managed to reduce all flow in this part of the rock. The fracture intensity was rather high at this position, which indicates a fracture zone which when sealed probably limited all flow in adjacent connected fractures.

However, the pre-grouting could not seal the fractures required for reaching the inflow requirements set for the KBS-3H project of 0.1 l/min per 10 meter. The groundwater situation gives a flow situation of up to 4-5 l/min in fracture apertures less than 100 µm, which is considered to be penetrability limitation. This information could be obtained from the hydraulic tests and from Äspö HRL in general, so it would probably have been possible in beforehand to comprehend that cement-based grouting would not give sufficient sealing.

The post-grouting project with silica sol achieved a sealing of smaller fractures, which reduced the total inflow to the drift to the required levels. The inflows in the not yet grouted positions increased as the surrounding positions were grouted in the Mega-Packer project, which could be a result of increasing groundwater pressure outside of the sealed zone. As a result of the grouting, the water flow in the finer fractures increased, which shows that there will always be some residual, minor inflows. The increased inflows at 11 and 17 m could be expected due to their closeness to position 1.

The spread of grout in fractures are dependent on several aspects such as the properties of the grout, the fracture geometry and the grouting technique (Eriksson & Stille, 2005). From the flow dimension evaluation it was suggested that there is in general two-dimensional flow around the drift. For the penetration of cement grout, it would mean that the grout spread around 15-35 m in the fractures possible to penetrate. These rather long penetrations could be a problem when constructing several tunnels in each others' vicinity. During the sealing of the drift, the silica sol grout was estimated to spread 2-8 metres. The predictions of grout penetrations are affected by uncertainties regarding the real grout properties and pressure used, incorrect interpretation of fracture geometry and deformation of the rock when grouting.

5 Conclusion

The groundwater control is of great importance for the KBS-3H repository design and the planning of a repository with high utilization degree is facilitated by inflow predictions and a thorough description of the water-conducting fracture system. The evaluation of horizontal drifts at Äspö HRL has shown that some information regarding the hydrogeological conditions are possible to evaluate from basic hydraulic testing, while other parts are more difficult. Properties such as fracture intensity, fracture set orientations, hydraulic apertures and flow dimension are not hard to estimate with existing evaluation methods if the quality of the data is good. But it is more difficult to create a general picture of the whole fracture system, with an understanding of why it behaves like it does and how good and accurate predictions concerning groundwater flow can be made.

The different characterisation methods used in this project have made it possible to describe the fracture network geometry surrounding the horizontal drifts at Äspö HRL and discuss the flow characteristics and the effect of grouting. This description could be made despite inconsistent hydraulic testing, but of course some assumptions and uncertainties could have been avoided if the test programme had been more complete. Missing measurements were for example those spanning longer time periods, from which variations in inflows and groundwater pressure could be evaluated. Another important part of a test programme would be to make more detailed and easily comparable measurements, e.g. by using shorter and uniform measuring sections for water pressure tests and inflow measurements.

The attained characteristics of the fracture network geometry indicate a fracture network described as a Type I permeability structure. This means that there is poor connectivity in the system and a 2D flow should be the dominating flow dimension. The water is flowing mainly in two fracture sets with a fairly small deviation in orientation (small angle between the sets), see Figure 3.10. The fact that it was possible to drastically reduce the inflow in a 95 m long drift (almost 90 % of the inflow disappeared with the grouting) through grouting of five separate position is an indication of a fracture network with low connectivity. The current stress field was of importance for the flow characteristics in this fracture network; a majority of the largest inflow positions had orientations of approximately the same strike as the largest horizontal stress, which dilates the fractures of favourable orientations.

The transmissivities evaluated from the different hydraulic tests, such as water pressure tests and inflow measurements, were correlating well. This especially when a short, well-defined measurement section was used, such as the Mega-Packer measurement in the drift. The Pareto distributions did fit reasonably well to the transmissivity data obtained from the hydraulic tests and the inflow simulations did give reasonably good predictions of groundwater inflow to boreholes and drifts, considering the extent and quality of the input data. The coefficient of distribution, k, for Pareto distributions of the rock at Äspö seems to be in the range of 0.35 to 0.5. Using probabilistic tools is probably a good way of describing the flow in a fracture system, but it is important that the quality of the data and the accuracy of the evaluation method are satisfying.

The inflow positions and the grouting have also been investigated. It was found that there are some difficulties when determining the inflow positions in drift solely based on inflow positions in the core borehole, but the detection of inflow positions were facilitated by combining information from hydraulic tests with fracture intensity (though this gave overestimations). The two grouting sessions both affected the fracture network, but estimations implies that cement grouting only gave sufficient sealing in fractures with a hydraulic aperture larger than 100 µm, which corresponds to an inflow of around 4 l/min.

5.1 Future work

In the KBS-3H repository design there are still many design issues to consider, and the findings in this project suggests that a more consistent hydrogeology investigation programme is set up for future demonstration drifts. The test programme should be improved to generate data foremost appropriate for transmissivity distributions and inflow simulations, e.g. by using shorter measurement sections and more precise equipment.

The modelling of the hydrogeological conditions could be further developed, as well as the questions regarding the water pressure situation around the drifts. The pressure head increased around the drifts as the inflow positions were grouted, and this induced new inflow positions and caused increased flow in nearby, not sealed, structures. The extent of the pressure increase is a topic that could be of importance when constructing several underground constructions close to each other. The lowering of the pressure head over a long time span is another subject that could be interesting to investigate in detail if sufficient pressure data is available.

The interpretation of flow dimensions is a part of the project associated with uncertainties, which can be developed in future characterisations. A combination of detailed logging from grouting sessions and long duration hydraulic tests could give a more reliable description of the flow dimensions in the fracture system. Other parameters of the fracture system, such as fracture intensity and fracture frequency distributions, could be better utilized, e.g. by using them in flow simulations and modelling.

6 References

Andersson J. Berglund J. Follin S. Hakami E. Halvarson J. Hermanson J. Laaksoharju M. Rhén I. Wahlgren C-H. (2002): *Testing the methodology for site descriptive modelling: Application for the Laxemar area.* Svensk Kärnbränslehantering AB, Technical Report TR-02-19, Stockholm, Sweden.

Anttila P. Autio J. Berghäll J. Börgesson L. Eriksson M. Hagros A. Halvarsson B. Johansson E. Kotola R. Parkkinen I. Rönnqvist P-E. Sandén T. (2008): *KBS-3H Design Description 2007*. Posiva OY, Posiva 2008-01, Eurajoki, Finland, 308 pp.

Berglund J. Curtis P. Eliasson T. Ohlsson T. Starzec P. Tullborg E-L. (2003): *Update of the geological model 2002.* Svensk Kärnbränslehantering AB, International Progress Report IPR-03-34, Stockholm, Sweden, 130 pp.

Butrón C. Gustafson G. Fransson Å. Funehag J. (2009): Drip sealing of tunnels in hard rock: A new concept for the design and evaluation of permeation grouting, *Tunnelling and Underground Space Technology*, Vol. 25. Issue 2, March 2010, pp. 114-121.

Bäckblom G. Lindgren E. (2005): *KBS-3H – Excavation of two horizontal drifts at the Äspö Hard Rock Laboratory during year 2004–2005: Work description, summary of results and experience.* Svensk Kärnbränslehantering AB, Report R-05-44, Stockholm, Sweden, 87 pp.

Cox I. Gylling B. Hartley L. Hunter F. Jackson P. Joyce S. Marsic N. Swift B. (2005): *Regional hydrogeological simulations for Forsmark: Numerical modelling using CONNECTFLOW*. Svensk Kärnbränslehantering AB, Report R-05-32, Stockholm, Sweden, 254 pp.

Dershowitz W. Herda H H. (1992): *Interpretation of fracture spacing and intensity*. 33rd US Symposium on Rock Mechanics, pp. 757-766. Balakema. Rotterdam, the Netherlands.

Doe T W. Geier J E. (1991): *Interpretation of fracture system geometry using well test data.* Svensk Kärnbränslehantering AB, Stripa Project Technical report 91-03, Stockholm, Sweden

Draganovic A. (2009): *Provning av injekteringsbruk Bangårdstunneln/Citybanan*. Kungliga Tekniska Högskolan. Project PM.

Eriksson M. Lindström L. (2008): *KBS-3H post-grouting: Mega-Packer test at -220 m level at Äspö HRL.* Svensk Kärnbränslehantering AB, Report R-08-42, Stockholm, Sweden, 67 pp.

Eriksson M. Stille H. (2005): *Cementinjektering i hårt berg*. SveBeFo Rapport K22, Stockholm, Sweden.

Follin S. Hartley L. Jackson P. Joyce S. Levén J. Roberts D. Swift B. (2007): *Hydrogeological characterisation and modelling of deformation zones and*

fracture domains: Forsmark modelling stage 2.2. Svensk Kärnbränslehantering AB, Report R-07-48, Stockholm, Sweden, 240 pp.

Forssberg O. Fox A. Hermanson J. La Pointe P. (2005): *Statistical model of fractures and deformation zones - Preliminary site description, Laxemar subarea, version 1.2.* Svensk Kärnbränslehantering AB, Report R-05-45, Stockholm, Sweden, 318 pp.

Fransson Å. (2001): *Characterisation of a Fractured Rock for Grouting Using Hydrogeological Methods.* Ph. D. Thesis. Department of Geology, Chalmers University of Technology, Publ A 97, Göteborg, Sweden.

Fransson Å. (2008): *Grouting design based on characterization of the fractured rock: Presentation and demonstration of a methodology.* Svensk Kärnbränslehantering AB, Report R-08-127, Stockholm, Sweden, 24 pp.

Fransson Å. Hernqvist L. (2010): *Geology, Water Inflow Prognosis and Grout Selection for Tunnel Sealing: Case Studies from Two Tunnels in Hard Rock, Sweden.* Chalmers University of Technology, Göteborg, Sweden. *In publishing*

Funehag J. (2007): *Grouting of Fractured Rock with Silica Sol: Grouting design based on penetration length.* Ph.D. Thesis. Department of Civil and Environmental Engineering, Chalmers University of Technology, Göteborg, Sweden.

Gustafson G. (2009): *Hydrogeologi för bergbyggare*. Formas, Stockholm, Sweden.

Gustafson G. Fransson Å. (2005): The use of the Pareto distribution for fracture transmissivity assessment. *Hydrogeology Journal*, Vol. 14, No. 1-2, pp. 15-20.

Gustafson G. Stille H. (2005*): Stop criteria for cement grouting*. *Felsbau*, Vol. 23, No. 3 pp. 62-68.

Hernqvist L. (2009): *Characterization of the Fracture System in Hard Rock for Tunnel Grouting*. Licentiate Thesis. Department of Civil and Environmental Engineering, Chalmers University of Technology, Göteborg, Sweden.

Hoek E. Brown E.T. (1990): *Underground excavations in rock*. Taylor & Francis, Abingdon, UK.

Johansson Å. (2005). *KBS-3H – Rapportering av resultat vid kärnborrning, vattenförlustmätning och injektering.* SKB internal PM.

Kamb W B. (1959): Ice petrofabric observations from Blue Glacier, Washington, in relation to theory and experiment. *J. Geophys. Res*. Vol 64, pp. 1891–1909.

Kozubowski T J. Meerschaert M M. Gustafson G. (2008): A new stochastic model for fracture transmissivity assessment. *Water Resources Research*, Vol. 44, W02435, doi:10.1029/2007WR006053.

De Marsily G. (1986): *Quantitative Hydrogeology. Groundwater Hydrology for Engineers*: Academic Press, Inc., San Diego, USA, 440 pp.

Munier R. (2004): *Statistical analysis of fracture data, adapted for modelling Discrete Fracture Networks-Version 2*. Svensk Kärnbränslehantering AB, Report R-04-66, Stockholm, Sweden, 60 pp.

Nordman C. (2003): *Boremap mapping KBS-3H*. SKB internal PM .

Rhén I. Bäckblom G. Gustafson G. Stanfors R. Wikberg P. (1997): *Äspö HRL – Geoscientific evaluation 1997/2. Results from pre-investigations and detailed site characterization*. Svensk Kärnbränslehantering AB, Technical Report TR-97-03, Stockholm, Sweden.

Robin P Y F. Jowett E C. (1986): Computerized density contouring and statistical evaluation of orientation data using counting circles and continuous weighting functions. *Tectonophysics.* Vol 121 (2–4), pp. 207–223.

Smith P A. Johnson L H. Snellman M. Pastina B. Gribi P. (2007): *Safety assessment for a KBS-3H spent nuclear fuel repository at Olkiluoto - Evolution report*. Svensk Kärnbränslehantering AB, Report R-08-37, Stockholm, Sweden.

Snow D T. (1968): Rock fracture spacings, openings and porosities. *Journal of the Soil Mechanics and Foundation Division, Proceedings of the American Society of Civil Engineers*, Vol. 94, pp 73-91.

Starzec P. (2001): *Characterisation and Modeling of Discontinuous Rock Mass.* Ph. D. Thesis. Department of Geology, Chalmers University of Technology, Göteborg, Sweden.

Stille B. Stille H. Gustafson G. Kobayashi S. (2009): Experience with the real time grouting control method. *Geomechanics and Tunnelling.* Vol. 2:5, pp. 447-459.

Talbot C J. Sirat M. (2001): Stress control of hydraulic conductivity in fracture-saturated Swedish bedrock. *Engineering Geology*, Vol. 61, Issues 2-3, pp. 145-153.

Vidstrand P. Ericsson L O. (2008): *A compilation of size-dependent fracture transmissivity*. IAHR, International Groundwater Symposium, June 18-20 2008. Istanbul, Turkey.

Contents - Appendices

A Evaluation of pre-investigation data

This appendix contains the evaluations performed on the data obtained in the pre-investigation of the KBS-3H project site at the 220 m-level at Äspö HRL. The evaluations concern:

1. Fracture intensity based on core mapping, with cumulative frequencies of the fracture data, compared to a fitted negative binomial distribution.

2. Visualisations of the mapped fractures, with investigations of intensities of interpreted fracture sets.

3. Transmissivity and hydraulic apertures in sections of boreholes based on inflow measurements and water pressure tests.

4. Distribution of transmissivities, represented with lognormal and Pareto distributions.

5. Penetration of cementitious grout, and transmissivity distribution after grouting.

The methods used for the evaluation are described in Chapter 2.

A.1 Fracture intensity in boreholes

The mapping of the core boreholes in 2003 was performed using both core mapping and BIPS images. Properties of the fractures, such as orientations and positions were investigated, as well as categorisation into open or sealed fractures. The fracture data from the boreholes has been divided into 3 m-sections, see Table A.1, with a total of 286 fractures and 156 open fractures.

Next, the frequency of the number of fractures per 3 m-section was determined and a negative binomial distribution was fitted to the fracture frequency data; see Table A.2 and Figure A.1. There are a total of 286 fractures, distributed in 53 3 m-sections. The calculated average is 5.4 fractures per section, and the standard deviation is 5.2.

Table A.1 Compilation of fracture data in 3 m sections. Based on data from delivery SICADA-10-033.

KA1619A01			KA1621A01			KA1616A01		
Section [m]	All fractures	Open fractures	Section [m]	All fractures	Open fractures	Section [m]	All fractures	Open fractures
0-3	1	1	0-3	9	5	0-3	8	6
3-6	6	5	3-6	14	5	3-6	8	3
6-9	4	3	6-9	2	1	6-9	4	2
9-12	5	5	9-12	0	0	9-12	2	1
12-15	4	4	12-15	2	2	12-15	1	1
15-18	2	2	15-18	2	1	15-18	7	3
18-21	4	3	18-21	0	0	18-21	0	0
21-24	9	5	21-24	4	3	21-24	14	5
24-27	5	2	24-27	6	2	24-27	5	1
27-30	23	8	27-30	5	1	27-30	3	0
30-33	5	1						
33-36	21	14						
36-39	2	1						
39-42	0	0						
42-45	3	3						
45-48	8	2						
48-51	7	3						
51-54	9	8						
54-57	6	3						
57-60	5	4						
60-63	1	1						
63-66	2	1						
66-69	0	0						
69-72	4	3						
72-75	2	0						
75-78	0	0						
78-81	3	2						
81-84	5	1						
84-87	21	13						
87-90	6	3						
90-93	4	2						
93-96	2	2						
96-100	11	9						

Appendix A

Table A.2 Frequency data for a negative binomial distribution of fractures.

Number of fracture/3m	Section frequency data	Cumulative section data	Nbiom distribution	Nbiom section frequency distr.	Nbiom cumulative section distr.
0	6	6	0.1036	5.490	5.490
1	3	9	0.1211	6.418	11.908
2	9	18	0.1180	6.253	18.160
3	3	21	0.1073	5.686	23.846
4	7	28	0.0941	4.986	28.832
5	7	35	0.0807	4.275	33.107
6	4	39	0.0681	3.610	36.717
7	2	41	0.0569	3.015	39.732
8	3	44	0.0471	2.497	42.229
9	3	47	0.0388	2.054	44.283
10	0	47	0.0317	1.681	45.964
11	1	48	0.0259	1.370	47.335
12	0	48	0.0210	1.113	48.447
13	0	48	0.0170	0.901	49.348
14	2	50	0.0137	0.727	50.075
15	0	50	0.0110	0.586	50.660
16	0	50	0.0089	0.471	51.131
17	0	50	0.0071	0.378	51.509
18	0	50	0.0057	0.303	51.812
19	0	50	0.0046	0.242	52.054
20	0	50	0.0036	0.193	52.247
21	2	52	0.0029	0.154	52.402
22	0	52	0.0023	0.123	52.525
23	1	53	0.0018	0.098	52.623
24	0	53	0.0015	0.078	52.701
25	0	53	0.0012	0.062	52.763

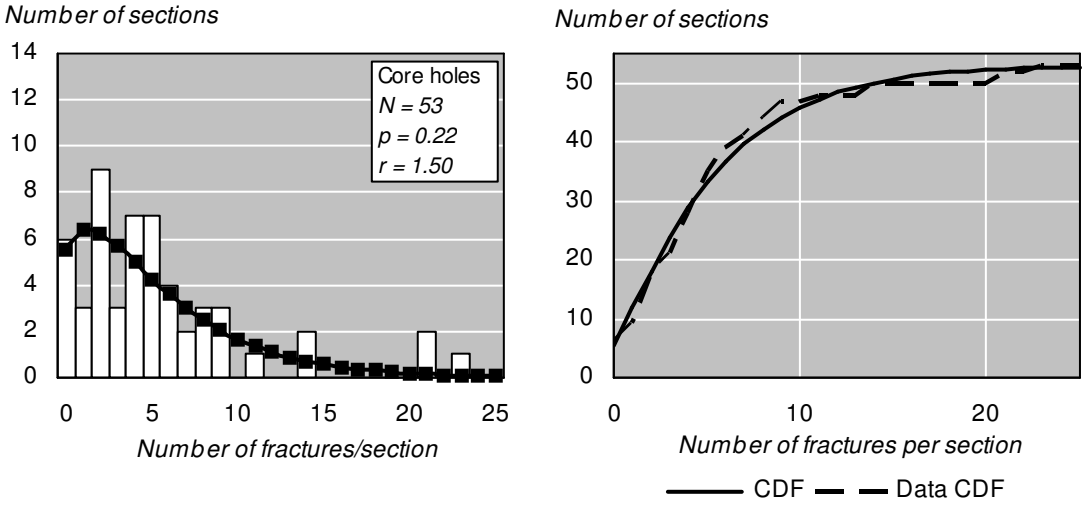

Figure A.1 Left: Frequency diagram for the number of fractures per 3 m-section in boreholes KA1616A01, KA1619A01 and KA1621A01, and a negative binomial distribution fitted to the data. Total number of fractures is 286. Right: The cumulative distribution function, CDF in comparison with cumulative data.

A.2 Fracture orientations

The fractures along the core boreholes were mapped in 2003, and a total of 286 fractures were orientated. These have been visualized in sterographic equal-area projections (Schmidt nets), created in the software GeoPlot. The visualisation has been performed using all fractures, and only open fractures, see Figure A.2.

Nordman (2003) interpreted two fracture sets from the open fracture data: 310/80-90° and 25/80°. The fractures identified within the sets are presented in Table A.3 and Table A.4, with information of orientation and position. The positions of the fractures belonging to these fracture sets are illustrated in Figure A.3. Fracture frequency diagrams and cumulative distribution functions for these sets are shown in Figure A.5 and Figure A.4.

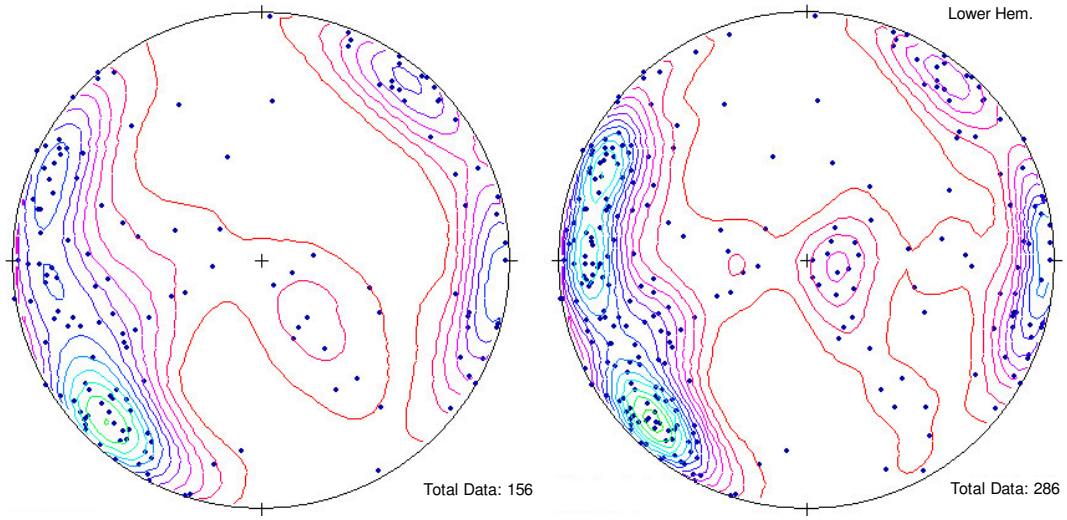

Figure A.2 *Stereo plots showing the orientation of fractures along the three cored boreholes. Left: Open fractures (N=156). Right: All fractures mapped (N=286).*

Table A.3 *The open fractures identified within fracture set 25/80º, with information of orientation and observation point.*

No.	Borehole	Borehole position [m]	Strike	Dip	No.	Borehole	Borehole position [m]	Strike	Dip
1	1616	0.095	193.9	75.3	18	1619	56.521	27.7	87.9
2	1616	0.179	195.6	87.9	19	1619	56.915	28.6	81.6
3	1616	0.201	197.9	76.2	20	1619	80.269	25.0	81.1
4	1616	26.160	24.2	69.7	21	1619	86.126	203.6	86.5
5	1619	17.192	208.9	85.0	22	1619	86.395	6.5	78.0
6	1619	31.228	29.7	78.6	23	1619	87.121	205.7	78.2
7	1619	35.364	23.1	84.4	24	1619	90.472	210.3	89.4
8	1619	35.627	18.1	77.0	25	1621	5.973	194.8	88.1
9	1619	35.962	28.2	79.9	26	1621	12.239	194.9	87.9
10	1619	36.190	30.8	71.9	27	1621	30.052	195.4	87.6
11	1619	36.217	14.5	84.1					
12	1619	36.267	13.0	79.5					
13	1619	38.918	20.6	80.3					
14	1619	53.232	25.6	89.5					
15	1619	53.323	12.5	81.4					
16	1619	53.380	31.3	84.1					
17	1619	56.396	25.4	81.3					

Table A.4 The open fractures identified within fracture set 310/80º, with information of orientation and observation point.

No.	Borehole	Borehole position [m]	Strike	Dip	No.	Borehole	Borehole position [m]	Strike	Dip
1	1616	13.998	132.0	88.6	24	1619	34.944	309.0	77.1
2	1616	6.913	144.1	85.7	25	1619	46.382	316.2	87.8
3	1616	6.918	320.3	83.5	26	1619	46.675	318.0	84.9
4	1616	22.132	307.1	79.2	27	1619	49.621	135.2	88.0
5	1616	23.340	317.9	66.7	28	1619	49.929	316.8	86.1
6	1619	2.956	325.8	86.7	29	1619	50.701	311.9	77.0
7	1619	10.158	298.5	80.3	30	1619	53.400	330.2	89.5
8	1619	14.879	316.6	69.5	31	1619	60.329	297.3	89.3
9	1619	14.899	125.4	85.7	32	1619	60.377	297.5	87.0
10	1619	15.116	138.1	86.0	33	1619	60.469	317.7	83.5
11	1619	15.118	137.6	85.3	34	1619	61.065	301.1	85.1
12	1619	18.335	144.0	72.7	35	1619	63.751	322.5	83.2
13	1619	18.478	129.2	76.7	36	1619	71.954	303.1	72.0
14	1619	19.880	126.0	77.9	37	1619	85.362	301.4	74.2
15	1619	20.172	123.7	89.4	38	1619	85.656	301.0	79.0
16	1619	21.466	131.1	87.9	39	1621	5.750	324.6	74.7
17	1619	21.714	318.4	70.4	40	1621	17.164	127.0	76.2
18	1619	22.063	124.4	73.9	41	1621	21.184	317.6	74.9
19	1619	22.064	311.3	87.9	42	1621	21.235	322.6	75.1
20	1619	22.660	305.8	89.1	43	1621	23.119	314.6	75.2
21	1619	24.894	313.7	56.5	44	1621	25.523	131.6	74.6
22	1619	25.679	310.6	68.7	45	1621	26.749	308.4	74.6
23	1619	34.912	307.9	81.3					

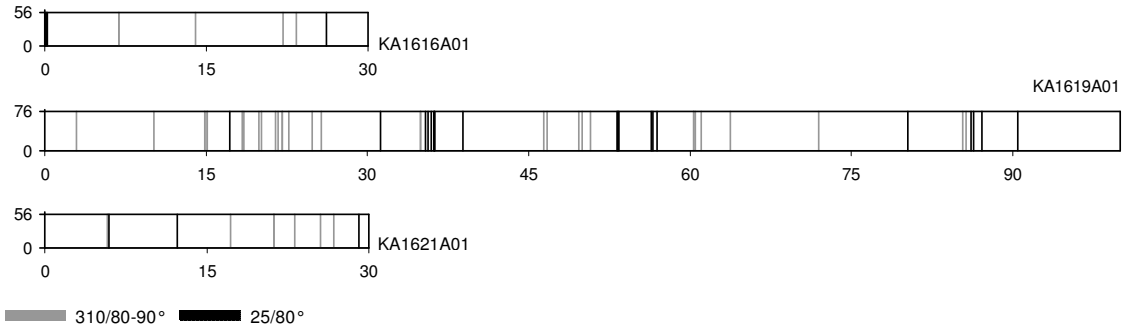

Figure A.3 Illustration of the open fractures belonging to the interpreted fracture sets, along the core boreholes.

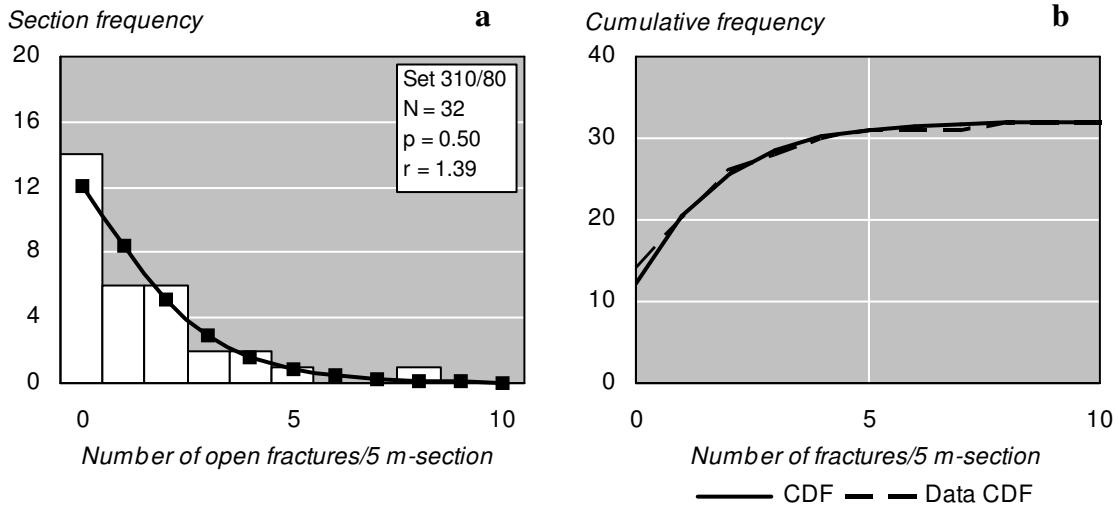

*Figure A.4 Frequency diagrams in 5 m-sections for fractures belong to interpreted fracture sets, with negative binomial distributions fitted to the data (black lines). **a**: frequency diagrams and **b**: CDF for set 310/80º.*

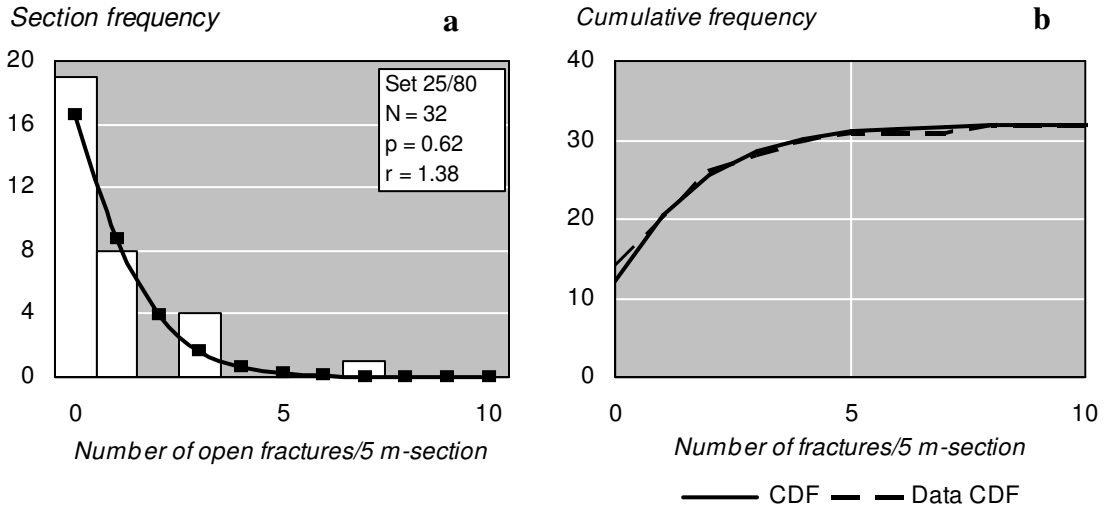

Figure A.5 *Frequency diagrams in 5 m-sections for fractures belong to interpreted fracture sets, with negative binomial distributions fitted to the data (black lines).* ***a****: Frequency diagram and* ***b****: CDF for set 25/80º.*

A.3 Transmissivity and hydraulic aperture

The hydraulic tests performed in the core boreholes during the pre-investigation consisted of inflow measurements in 3 m-intervals and water pressure tests in 5 m-intervals in parts of the core boreholes. The calculation of the transmissivity and the hydraulic apertures, based on the inflow measurements, are performed using the following input data:

Hydraulic head =158 m
g = 9.81 m/s^2
μ = 0.001308 N s/m^2
r = 998 kg/m^3
r_{w1} = 0.028 m, r_{w2} = 0.038 m

The corresponding estimations from water pressure tests are based on following:
Hydraulic head: 158 m
Overpressure: 1 MPa = 98 m
Length of section: 5 m
r_{w1}: 0.028 m, r_{w2}: 0.038 m
R_0 = 100 x r_w
g = 9.81 m/s^2
μ = 0.001308 N s/m^2
ρ = 998 kg/m^3

The correlation between the hydraulic apertures obtained from these to data sets are shown in Table A.5 and Figure A.6.

Table A.5 Correlation between hydraulic apertures based on water inflow measurements and WPTs in corresponding sections.

Borehole [-]	Section [m]	*b* [µm] (Inflow, *Q/dh*)	*b* [µm] (WPT, Thiem)
KA1621A01	20-25	60	62
KA1616A01	3-6	123	43
	20-25	0	76
	25-30	0	71
KA1619A01	96-100	172	157
	90-95	0	34

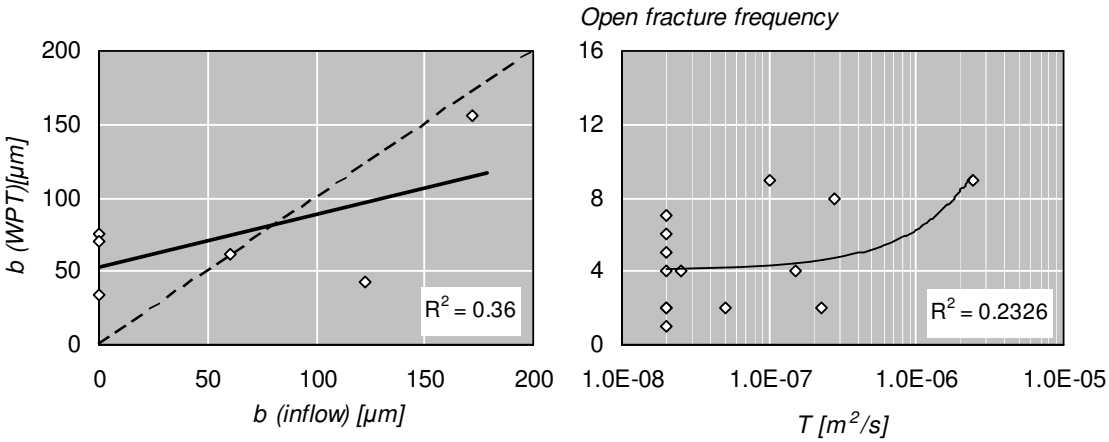

Figure A.6 Left: Aperture correlation based on values in Table A.5, with the squared correlation coefficient, R^2. Right: Correlation of the open fracture frequency and the calculated transmissivity based on WPT.

A.4 Transmissivity distributions

The transmissivities evaluated from the water pressure tests in 5 m-sections, and inflow measurements in 3 m-sections along the core boreholes, have been used to derive statistical distributions of the transmissivity in the rock.

Lognormal distribution

A lognormal distribution has been fitted to the WPT transmissivity data. The data used in the evaluation is truncated; 50 % of the values in the lower measurement interval is missing since the measurement limit was around $2 \cdot 10^{-8}$ m^2/s. Some assumptions of geometric mean and standard deviation are therefore made, see Chapter 2. Three boreholes were used in the calculations with a total of 14 measured sections of which 7 had water losses. It is assumed that each section has one fracture conducting the water.

The resulting parameters, used to calculate the lognormal distribution, are T_{50} = *2.25E-08*, T_{84} = *2.18E-07*. The result is presented in Table A.6 and Figure A.7. The median of the distribution, $T_{50,distr}$, is $2.29 \cdot 10^{-8}$ m^2/s. The transmissivity distribution derived corresponds to inflows between 0.01 and 4.9 l/min, in total 5.0 l/min. The actual flow in these 14 sections was 42.3 l/min.

Table A.6 Measured transmissivities and calculated lognormal distribution with corresponding flow, based on WPT transmissivities.

i	Measured transmissivity [m^2/s]	$p\ (T \leq T_i) = n_i/(N+1)$	Calculated log inv. [m^2/s]	Corresponding inflow [l/min]
1	2.00E-08	0.07	7.39E-10	0.01
2	2.00E-08	0.13	1.80E-09	0.01
3	2.00E-08	0.20	3.31E-09	0.02
4	2.00E-08	0.27	5.45E-09	0.04
5	2.00E-08	0.33	8.43E-09	0.06
6	2.00E-08	0.40	1.26E-08	0.09
7	2.00E-08	0.47	1.86E-08	0.13
8	2.49E-08	0.53	2.72E-08	0.19
9	4.98E-08	0.60	4.00E-08	0.29
10	9.96E-08	0.67	5.98E-08	0.43
11	1.49E-07	0.73	9.26E-08	0.66
12	2.24E-07	0.80	1.52E-07	1.09
13	2.74E-07	0.87	2.81E-07	2.01
14	2.39E-06	0.93	6.82E-07	4.88

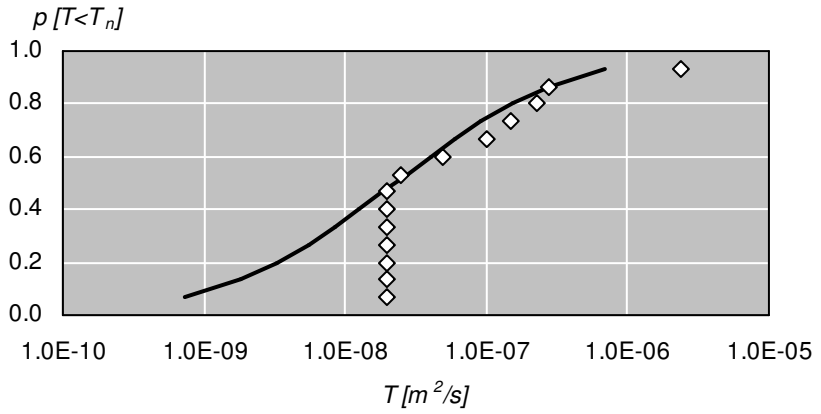

Figure A.7 WPT transmissivity values with a fitted lognormal distribution.

Appendix A

Pareto distribution

A fracture transmissivity distribution has also been obtained with the Pareto distribution (see Chapter 2). From this distribution was also a Pareto distribution of fracture apertures derived. The measured data set of transmissivities from water inflow measurements in the core boreholes have been used to simulate 114 open fractures mapped in KA16*19*A01 (see Table A.7). The distribution parameter *k* was evaluated from a linear trend-line fitted by the least square method to the dataset in a log-log plot, and was evaluated to 0.3701. The corresponding distribution of inflow from these 114 open fractures can be seen in Table A.7; the total simulated inflow is 41.4 l/min.

Table A.7 Simulated transmissivities and hydraulic apertures with corresponding inflow for 114 open fractures along KA1619A01, based on inflow measurements.

r	*1-p*	T_n	*b* [mm]	*Q* [l/min]	*r*	*1-p*	T_n	*b* [mm]	*Q* [l/min]
1	0.991	4.54E-06	0.194	3.25E+01	58	0.496	7.81E-11	0.005	5.59E-04
2	0.983	6.98E-07	0.104	4.99E+00	59	0.487	7.46E-11	0.005	5.33E-04
3	0.974	2.34E-07	0.072	1.67E+00	60	0.478	7.13E-11	0.005	5.10E-04
4	0.965	1.07E-07	0.056	7.67E-01	61	0.470	6.82E-11	0.005	4.87E-04
5	0.957	5.87E-08	0.045	4.20E-01	62	0.461	6.52E-11	0.005	4.66E-04
6	0.948	3.59E-08	0.039	2.57E-01	63	0.452	6.25E-11	0.005	4.47E-04
7	0.939	2.37E-08	0.034	1.69E-01	64	0.443	5.99E-11	0.005	4.28E-04
8	0.930	1.65E-08	0.030	1.18E-01	65	0.435	5.74E-11	0.005	4.11E-04
9	0.922	1.20E-08	0.027	8.58E-02	66	0.426	5.51E-11	0.004	3.94E-04
10	0.913	9.03E-09	0.024	6.45E-02	67	0.417	5.29E-11	0.004	3.78E-04
11	0.904	6.98E-09	0.022	4.99E-02	68	0.409	5.08E-11	0.004	3.63E-04
12	0.896	5.52E-09	0.021	3.94E-02	69	0.400	4.89E-11	0.004	3.49E-04
13	0.887	4.44E-09	0.019	3.18E-02	70	0.391	4.70E-11	0.004	3.36E-04
14	0.878	3.64E-09	0.018	2.60E-02	71	0.383	4.52E-11	0.004	3.23E-04
15	0.870	3.02E-09	0.017	2.16E-02	72	0.374	4.36E-11	0.004	3.11E-04
16	0.861	2.54E-09	0.016	1.81E-02	73	0.365	4.20E-11	0.004	3.00E-04
17	0.852	2.15E-09	0.015	1.54E-02	74	0.357	4.04E-11	0.004	2.89E-04
18	0.843	1.84E-09	0.014	1.32E-02	75	0.348	3.90E-11	0.004	2.79E-04
19	0.835	1.59E-09	0.014	1.14E-02	76	0.339	3.76E-11	0.004	2.69E-04
20	0.826	1.39E-09	0.013	9.92E-03	77	0.330	3.63E-11	0.004	2.60E-04
21	0.817	1.22E-09	0.012	8.69E-03	78	0.322	3.51E-11	0.004	2.51E-04
22	0.809	1.07E-09	0.012	7.67E-03	79	0.313	3.39E-11	0.004	2.42E-04
23	0.800	9.51E-10	0.012	6.80E-03	80	0.304	3.28E-11	0.004	2.34E-04
24	0.791	8.48E-10	0.011	6.06E-03	81	0.296	3.17E-11	0.004	2.27E-04
25	0.783	7.59E-10	0.011	5.43E-03	82	0.287	3.06E-11	0.004	2.19E-04
26	0.774	6.83E-10	0.010	4.88E-03	83	0.278	2.97E-11	0.004	2.12E-04
27	0.765	6.17E-10	0.010	4.41E-03	84	0.270	2.87E-11	0.004	2.05E-04
28	0.757	5.59E-10	0.010	4.00E-03	85	0.261	2.78E-11	0.004	1.99E-04
29	0.748	5.08E-10	0.009	3.63E-03	86	0.252	2.69E-11	0.004	1.93E-04
30	0.739	4.64E-10	0.009	3.32E-03	87	0.243	2.61E-11	0.003	1.87E-04
31	0.730	4.25E-10	0.009	3.04E-03	88	0.235	2.53E-11	0.003	1.81E-04
32	0.722	3.90E-10	0.009	2.79E-03	89	0.226	2.46E-11	0.003	1.76E-04
33	0.713	3.59E-10	0.008	2.56E-03	90	0.217	2.38E-11	0.003	1.70E-04
34	0.704	3.31E-10	0.008	2.36E-03	91	0.209	2.31E-11	0.003	1.65E-04
35	0.696	3.06E-10	0.008	2.19E-03	92	0.200	2.25E-11	0.003	1.61E-04
36	0.687	2.83E-10	0.008	2.03E-03	93	0.191	2.18E-11	0.003	1.56E-04
37	0.678	2.63E-10	0.008	1.88E-03	94	0.183	2.12E-11	0.003	1.52E-04
38	0.670	2.45E-10	0.007	1.75E-03	95	0.174	2.06E-11	0.003	1.47E-04
39	0.661	2.28E-10	0.007	1.63E-03	96	0.165	2.00E-11	0.003	1.43E-04
40	0.652	2.13E-10	0.007	1.52E-03	97	0.157	1.95E-11	0.003	1.39E-04
41	0.643	1.99E-10	0.007	1.43E-03	98	0.148	1.89E-11	0.003	1.35E-04
42	0.635	1.87E-10	0.007	1.34E-03	99	0.139	1.84E-11	0.003	1.32E-04
43	0.626	1.75E-10	0.007	1.25E-03	100	0.130	1.79E-11	0.003	1.28E-04
44	0.617	1.65E-10	0.006	1.18E-03	101	0.122	1.75E-11	0.003	1.25E-04
45	0.609	1.55E-10	0.006	1.11E-03	102	0.113	1.70E-11	0.003	1.22E-04
46	0.600	1.46E-10	0.006	1.04E-03	103	0.104	1.66E-11	0.003	1.18E-04
47	0.591	1.38E-10	0.006	9.86E-04	104	0.096	1.61E-11	0.003	1.15E-04
48	0.583	1.30E-10	0.006	9.31E-04	105	0.087	1.57E-11	0.003	1.12E-04
49	0.574	1.23E-10	0.006	8.81E-04	106	0.078	1.53E-11	0.003	1.10E-04
50	0.565	1.17E-10	0.006	8.34E-04	107	0.070	1.49E-11	0.003	1.07E-04
51	0.557	1.11E-10	0.006	7.91E-04	108	0.061	1.46E-11	0.003	1.04E-04
52	0.548	1.05E-10	0.006	7.50E-04	109	0.052	1.42E-11	0.003	1.02E-04
53	0.539	9.97E-11	0.005	7.13E-04	110	0.043	1.39E-11	0.003	9.91E-05
54	0.530	9.48E-11	0.005	6.78E-04	111	0.035	1.35E-11	0.003	9.67E-05
55	0.522	9.02E-11	0.005	6.45E-04	112	0.026	1.32E-11	0.003	9.44E-05
56	0.513	8.59E-11	0.005	6.14E-04	113	0.017	1.29E-11	0.003	9.21E-05
57	0.504	8.19E-11	0.005	5.85E-04	114	0.009	1.26E-11	0.003	9.00E-05

A.5 Pre-grouting in boreholes

Pre-grouting of the three core boreholes was performed in March 2004, using cementitious grout. It was assumed that the grout only filled the two shorter boreholes, and hence the grouting evaluation only concerns the long borehole where grout spread into fractures in all three grouting sections. The injected volumes in KA1619A01 are presented in Table A.8.

Table A.8 Injected volumes of grout in KA1619A01.

Section [m]	Pressure [MPa]	Total volume [l]	Penetration volume [l]
0-35	3.78	554	395
35-70	3.79	523	364
70-100	3.83	1069	933

The input for the calculation of grout spread in the three fractures larger than 100 µm is presented below and in Table A.9.

Grouting pressure: 2 MPa
W/C =1.47 *W/C* =1.55
τ_0: 1 Pa τ_0: 1 Pa
μ_g: 0.01 Pas μ_g: 0.01 Pas

Table A.9 Estimated penetration of the cement grouting performed in the 100 m core borehole. Only the three fractures with a hydraulic aperture larger than 100 µm are evaluated.

Inflow section	*b* [µm]	W/C-ratio	t_0 [min]	Grouting time, *t* [min]	l_{1D} [m]	l_{2D} [m]
60 m	180	1.47	2000	82	59	32
86 m (grout I)	107	1.47	2000	101	38	21
86 m (grout II)	107	1.55	2000	66	32	18
99 m (grout I)	194	1.47	2000	101	69	38
99 m (grout II)	194	1.55	2000	66	58	32

Control hole

The control borehole was drilled to be able to evaluate the performance of the cement grouting. The transmissivity of the sections in the 96 m-long hole have been evaluated from the WPT conducted after grouting. The evaluation is based on the following input and the result can be seen in Chapter 3.

Hydraulic head: 158 m
Overpressure: 1 MPa = 98 m
Length of section: 5 m
r_{w2}: 0.038 m
R_0 = 100 x r_w
g = 9.81 m/s^2
μ = 0.001308 N s/m^2
ρ = 998 kg/m^3

A transmissivity distribution of the values obtained from the WTP has been made using the Pareto statistical distribution; see Table A.10, Figure A.8. The distribution parameter, k is 0.7212, and the largest hydraulic aperture is 100 µm. The total simulated inflow is 13.7 l/min.

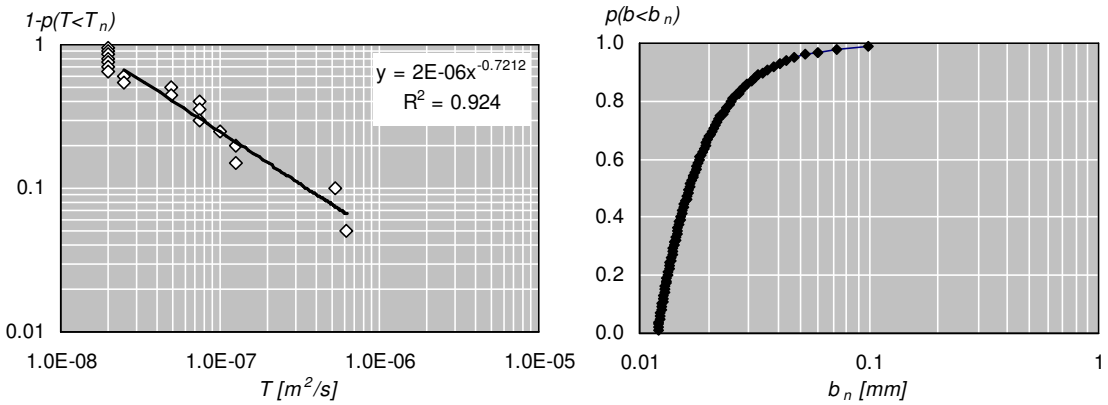

Figure A.8 *Left: Pareto distribution from fracture transmissivity data of the control hole (from WPT). Right: Cumulative distribution plot of simulated hydraulic apertures.*

Table A.10 *Simulated transmissivities and hydraulic apertures with corresponding inflow for 98 open fractures along the control hole.*

r	*1-p*	T_n	*b* [mm]	*Q* [l/min]	*r*	*1-p*	T_n	*b* [mm]	*Q* [l/min]
1	0.990	6.23E-07	0.100	4.75E+00	50	0.495	2.75E-09	0.016	2.09E-02
2	0.980	2.38E-07	0.073	1.82E+00	51	0.485	2.67E-09	0.016	2.04E-02
3	0.970	1.36E-07	0.060	1.04E+00	52	0.475	2.60E-09	0.016	1.98E-02
4	0.960	9.11E-08	0.053	6.95E-01	53	0.465	2.53E-09	0.016	1.93E-02
5	0.949	6.69E-08	0.048	5.10E-01	54	0.455	2.47E-09	0.016	1.88E-02
6	0.939	5.19E-08	0.044	3.96E-01	55	0.444	2.41E-09	0.016	1.83E-02
7	0.929	4.19E-08	0.041	3.20E-01	56	0.434	2.35E-09	0.016	1.79E-02
8	0.919	3.48E-08	0.038	2.66E-01	57	0.424	2.29E-09	0.015	1.75E-02
9	0.909	2.96E-08	0.036	2.26E-01	58	0.414	2.23E-09	0.015	1.70E-02
10	0.899	2.56E-08	0.034	1.95E-01	59	0.404	2.18E-09	0.015	1.66E-02
11	0.889	2.24E-08	0.033	1.71E-01	60	0.394	2.13E-09	0.015	1.63E-02
12	0.879	1.99E-08	0.032	1.51E-01	61	0.384	2.08E-09	0.015	1.59E-02
13	0.869	1.78E-08	0.031	1.36E-01	62	0.374	2.04E-09	0.015	1.55E-02
14	0.859	1.60E-08	0.030	1.22E-01	63	0.364	1.99E-09	0.015	1.52E-02
15	0.848	1.46E-08	0.029	1.11E-01	64	0.354	1.95E-09	0.015	1.49E-02
16	0.838	1.33E-08	0.028	1.02E-01	65	0.343	1.91E-09	0.015	1.45E-02
17	0.828	1.23E-08	0.027	9.34E-02	66	0.333	1.87E-09	0.014	1.42E-02
18	0.818	1.13E-08	0.026	8.63E-02	67	0.323	1.83E-09	0.014	1.39E-02
19	0.808	1.05E-08	0.026	8.01E-02	68	0.313	1.79E-09	0.014	1.37E-02
20	0.798	9.78E-09	0.025	7.46E-02	69	0.303	1.76E-09	0.014	1.34E-02
21	0.788	9.14E-09	0.024	6.97E-02	70	0.293	1.72E-09	0.014	1.31E-02
22	0.778	8.57E-09	0.024	6.53E-02	71	0.283	1.69E-09	0.014	1.29E-02
23	0.768	8.06E-09	0.023	6.14E-02	72	0.273	1.66E-09	0.014	1.26E-02
24	0.758	7.60E-09	0.023	5.79E-02	73	0.263	1.62E-09	0.014	1.24E-02
25	0.747	7.18E-09	0.023	5.47E-02	74	0.253	1.59E-09	0.014	1.22E-02
26	0.737	6.80E-09	0.022	5.18E-02	75	0.242	1.56E-09	0.014	1.19E-02
27	0.727	6.45E-09	0.022	4.92E-02	76	0.232	1.54E-09	0.014	1.17E-02
28	0.717	6.13E-09	0.021	4.68E-02	77	0.222	1.51E-09	0.013	1.15E-02
29	0.707	5.84E-09	0.021	4.45E-02	78	0.212	1.48E-09	0.013	1.13E-02
30	0.697	5.57E-09	0.021	4.25E-02	79	0.202	1.46E-09	0.013	1.11E-02
31	0.687	5.33E-09	0.020	4.06E-02	80	0.192	1.43E-09	0.013	1.09E-02
32	0.677	5.10E-09	0.020	3.89E-02	81	0.182	1.41E-09	0.013	1.07E-02
33	0.667	4.88E-09	0.020	3.72E-02	82	0.172	1.38E-09	0.013	1.05E-02
34	0.657	4.69E-09	0.020	3.57E-02	83	0.162	1.36E-09	0.013	1.04E-02
35	0.646	4.50E-09	0.019	3.43E-02	84	0.152	1.34E-09	0.013	1.02E-02
36	0.636	4.33E-09	0.019	3.30E-02	85	0.141	1.32E-09	0.013	1.00E-02
37	0.626	4.17E-09	0.019	3.18E-02	86	0.131	1.29E-09	0.013	9.87E-03
38	0.616	4.02E-09	0.019	3.06E-02	87	0.121	1.27E-09	0.013	9.71E-03
39	0.606	3.87E-09	0.018	2.95E-02	88	0.111	1.25E-09	0.013	9.56E-03
40	0.596	3.74E-09	0.018	2.85E-02	89	0.101	1.23E-09	0.013	9.41E-03
41	0.586	3.61E-09	0.018	2.76E-02	90	0.091	1.22E-09	0.012	9.26E-03
42	0.576	3.50E-09	0.018	2.67E-02	91	0.081	1.20E-09	0.012	9.12E-03
43	0.566	3.38E-09	0.018	2.58E-02	92	0.071	1.18E-09	0.012	8.99E-03
44	0.556	3.28E-09	0.017	2.50E-02	93	0.061	1.16E-09	0.012	8.85E-03
45	0.545	3.18E-09	0.017	2.42E-02	94	0.051	1.14E-09	0.012	8.72E-03
46	0.535	3.08E-09	0.017	2.35E-02	95	0.040	1.13E-09	0.012	8.60E-03
47	0.525	2.99E-09	0.017	2.28E-02	96	0.030	1.11E-09	0.012	8.47E-03
48	0.515	2.91E-09	0.017	2.21E-02	97	0.020	1.10E-09	0.012	8.35E-03
49	0.505	2.82E-09	0.017	2.15E-02	98	0.010	1.08E-09	0.012	8.23E-03

B Evaluation of data from Mega-Packer project

This appendix includes the evaluations performed on the data obtained during the excavation and post-grouting of the horizontal drifts at the KBS-3H project site at the 220 m level at Äspö HRL. The methods used for the evaluation are further described in Chapter 2. The evaluations concerns:

1. Fracture- and surface intensity based on tunnel mapping.

2. Transmissivity and hydraulic aperture of the five positions, based on the data obtained from pressure build-up tests.

3. Pareto distribution for the 92 water-conducting fractures in the drift.

4. Dimensionality analysis using PBT data and loggings from the grouting sessions.

5. Penetration of silica sol.

B.1 Fracture intensity from tunnel mapping

The fractures mapped in the two drifts have been sorted into 3 m sections with information of the length of the traces, see Table B.1. From this compilation, evaluation of fracture frequency in 3 m sections (fitted to a negative binomial distribution) was performed (Table B.2 and Figure B.1). The fracture trace length distribution can be seen in Table B.3 and Figure B.2.

Table B.1 Compilation of fracture data in 3 m sections of the two drifts. Based on data from SICADA.

	DA1619A02				DA1622A01				
[m]	All fractures	Length: fracture traces	Water cond. fractures	Length: water fracture traces	[m]	All fractures	Length: fracture traces	Water cond. fractures	Length: water fracture traces
0-3	12	31.68	0	0	0-3	19	39.63	0	0
3-6	10	35.3	1	2.43	3-6	23	47.43	9	24.74
6-9	28	51.11	1	6.31	6-9	25	29.88	18	12.41
9-12	7	16.79	2	15.53	9-12	18	30.07	1	3.90
12-15	12	38.95	4	13.22	12-15	16	42.35	5	10.59
15-18	11	41.17	7	32.69					
18-21	19	67.46	2	19.12					
21-24	11	40.03	2	6.2					
24-27	18	36.65	0	0					
27-30	29	51.84	2	8.6					
30-33	32	72.7	7	21.62					
33-36	18	45.51	6	19.25					
36-39	11	30.22	4	12.01					
39-42	10	17.82	3	10.49					
42-45	7	22.84	2	4.43					
45-48	33	43.99	12	15.91					
48-51	29	60.43	3	7.09					
51-54	12	30.31	3	13.66					
54-57	14	32.70	1	1					
57-60	17	39.98	2	7.79					
60-63	11	25.36	2	7.81					
63-66	3	25.02	2	16.5					
66-69	5	15.65	1	2.08					
69-72	18	50.81	1	9.86					
72-75	15	48.33	5	6.56					
75-78	14	41.92	0	0					
78-81	17	38.35	2	12.5					
81-84	23	78.74	3	5.92					
84-87	68	32.79	1	1.03					
87-90	46	65.47	3	13.77					
90-93	21	55.39	8	12.8					
93-95	10	15.21	0	0					

Table B.2 Water-conducting fracture frequency of all 3 m-sections in the drifts.

Number of fracture/3 m	Section frequency data	Cumulative section data	Nbiom distribution	Nbiom section frequency distr.	Nbiom cumulative section distr.
0	5	5	0.17311	6.4052	6.405
1	7	12	0.17724	6.5580	12.963
2	9	21	0.15250	5.6425	18.606
3	5	26	0.12290	4.5473	23.153
4	2	28	0.09570	3.5409	26.694
5	2	30	0.07295	2.6993	29.393
6	1	31	0.05482	2.0283	31.421
7	2	33	0.04077	1.5083	32.930
8	1	34	0.03008	1.1128	34.043
9	1	35	0.02205	0.8160	34.859
10	0	35	0.01609	0.5954	35.454
11	0	35	0.01169	0.4326	35.887
12	1	36	0.00847	0.3133	36.200
13	0	36	0.00611	0.2262	36.426
14	0	36	0.00440	0.1630	36.589
15	0	36	0.00317	0.1171	36.706
16	0	36	0.00227	0.0840	36.790
17	0	36	0.00163	0.0602	36.850
18	1	37	0.00116	0.0430	36.893
19	0	37	0.00083	0.0307	36.924
20	0	37	0.00059	0.0219	36.946

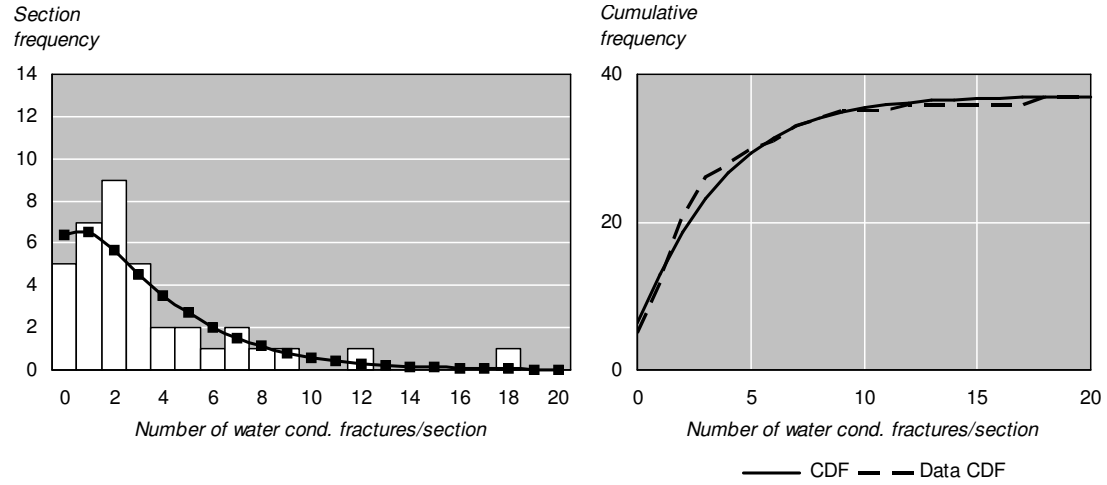

Figure B.1 *Left: Frequency diagram for water-conducting fractures per 3 m-section in the drifts, DA1619A02 and DA1622A01, with a negative binomial distribution fitted to the data. Right: The cumulative distribution function, CDF in comparison with cumulative data.*

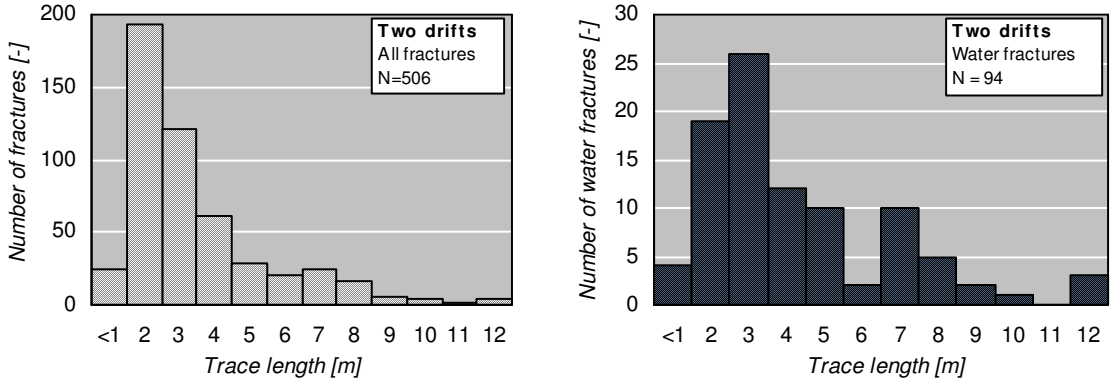

Figure B.2 *Fracture trace length distributions from mapping of the two drifts. Left: All fractures. Right: Only water-conducting fractures.*

Table B.3 *Trace lengths for fractures in the two drifts.*

All fractures		Water-conducting	
Fracture length [m]	**Number of fractures**	**Fracture length [m]**	**Number of fractures**
<1	24	<1	4
2	193	2	19
3	121	3	26
4	61	4	12
5	29	5	10
6	21	6	2
7	25	7	10
8	17	8	5
9	6	9	2
10	4	10	1
11	1	11	0
12	4	12	3

B.2 Evaluation of transmissivity and skin factor from PBT data

The transmissivity based on pressure build-up tests performed in the post-grouting project have been re-evaluated in this thesis using Jacob's method. A total of six pressure build-up curves have been used in the evaluation. Three were obtained in November 2007 before grouting, and three in March 2008 in positions not yet grouted. Position 1 and 2 in November 2007 are not evaluated due to uncertainties related to the pressure build-up curves.

Position 3. November 2007

ds'' = 12.3 m
Q = 8.17E-06 m^3/s

T =1.22E-07 m^2/s
b = *58 µm*

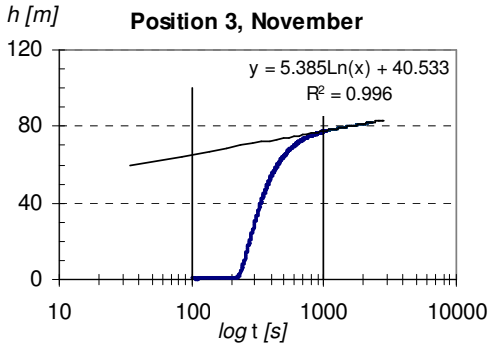

Position 4. November 2007

ds'' = 46.5 m
Q = 2.93E-05 m^3/s

T = 1.15E-07 m^2/s
b = *57 µm*

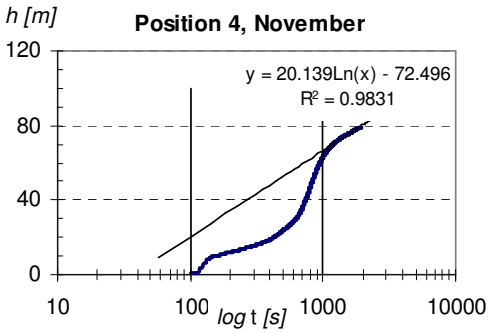

Position 5. November 2007

ds'' = 9.6 m
Q = 2.47E-06 m^3/s

T = 4.70E-08 m^2/s
b = *42 µm*

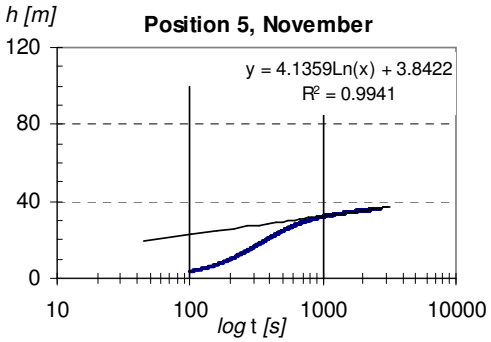

Position 2. March 2008

ds'' = 6.5 m
Q = 2.42E-06 m^3/s

T = 6.80E-08 m^2/s
b = *48 µm*

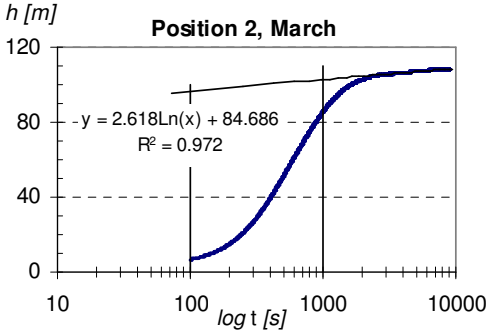

Position 4. March 2008

ds'' = 26.5 m
Q = 2.93E-05 m^3/s

T = 2.03E-07 m^2/s
b = 69 μm

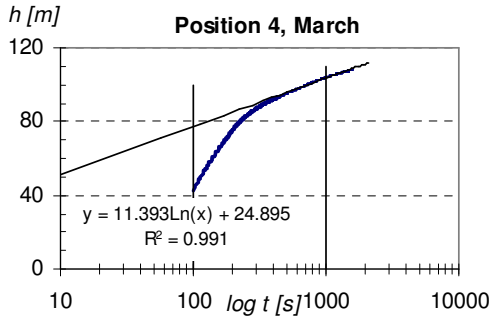

Position 5. March 2008

ds'' = 19 m
Q = 3.17E-06 m^3/s

T = 3.05E-08 m^2/s
b = 36 μm

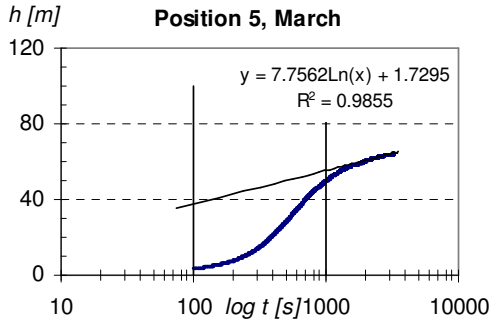

Table B.4 Compilation of evaluated transmissivities based on PBT.

	Position 3 November	Position 4 November	Position 5 November	Position 2 March	Position 4 March	Position 5 March
T [m²/s]	1.22E-07 m^2/s	1.15E-07 m^2/s	4.70E-08 m^2/s	6.80E-08 m^2/s	2.03E-07 m^2/s	3.05E-08 m^2/s
b [μm]	58	57	42	48	69	36

Skin factor

The evaluation of the skin factor in the drift at the characterised positions have been based on the pressure build-up test performed (position 1 and 2 in November 2007 are excluded). The evaluations have been performed with the following equations:

$$\zeta = \frac{2\pi \cdot T \cdot s_{1\min}}{Q} - \ln\left(\frac{\sqrt{135T/S}}{r_w}\right)$$

$$S = 0.0007\sqrt{T}$$

Position 3. November 2007

radius = 0.925 m
s_{1min} = 62.6 m
T = 1.22E-07 m^2/s
Q = 8.17E-06 m^3/s
S = 2.44E-07
Skin = 4

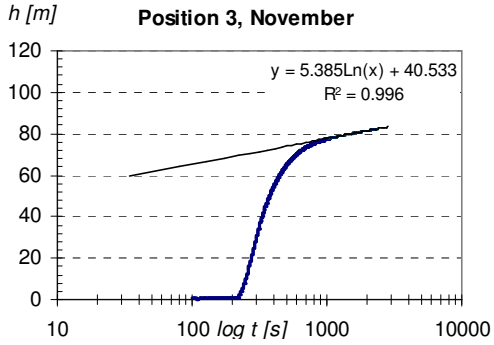

Position 4. November 2007

radius = 0.925 m
s_{1min} = 10.0 m
T = 6.80E-08 m^2/s
Q = 2.45E-05 m^3/s
S = 1.83E-07
Skin = -2

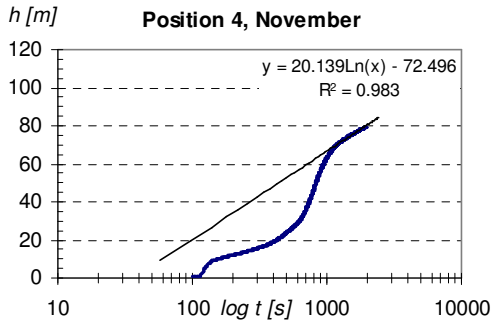

Position 5. November 2007
radius = 0.925 m
s_{1min} = 20.8 m
T = 4.70E-08 m^2/s
Q = 3.17E-06 m^3/s
S = 1.52E-07

Skin = 0

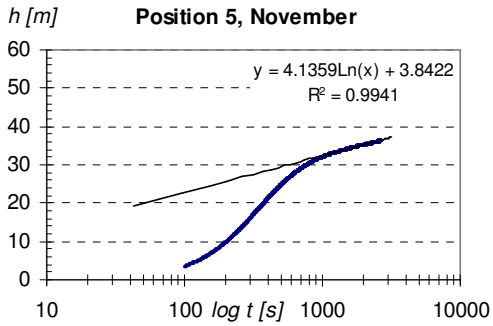

Position 2. March 2008
radius = 0.925 m
s_{1min} = 95.3 m
T = 6.80E-08 m^2/s
Q = 2.42E-06 m^3/s
S = 1.83E-07

Skin = 15

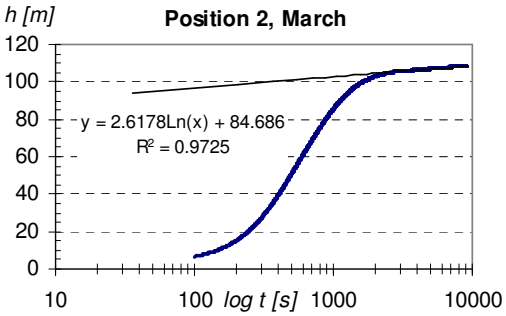

Position 4. March 2008
radius = 0.925 m
s_{1min} = 71.5 m
T = 2.03E-07 m^2/s
Q = 2.93E-05 m^3/s
S = 3.15E-07

Skin = 1

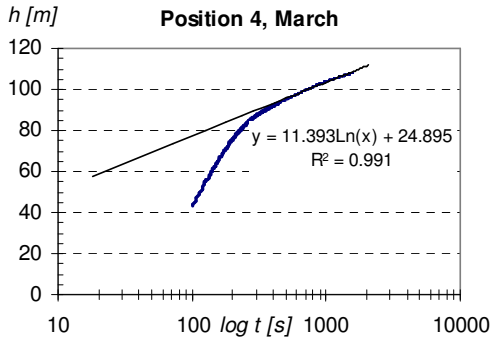

Position 5. March 2008
radius = 0.925 m
s_{1min} = 33.5 m
T = 3.05E-08 m^2/s
Q = 3.17E-06 m^3/s
S = 1.22E-07

Skin = 0

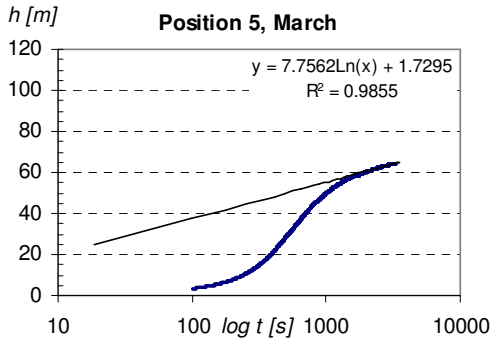

Table B.5 Compilation of evaluated skin factors based on PBT.

	Position 1		Position 2		Position 3		Position 4		Position 5	
	Nov.	March	Nov.	March	Nov.	March	Nov.	March	Nov.	March
Skin factor, ξ	-	-	-	15	4	-	-2	1	0	0

B.3 Pareto distribution for water-conducting fractures in the drift

The drift was divided into 12 five meter long sections, with 5 sections having an inflow that was measured before the Mega-Packer post-grouting project. The evaluation is made for 92 water-conducting fractures, based on the following input (inflow measurements, see Chapter 3.4.6). The result is presented in Chapter 3.

Hydraulic head: 80 m
Position 2 1.25E-08 m^2/s
Position 5 2.99E-08 m^2/s
Position 3 7.97E-08 m^2/s
Position 4 2.39E-07 m^2/s
Position 1 1.20E-06 m^2/s

A transmissivity distribution from inflow measurements, using the Pareto statistical distribution is presented in Table B.6. The distribution parameter, *k* is 0.3638, and the largest hydraulic aperture is 124 µm. The total simulated inflow is 5.96 l/min.

Table B.6 Simulated transmissivities and hydraulic apertures with corresponding inflow for 98 open fractures along the control hole.

r	*1-p*	T_n	*b* [mm]	*Q* [l/min]	*r*	*1-p*	T_n	*b* [mm]	*Q* [l/min]
1	0.989	1.20E-06	0.124	4.73E+00	47	0.495	3.04E-11	0.004	1.20E-04
2	0.978	1.79E-07	0.066	7.04E-01	48	0.484	2.87E-11	0.004	1.13E-04
3	0.968	5.86E-08	0.045	2.31E-01	49	0.473	2.71E-11	0.004	1.07E-04
4	0.957	2.66E-08	0.035	1.05E-01	50	0.462	2.57E-11	0.003	1.01E-04
5	0.946	1.44E-08	0.028	5.67E-02	51	0.452	2.43E-11	0.003	9.57E-05
6	0.935	8.71E-09	0.024	3.43E-02	52	0.441	2.30E-11	0.003	9.08E-05
7	0.925	5.70E-09	0.021	2.25E-02	53	0.430	2.19E-11	0.003	8.61E-05
8	0.914	3.95E-09	0.019	1.56E-02	54	0.419	2.08E-11	0.003	8.18E-05
9	0.903	2.86E-09	0.017	1.13E-02	55	0.409	1.97E-11	0.003	7.78E-05
10	0.892	2.14E-09	0.015	8.43E-03	56	0.398	1.88E-11	0.003	7.40E-05
11	0.882	1.65E-09	0.014	6.49E-03	57	0.387	1.79E-11	0.003	7.05E-05
12	0.871	1.30E-09	0.013	5.11E-03	58	0.376	1.71E-11	0.003	6.72E-05
13	0.860	1.04E-09	0.012	4.10E-03	59	0.366	1.63E-11	0.003	6.41E-05
14	0.849	8.49E-10	0.011	3.34E-03	60	0.355	1.55E-11	0.003	6.12E-05
15	0.839	7.02E-10	0.010	2.77E-03	61	0.344	1.49E-11	0.003	5.85E-05
16	0.828	5.88E-10	0.010	2.32E-03	62	0.333	1.42E-11	0.003	5.60E-05
17	0.817	4.98E-10	0.009	1.96E-03	63	0.323	1.36E-11	0.003	5.36E-05
18	0.806	4.25E-10	0.009	1.68E-03	64	0.312	1.30E-11	0.003	5.13E-05
19	0.796	3.67E-10	0.008	1.44E-03	65	0.301	1.25E-11	0.003	4.92E-05
20	0.785	3.18E-10	0.008	1.25E-03	66	0.290	1.20E-11	0.003	4.71E-05
21	0.774	2.78E-10	0.008	1.10E-03	67	0.280	1.15E-11	0.003	4.52E-05
22	0.763	2.45E-10	0.007	9.66E-04	68	0.269	1.10E-11	0.003	4.34E-05
23	0.753	2.17E-10	0.007	8.55E-04	69	0.258	1.06E-11	0.003	4.17E-05
24	0.742	1.93E-10	0.007	7.60E-04	70	0.247	1.02E-11	0.003	4.01E-05
25	0.731	1.72E-10	0.007	6.80E-04	71	0.237	9.78E-12	0.003	3.86E-05
26	0.720	1.55E-10	0.006	6.10E-04	72	0.226	9.41E-12	0.002	3.71E-05
27	0.710	1.40E-10	0.006	5.50E-04	73	0.215	9.06E-12	0.002	3.57E-05
28	0.699	1.26E-10	0.006	4.98E-04	74	0.204	8.73E-12	0.002	3.44E-05
29	0.688	1.15E-10	0.006	4.52E-04	75	0.194	8.42E-12	0.002	3.32E-05
30	0.677	1.04E-10	0.006	4.12E-04	76	0.183	8.11E-12	0.002	3.20E-05
31	0.667	9.55E-11	0.005	3.76E-04	77	0.172	7.83E-12	0.002	3.09E-05
32	0.656	8.75E-11	0.005	3.45E-04	78	0.161	7.56E-12	0.002	2.98E-05
33	0.645	8.04E-11	0.005	3.17E-04	79	0.151	7.30E-12	0.002	2.88E-05
34	0.634	7.40E-11	0.005	2.92E-04	80	0.140	7.05E-12	0.002	2.78E-05
35	0.624	6.84E-11	0.005	2.69E-04	81	0.129	6.81E-12	0.002	2.68E-05
36	0.613	6.33E-11	0.005	2.49E-04	82	0.118	6.59E-12	0.002	2.60E-05
37	0.602	5.87E-11	0.005	2.31E-04	83	0.108	6.37E-12	0.002	2.51E-05
38	0.591	5.45E-11	0.004	2.15E-04	84	0.097	6.16E-12	0.002	2.43E-05
39	0.581	5.08E-11	0.004	2.00E-04	85	0.086	5.97E-12	0.002	2.35E-05
40	0.570	4.74E-11	0.004	1.87E-04	86	0.075	5.78E-12	0.002	2.28E-05
41	0.559	4.43E-11	0.004	1.74E-04	87	0.065	5.60E-12	0.002	2.21E-05
42	0.548	4.14E-11	0.004	1.63E-04	88	0.054	5.42E-12	0.002	2.14E-05
43	0.538	3.88E-11	0.004	1.53E-04	89	0.043	5.26E-12	0.002	2.07E-05
44	0.527	3.65E-11	0.004	1.44E-04	90	0.032	5.10E-12	0.002	2.01E-05
45	0.516	3.43E-11	0.004	1.35E-04	91	0.022	4.95E-12	0.002	1.95E-05
46	0.505	3.23E-11	0.004	1.27E-04	92	0.011	4.80E-12	0.002	1.89E-05

B.4 Dimensionality analysis

Dimensionality analyses have been performed using pressure, volume and time recordings from water pressure tests and grouting sessions. The analysis based on WPTs performed in October and November 2007 is presented below, with pressure-flow curves, flow dimension curves and accumulated flow curves for each position.

WPT Position 1

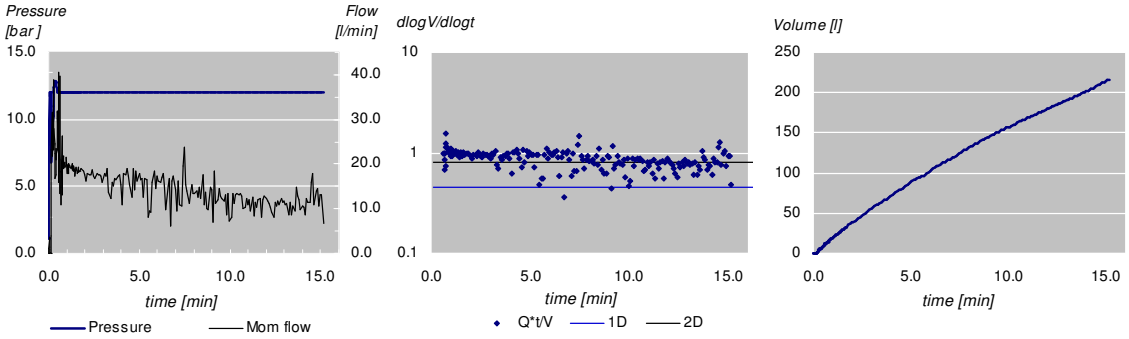

WPT Position 2

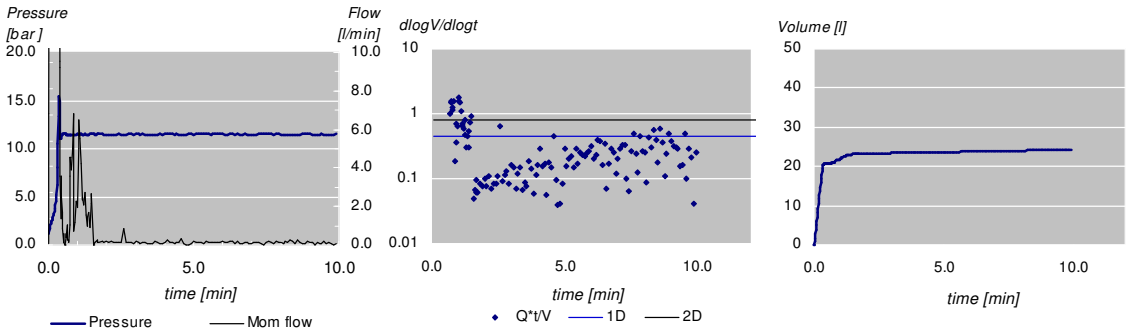

WPT Position 3

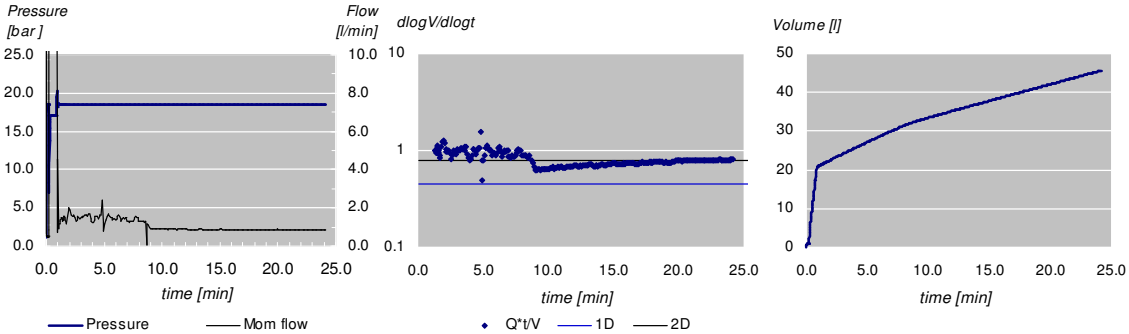

Appendix B

WPT Position 4

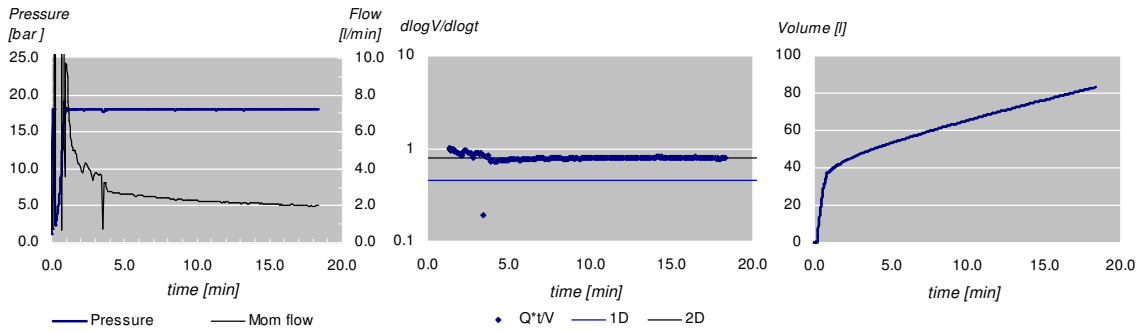

WPT Position 5

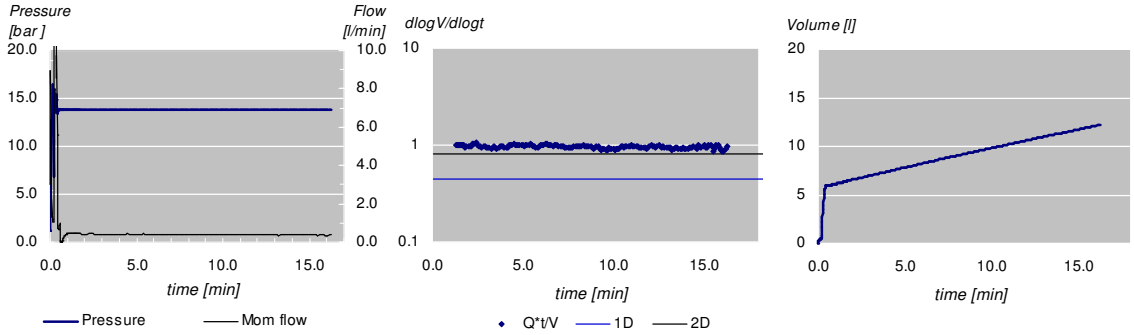

Below is the dimensionality analysis based on grouting data presented with pressure-flow curves, flow dimensionality curves and accumulated flow curves.

Grouting Position 1, November

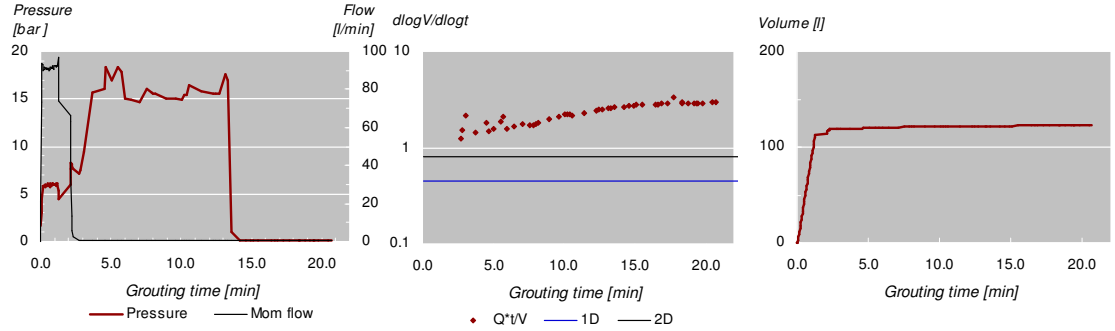

Grouting Position 2, March

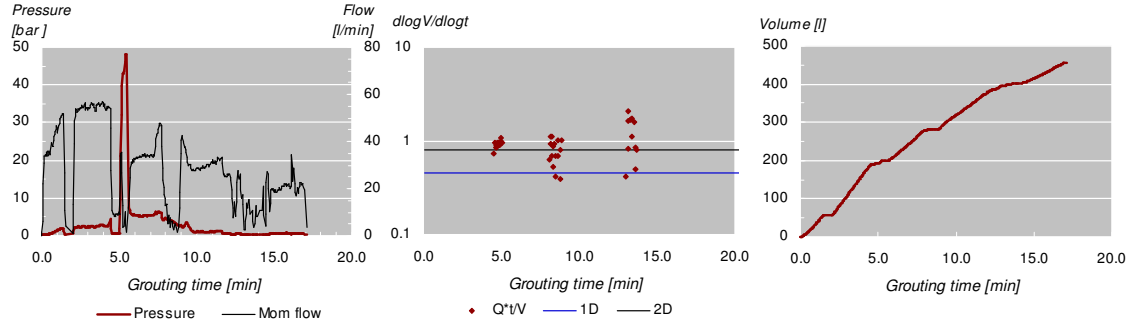

Grouting Position 3, November

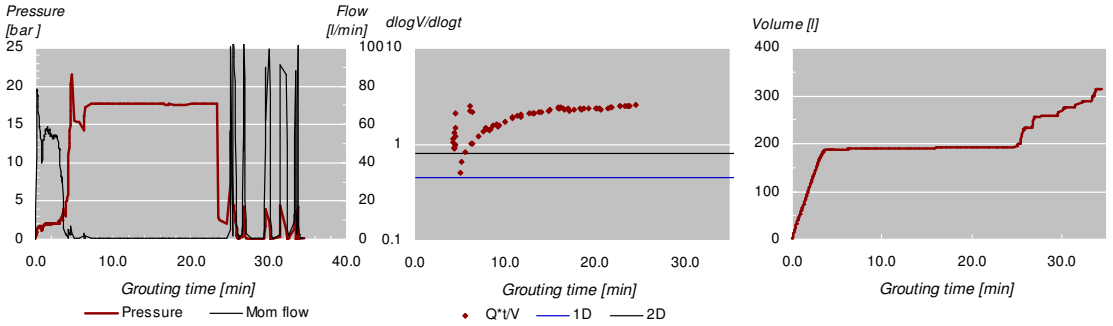

Grouting Position 4, March

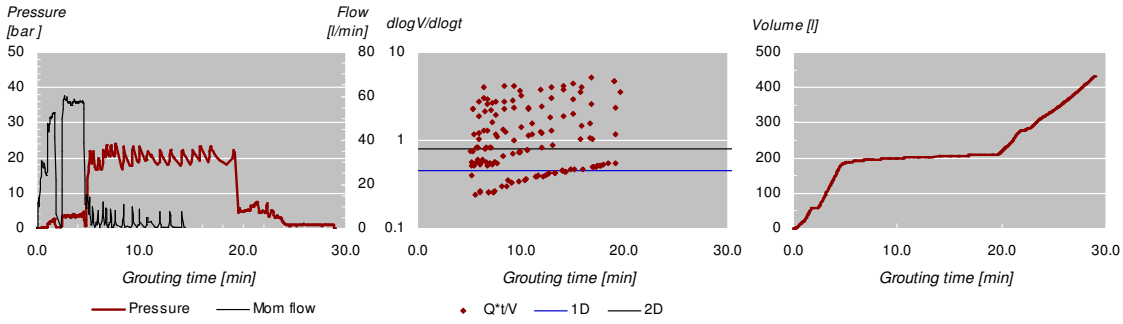

Grouting Position 5-1, March

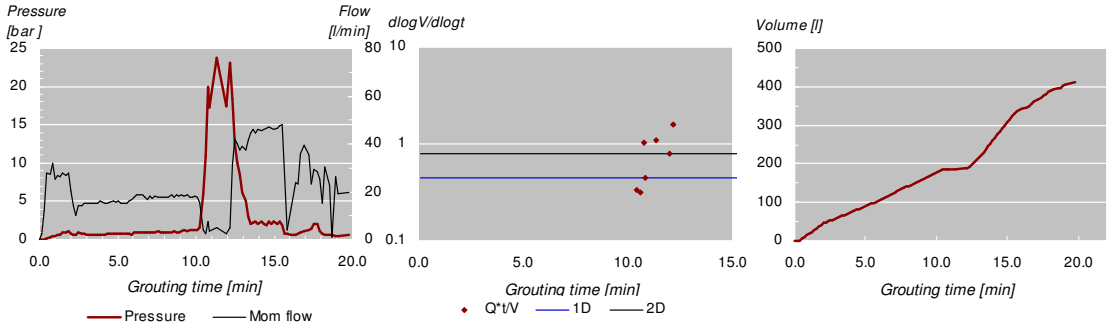

Grouting Position 5-2, March

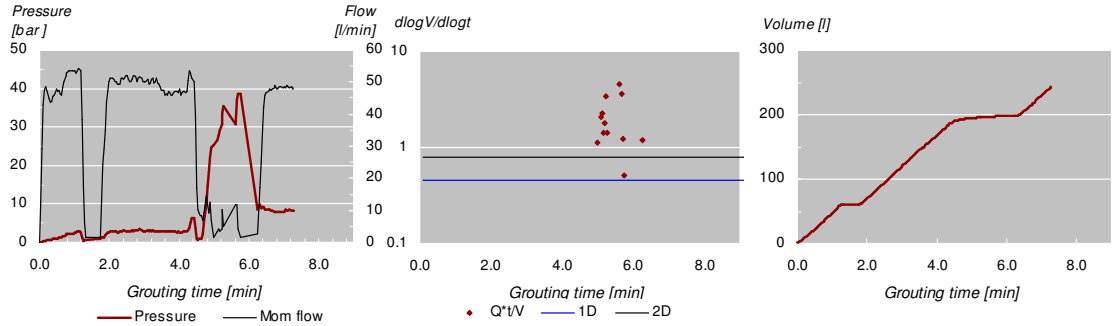

B.5 Penetration of silica sol

The maximum penetration of silica sol in the five Mega-Packer positions has been calculated using following equations and input data. The result can be seen in Table B.7.

Groundwater pressure: 0.8 MPa
Initial viscosity, μ_0: 5 mPas

Table B.7 Calculation of maximum penetration of silica sol.

POSITION	1	2	3	4	5A
Geltime [min]	40	43	40	43	31
Total pressure	1.4	2.1	1.8	2.1	1.7
Δp [MPa]	0.6	1.3	1	1.3	0.9
b [µm]	133	33	55	76	42
t_G, (1/3 of the geltime) [s]	800	860	800	860	620
l_{max} 2D [m]	**7.6**	**2.9**	**4.0**	**6.6**	**2.6**
l_{max} 1D [m]	**16.8**	**6.4**	**9.0**	**14.7**	**5.7**